
# NAVAL POSTGRADUATE SCHOOL

**MONTEREY, CALIFORNIA**

# THESIS

**CALIBRATION AND VALIDATION OF HIGH FREQUENCY RADAR FOR OCEAN SURFACE CURRENT MAPPING**

by

Kyung Cheol Kim

June 2004

Thesis Advisor: Jeffrey D. Paduan
Second Reader: Steven R. Ramp

**Approved for public release; distribution is unlimited**

THIS PAGE INTENTIONALLY LEFT BLANK

| REPORT DOCUMENTATION PAGE | | | Form Approved OMB No. 0704-0188 |
|---|---|---|---|
| Public reporting burden for this collection of information is estimated to average 1 hour per response, including the time for reviewing instruction, searching existing data sources, gathering and maintaining the data needed, and completing and reviewing the collection of information. Send comments regarding this burden estimate or any other aspect of this collection of information, including suggestions for reducing this burden, to Washington headquarters Services, Directorate for Information Operations and Reports, 1215 Jefferson Davis Highway, Suite 1204, Arlington, VA 22202-4302, and to the Office of Management and Budget, Paperwork Reduction Project (0704-0188) Washington DC 20503. | | | |
| **1. AGENCY USE ONLY** ***(Leave blank)*** | **2. REPORT DATE**<br>June 2004 | **3. REPORT TYPE AND DATES COVERED**<br>Master's Thesis | |
| **4. TITLE AND SUBTITLE**:<br>Calibration and Validation of High Frequency Radar for Ocean Surface Current Mapping | | | **5. FUNDING NUMBERS** |
| **6. AUTHOR(S)**<br>Kim, Kyung Cheol | | | |
| **7. PERFORMING ORGANIZATION NAME(S) AND ADDRESS(ES)**<br>Naval Postgraduate School<br>Monterey, CA 93943-5000 | | | **8. PERFORMING ORGANIZATION REPORT NUMBER** |
| **9. SPONSORING /MONITORING AGENCY NAME(S) AND ADDRESS(ES)**<br>N/A | | | **10. SPONSORING/MONITORING AGENCY REPORT NUMBER** |
| **11. SUPPLEMENTARY NOTES** The views expressed in this thesis are those of the author and do not reflect the official policy or position of the Department of Defense or the U.S. Government. | | | |
| **12a. DISTRIBUTION / AVAILABILITY STATEMENT**<br>Approved for public release; distribution unlimited | | | **12b. DISTRIBUTION CODE** |


**13. ABSTRACT (maximum 200 words)**

High Frequency (HF) radar backscatter instruments are being developed and tested in the marine science and defense science communities for their abilities to sense surface parameters remotely in the coastal ocean over large areas. In the Navy context, the systems provide real-time mapping of ocean surface currents and waves critical for characterizing and forecasting the battle space environment.

In this study, the performance of a network of four CODAR (Coastal Ocean Dynamics Application Radar) SeaSonde HF radars, using the Multiple Signal Classification (MUSIC) algorithm for direction finding, is described for the period between July to September 2003. Comparisons are made in Monterey Bay with moored velocity observations, with four radar baseline pairs, and with velocity observations from sixteen drifter deployments.

All systems measure ocean surface current and all vector currents are translated into radial current components in the direction of the various radar sites. Measurement depths are ~1 m for the HF radar-derived currents, 12 to 20 m for the ADCP bin nearest to the surface at the M1 mooring site, and ~8 m for the drifter-derived velocity estimates.

Comparisons of HF radar-M1 mooring buoy, HF radar-HF radar (baseline), and HF radar-drifter data yield improvements of –1.7 to 16.7 cm/s rms differences and –0.03 to 0.35 correlation coefficients when measured antenna patterns are used. The mooring comparisons and the radar-to-radar baseline comparisons indicate angular shifts of 10˚ to 30˚ for radial currents produced using ideal antenna patterns and 0˚ to 15˚ angular shifts for radial currents produced using measured patterns. The comparisons with drifter-derived radial currents indicate that these angular biases are not constant across all look directions, even though the local antenna pattern distortions were taken into account through the use of measured antenna patterns. In particular, data from the SCRZ and MLNG radar sites show varied pointing errors across the range of angles covered.


| **14. SUBJECT TERMS**<br>HF radar, Ocean surface current, Calibration, MUSIC algorithm | | | **15. NUMBER OF PAGES**<br>92 |
|---|---|---|---|
| | | | **16. PRICE CODE** |
| **17. SECURITY CLASSIFICATION OF REPORT**<br>Unclassified | **18. SECURITY CLASSIFICATION OF THIS PAGE**<br>Unclassified | **19. SECURITY CLASSIFICATION OF ABSTRACT**<br>Unclassified | **20. LIMITATION OF ABSTRACT**<br>UL |

NSN 7540-01-280-5500

Standard Form 298 (Rev. 2-89)
Prescribed by ANSI Std. 239-18

THIS PAGE INTENTIONALLY LEFT BLANK

**Approved for public release; distribution unlimited**

**CALIBRATION AND VALIDATION OF HIGH FREQUENCY RADAR FOR OCEAN SURFACE CURRENT MAPPING**

Kyung Cheol Kim
Lieutenant Commander, Republic of Korea Navy
B.S., Republic of Korea Naval Academy, 1993

Submitted in partial fulfillment of the
requirements for the degree of

**MASTER OF SCIENCE IN PHYSICAL OCEANOGRAPHY**

from the

**NAVAL POSTGRADUATE SCHOOL**
**June 2004**

Author: Kyung Cheol Kim

Approved by: Jeffrey D. Paduan
Thesis Advisor

Steven R. Ramp
Second Reader

Mary L. Batteen
Chairman, Department of Oceanography

THIS PAGE INTENTIONALLY LEFT BLANK

# ABSTRACT

High Frequency (HF) radar backscatter instruments are being developed and tested in the marine science and defense science communities for their abilities to sense surface parameters remotely in the coastal ocean over large areas. In the Navy context, the systems provide real-time mapping of ocean surface currents and waves critical for characterizing and forecasting the battle space environment.

In this study, the performance of a network of four CODAR (Coastal Ocean Dynamics Application Radar) SeaSonde HF radars, using the Multiple Signal Classification (MUSIC) algorithm for direction finding, is described for the period between July to September 2003. Comparisons are made in Monterey Bay with moored velocity observations, with four radar baseline pairs, and with velocity observations from sixteen drifter deployments.

All systems measure ocean surface current and all vector currents are translated into radial current components in the direction of the various radar sites. Measurement depths are ~1 m for the HF radar-derived currents, 12 to 20 m for the ADCP bin nearest to the surface at the M1 mooring site, and ~8 m for the drifter-derived velocity estimates.

Comparisons of HF radar-M1 mooring buoy, HF radar-HF radar (baseline), and HF radar-drifter data yield improvements of –1.7 to 16.7 cm/s rms differences and –0.03 to 0.35 correlation coefficients when measured antenna patterns are used. The mooring comparisons and the radar-to-radar baseline comparisons indicate angular shifts of 10˚ to 30˚ for radial currents produced using ideal antenna patterns and 0˚ to 15˚ angular shifts for radial currents produced using measured patterns. The comparisons with drifter-derived radial currents indicate that these angular biases are not constant across all look directions, even though the local antenna pattern distortions were taken into account through the use of measured antenna patterns. In particular, data from the SCRZ and MLNG radar sites show varied pointing errors across the range of angles covered.

THIS PAGE INTENTIONALLY LEFT BLANK

# TABLE OF CONTENTS

THIS PAGE INTENTIONALLY LEFT BLANK

# LIST OF FIGURES

THIS PAGE INTENTIONALLY LEFT BLANK

# LIST OF TABLES

# ACKNOWLEDGMENTS

This work would not have been possible without the enormous support of many people. First of all, I would like to extend my deepest appreciation to my thesis advisor, Professor Jeffrey D. Paduan, and the second reader, Professor Steven R. Ramp. Their expert advice, directions and patience have expanded and enhanced my knowledge, and allowed me to complete my thesis. Professor Paduan who provided me with the opportunity to explore the incredible world of HF radar deserves my highest respect and appreciation.

I also owe a great deal of thanks to Dr. Hyong Rok Kim and Dr. Sung Hyea Park of the Naval Postgraduate School Oceanography Department. Their recommendations on my thesis and the studies of physical oceanography opened my eyes toward an academic world.

I also would like to thank to Mike Cook and Fred Bahr for supplying their data and assisting with the data processing.

Additionally, I wish to thank my wife Hyo Jung, my son Jae Hwan, and my lovely daughter, Do Hyun, for supporting me during the long hours I have spent away from home while finishing this thesis. They have been the greatest supporters and inspirers whenever I was discouraged. Also, I greatly appreciate my country, the Republic of Korea, and its Navy for all the support during my journey to the Naval Postgraduate School.

THIS PAGE INTENTIONALLY LEFT BLANK

# I. INTRODUCTION

## A. HIGH FREQUENCY RADAR

Since the first identification of the Doppler spectrum of sea echo by Crombie (1955), High Frequency (HF) radars have been developed mainly to measure surface current and to extract information about surface waves and winds from HF backscatter spectra (Paduan and Graber, 1997; Wyatt, 1997; Fernandez et al., 1997). The most common uses of HF radar systems are to produce the vector maps of the ~1 m deep currents over spatial scales ranging from hundreds of meters to hundreds of kilometers for near real-time applications (Stewart and Joy, 1974; Paduan and Graber, 1997).

A single radar can observe only the component receding from or approaching the radar at a given bearing and range called the "radial" component. For mapping radial current data, the system needs three pieces of information from each radar: range, speed, and bearing of the scattering source. Two or more radars are needed for mapping vectors currents.

To determine range, several methods exist related to the time delay of the scattered signal after transmission. Since the Doppler-frequency shift includes the speed of the reflecting ocean wave and the underlying current, differences between the measured speed and the known speed of the waves provide the speed of the underlying current. Two types of methods, called beam forming and direction finding, can determine the angle from which a return is coming. A beam forming system, such as the Ocean Surface Current Radar (OSCR; Hammond et al. 1987) and Wellen Radar (WERA; Gurgel et al. 1999) uses a linear array of receive antennae to steer the receive antennae look angle to different directions. In contrast, a direction finding system, such as the CODAR (Coastal Ocean Dynamics Application Radar) SeaSonde, uses the signal received by three different antennae, including two loop antennae oriented ninety degrees to each other, and a monopole to determine the angle. When the signals received by the two loop antennae are normalized with the monopole signal, the arctangent of two crossed-loop signal ratio is used to determine the direction of the signal (Kohut and Glenn, 2003). In practice, a much more robust algorithm called Multiple Signal

Classification (MUSIC; Schmidt 1986) is used to determine bearing. This MUSIC algorithm enables the CODAR configuration to resolve more complicated ocean surface current.

## B. MUSIC ALGORITHM AND ANTENNA PATTERNS

The CODAR SeaSonde systems use the MUSIC algorithm for direction finding, which requires accurate knowledge of the angular response pattern of each antenna element. Errors in the antenna patterns translate into errors in angular placement of radial current values around a given range cell. It is common to use one of two methods to ascertain the angular beam patterns: 1) assume the theoretical or "ideal" patterns based on the antenna design or 2) measure the actual antenna patterns after installation. The ideal patterns of the two cross-loop antennae are cosine-dependent and oriented orthogonal to each other. The measured patterns of the receive antenna elements can be obtained by moving a small battery-operated transponder around the shore site on a boat or, sometimes, by foot if space permits. Figure 1, 2, 3, and 4 illustrate the ideal and measured patterns of the four radar sites in Monterey Bay. The radial current vectors toward each radar site using the ideal antenna patterns (black arrows) and the measured (red arrows) are shown in the same figures.

The antenna patterns are sensitive to electromagnetic interference from the surrounding environment. Specifically, the efficiency of the monopole ground plane and whether the local environment is clear or cluttered with respect to conducting elements in the near field of the antenna, play important roles in antenna pattern distortion (Kohut and Glenn, 2003). If the actual beam patterns on site differ from the assumed patterns, this can introduce an angular bias as large as 35 degrees if they are not taken into account (Barrick and Lipa, 1986). Also Kohut and Glenn (2003) show that system accuracy depends on the distortion of the measured pattern.

## C. EVALUATION OF CODAR SEASONDE HF RADAR IN MONTEREY BAY

Validation of the algorithms used to produce current maps from HF radar backscatter is needed to create a better understanding of the system among the user community. The first validation studies were conducted using velocity estimates from drifters to compare with those from HF radar measurements (Stewart and Joy, 1974;

Barrick and Lipa, 1977; Frisch and Weber, 1980). Some later investigations compared the HF radar data with bottom-mounted Acoustic Doppler Current Profilers (ADCP) or moored instruments finding differences ranging from 9 to 17 cm/s (review by Chapman et al., 1997). A more recent study shows that the pointing error for a given radar is not constant but varied with bearing when using the ideal pattern data in the MUSIC algorithm of the CODAR SeaSonde HF radar (Emery et al., 2003).

When evaluating the accuracy of a new instrument, it is important that the two instruments are measuring the same physical quantities (Chapman et al., 1997). Differences in these comparisons are expected due to differences in time averaging, the depth of the observation, and geographical averaging in addition to inaccuracies of the instruments themselves.

The present study focuses on validating CODAR SeaSonde HF radar in comparison with moored velocity observations, with four radar baseline pairs, and with velocity observations from sixteen drifter deployments to understand the error in the CODAR SeaSonde HF radar and its MUSIC algorithm. First, accuracies of the direction-finding process of the MUSIC algorithm in ideal and measured patterns at one mooring location are estimated by comparing various statistical values of currents at selected locations from the HF radars with *in-situ* currents measured by a moored ADCP on the M1 buoy, located at the mouth of Monterey Bay. Through a comparison of M1 buoy data and HF radar data, some improvements in the statistical values are expected when shifting from data produced using ideal antenna patterns to data produced using measured antenna patterns. This is because it is expected that the measured antenna patterns will increase the accuracy of the direction finding.

Second, a comparison of radial currents on the baseline between two HF radar sites is made. Both ideal and measured antenna pattern data are used. Data from different angles for opposite radar sites are compared in the method of Melton (1995). These baseline analyses between the same HF radar systems provide the system accuracies including their direction finding capability. Also, use of multiple baseline pairs helps to determine if the pointing errors at one site are similar at different angles.

As an example, a comparison of the SCRZ radar site to PPIN, NPGS, and MLNG radar sites shows different pointing errors in direction finding at each site.

Lastly, HF radar data from ideal and measured patterns are compared with currents from surface drifters deployed in Monterey Bay. The drifter data distribution is scattered across Monterey Bay. Due to this scattered distribution, it is possible to see the statistical values at several angles from one radar site. Also, statistical changes can be seen at each angle from the ideal to the measured patterns, and the variations of these statistical values within certain angular ranges may also be seen through these comparisons.

The HF radar validation results presented here investigate and quantify through the comparison of moored ADCP data, baselines, and drifters, how the pointing errors vary at each angle of a radar site in both ideal and measured antenna patterns. The findings are presented after a brief summary of HF radar systems as background information. Chapter II outlines the data collection activities used in this investigation. Chapter III addresses the methods of data analysis and the results of each comparison. Chapter IV presents the discussion and summary of this work.

# II. DATA COLLECTION

## A. AUTONOMOUS OCEAN SAMPLING NETWORK (AOSN) PROJECT

The Autonomous Ocean Sensing Network (AOSN) in Monterey Bay used a variety of modern platforms such as gliders, Autonomous Underwater Vehicles (AUVs), drifters, floats, satellites, ships, moorings, and aircraft to produce a comprehensive view of the ocean. As a second field test for the AOSN program, a month-long experiment was conducted to study upwelling features in the Monterey Bay during the summer of 2003. More information is available at the Monterey Bay Aquarium Research Institute (MBARI) website (http://www.mbari.org/aosn/). This experiment used data from the HF radars, M1 buoy, and drifters. Figure 5 graphically illustrates the locations of the four HF radar sites, the M1 buoy, and drifter trajectories, while Table 1 summarizes the data that were used in the analyses presented here.

## B. HF RADAR

CODAR-Type HF Radar has been employed around Monterey Bay, CA, to measure ocean-surface currents since February 1992. These instruments are located at sites near the Naval Postgraduate School (NPGS) broadcasting at the frequency of 13.5 megahertz (MHz), Point Pinos (PPIN) at 13.2 MHz in the south, near Moss Landing (MLNG) at 24.6 MHz in the east, and near Santa Cruz (SCRZ) at 12.2 MHz on the northern shore of Monterey Bay. Different frequencies among the radar sites are designed to transmit signals without interference. The Bragg wavelength of the NPGS, PPIN and SCRZ sites is ~12 m and ~6 m at the MLNG site. The radial current velocity of the ocean surface is found from the difference between the Doppler shift of the returned signal and the expected Doppler shift of the ocean-surface gravity wave.

Each radar site has a transmit antenna, a receive antenna, radar electronics, and a computer for system control and data logging. The antennae were installed as close to the shore as possible but separated from each other. The data of each radar site are monitored and transmitted to a computer at NPGS Oceanography Department for current mapping in the Monterey bay. The near real-time observations of the currents in the Monterey Bay are available at the NPGS Oceanography Department website (http://www.oc.nps.navy.mil/~cook/Real/Totals/).

The HF data is a one-hour mean measurement of thirty minutes before and after each hour and has a radial speed toward or away from each radar site measured in cm/s. For the purpose of this study, ideal and measured pattern data from each radar site from 22 July to 9 September 2003 are used. A total of four paired mooring-HF radar, HF-HF radar, and drifter-HF radar time series were available with maximum record lengths exceeding 50 days and minimum record lengths of 21 days.

## C. M1 BUOY

The M1 buoy is an instrumented mooring maintained by MBARI and located at 36.744°N, 122.021°W near the mouth of Monterey Bay. The buoy is anchored in 1,000 m of water and was established as part of a network designed to provide continuous in-situ observations of physical, chemical, and biological properties over long periods of time.

The M1 mooring carries downward-looking Acoustic Doppler Current Profiler (ADCP), which separates the current measurements into 8-m depth bins and returns an average value for each bin. The shallowest good bin measures currents between 12 and 20 meters, while the deeper bins extend to 500 m. The ADCP is programmed to take a three–minute measurement once every hour.

For more accurate current estimates, Global Positioning System (GPS) data on the movement of the M1 buoy was used to correct the U and V velocity components of the first ADCP current bin for the period from 23 July to 9 September 2003.

## D. DRIFTER

Four drifters were deployed on the northern end of Monterey Bay from 11 August to 5 September 2003. When a drifter made its way across to the other side of the bay, it was recovered and redeployed to a new position in the northern end of Monterey Bay: Each drifter was relocated four times for a total of sixteen measured drifts.

The drifters were equipped with differential global positioning system (DGPS) navigation to obtain improved position accuracy in conjunction with a Radio Direction Finding (RDF) beacon. The drifters were designed to be surface-level Lagrangian drifters moving with an 8 m depth current speed. Figure 6 shows a drifter with its drogue stretched out along the ocean surface in Monterey Bay shortly after deployment.

| Instrument | Period | Measured Depth | Measured Period | Data Interval |
|---|---|---|---|---|
| **HF Radar** | 2003. 07. 22. ~ 09. 09. | ~ 1 m | 1 hour | Hourly |
| **ADCP of M1 Buoy** | 2003. 07. 23. ~ 09. 09. | 12 – 20 m | 3 minutes | Hourly |
| **Drifter** | 2003. 08. 11 ~ 09. 05. | ~ 8 m | 1 hour | Hourly |

**Table 1. Summary of the Data Used for Analysis**

THIS PAGE INTENTIONALLY LEFT BLANK

# III. DATA ANALYSIS AND RESULTS

## A. COMPARISON WITH M1 BUOY ADCP DATA

Ideal and measured patterns of radial surface current data from each site were compared with moored current-meter data from the M1 buoy. To compare radials from HF radar with current measurements from the mooring, the components of moored current velocity $U_{M1}$ and $V_{M1}$ were translated into radial current components in the direction of the HF radar,

$$U'_{M1} = U_{M1} \times \cos\alpha + V_{M1} \times \sin\alpha \quad (1)$$

where, α is the angle of the M1 buoy to the radar sites, $U_{M1}$ and $V_{M1}$ are the east and north mooring current speed vectors, and $U'_{M1}$ is the radial speed of the M1 buoy toward the HF radar site.

Various statistical analyses were performed for each pair of radar and mooring time series: correlation coefficient, rms difference, slope and intercept, and residual rms difference. The correlation coefficient as well as other statistical data was computed between the HF radar and the M1 buoy radial velocity for the angle of the closest HF radar data point to the M1 buoy and for other angles with the same distance (i.e., range) but different angles from the HF radar site (see Figure 7). The matrix laboratory (MATLAB) code of corrcoef was used to compute the correlation coefficient. Also, the rms differences between the HF radar and the M1 buoy radial data were computed as,

$$rms \quad difference = \sqrt{\sum_{i=1}^{n} (U'_{hf}i - U'_{M1}i)^2} \quad (2)$$

and using the least square fitting, the slope and intercept of the scatter plot were computed as,

$$U'_{hf} = aU'_{M1} + b \quad (3)$$

where *a* and *b* represent the slope and y intercept, respectively. Additionally, the residual rms difference was computed using the slope and intercept above to form

$$U'_{Test} = aU'_{M1} + b \quad (4)$$

with the residual rms differences between the HF radar and the M1 buoy radial data computed as,

$$\textit{residual rms difference} = \sqrt{\sum_{i=1}^{n} (U'_{hf}i - U'_{Test}\,i)^2}\,. \quad (5)$$

This residual rms difference is meant to account for the effect of the surface shear, thus providing information that is supplementary to the direct rms difference between the radar observations at 1 m depth and the deeper moored (or drifting buoy) observations. All the numerical results are addressed in the Appendix.

**1. M1 Buoy vs. SCRZ HF RADAR**

Radial angles of SCRZ radar site and the mooring watch circle (red), indicated by the GPS positions of the M1 buoy during the observation period, are presented in Figure 7. There is a two-degree difference between the ideal and measured grid data points as obtained from the SCRZ radar site due to the different setting of angular interval.

Figure 8 shows the correlation coefficients and the rms differences between the HF radial data using the ideal and measured antenna pattern data plotted against the radial component of the M1 buoy data. In the ideal pattern, the maximum value of the correlation coefficient, 0.62, is found at the angle of $-68^{o}$, and the minimum value of the rms difference, 15.2 cm/s, is found at $-58^{o}$. In the measured pattern, the maximum value of the correlation coefficient, 0.65, is found at the angle of $-90^{o}$, and the minimum value of the rms difference, 15.5 cm/s, is found at $-70^{o}$. The values of the maximum correlation coefficient and the minimum rms difference show a minor difference between the two. However, the angles detecting the maximum correlation coefficient and minimum rms difference in the ideal pattern data are shifted about 10° to 20° from the angle of the M1 buoy. Also, the angles detecting the maximum correlation coefficient and the minimum rms difference in the measured pattern data are shifted about 10° from the angle of the M1 buoy.

Scatter plots of the ideal and measured data were graphed against the M1 buoy radial data (Figure 9). The ideal data at $-78^{o}$ gives a slope of 0.7 and an intercept of 9.52

(1073 observations). The measured data at 80$^{o}$ gives a slope of 0.93 and an intercept of 7.96 (942 observations). A comparison of the slopes of the ideal and measured data shows that the measured data is more accurate than the ideal data.

**2. M1 Buoy vs. MLNG HF RADAR**

The radial angles of the MLNG radar site and the mooring watch circle (red) are presented in Figure 10. There is no difference between the ideal and measured grid data points as measured from the MLNG radar site.

Figure 11 shows the correlation coefficients and rms difference between the HF radial data using the ideal and measured pattern data plotted against the radial component of the M1 buoy data. In the ideal pattern, the maximum value of the correlation coefficient, 0.49, is found at the angle of 215$^{o}$, and the minimum value of the rms difference, 12.7 cm/s, is found at 210$^{o}$. In the measured pattern, the maximum value of the correlation coefficient, 0.44, is found at the angle of 205$^{o}$, and the minimum value of the rms difference, 12.4 cm/s, is found at 200$^{o}$. The values of the maximum correlation coefficient and the minimum rms difference show a minor difference in the two. However, the angles detecting the maximum correlation coefficient and the minimum rms difference in the ideal pattern data are shifted about 10° to 15° from the angle of the M1 buoy. Also, the angles detecting the maximum correlation coefficient and the minimum rms difference in the measured pattern data are shifted about 5° from the angle of the M1 buoy.

The scatter plots of the ideal and measured data were graphed against the M1 buoy radial data (Figure 12). The ideal data at 200$^{o}$ gives a slope of 0.21 and intercepts of –4.41 (1041 observations). The measured data at 200$^{o}$ gives a slope of 0.45 and an intercept of –1.43 (973 observations). Comparing the slopes of ideal and measured data shows that the measured data is more accurate compared to the ideal data. However, the statistical values are relatively low at the MLNG radar site. This may be due, in part, to the fact that the magnitudes of the radial current components, as measured from the MLNG location, are relatively weak.

### 3. M1 Buoy vs. NPGS HF RADAR

The radial angles of the NPGS radar site and the mooring watch circle (red) are presented in Figure 13. There is a one-degree difference between the ideal and measured grid data points as measured from the NPGS radar site due to the different setting of angular interval used in the radial processing.

Figure 14 shows the correlation coefficients and the rms difference between the HF radial data using the ideal and measured pattern data plotted against the radial component of the M1 buoy data. In the ideal pattern, the maximum value of the correlation coefficient, 0.57, is found at the angle of 161$^{o}$, and the minimum value of the rms difference, 14.6 cm/s, is found at 146$^{o}$. In the measured pattern, the maximum value of the correlation coefficient, 0.59, is found at the angle of 135$^{o}$, and the minimum value of the rms difference, 14.9 cm/s, is found at 140$^{o}$. The values of the maximum correlation coefficient and the minimum rms difference show a minor difference in the two. However, the angles detecting the maximum correlation coefficient and the minimum rms difference in the ideal pattern data are shifted about 15° to 30° from the angle of the M1 buoy. Also, the angles detecting the maximum correlation coefficient and the minimum rms difference in the measured pattern data are shifted about 5$^{o}$ to 10° from the angle of the M1 buoy.

The scatter plots of the ideal and measured data were graphed against the M1 buoy radial data (Figure 15). The ideal data at 131$^{o}$ gives a slope of 0.28 and intercepts of 0.48 (637 observations). The measured data at 130$^{o}$ gives a slope of 0.94 and an intercept of -6.24 (822 observations). Comparing the slopes of the ideal and the measured data shows that the measured data is more accurate than the ideal data. Note that there is a positive improvement in the correlation coefficient with 0.32, but a worsening in the rms difference with –0.2 cm/s.

### 4. M1 Buoy vs. PPIN HF RADAR

Radial angles of the PPIN radar site and the mooring watch circle (red) are presented in Figure 16. A wide circle (expanded) view of the M1 buoy positions with respect to the PPIN HF radar grid points is shown in Figure 17. The mean position of the M1 buoy is located at the center between the two HF radar range arcs shown in the figure. The grid points on the shorter-range arc were used for the comparison due to the

fact that more than 63 % of the M1 locations were closer to that range arc. There is no angle difference between the ideal and measured grid data points as measured from the PPIN radar site.

Figure 18 shows the correlation coefficients and the rms differences between the HF radial data using the ideal and measured pattern data plotted against the radial component of the M1 buoy data. For the ideal pattern, the maximum value of the correlation coefficient, 0.63, is found at the angles of $131^o$, $136^o$, and $141^o$, and the minimum value of the rms difference, 14.0 cm/s, is found at $151^o$. In the measured pattern, the maximum value of the correlation coefficient, 0.62, is found at the angles of $121^o$ and $126^o$, and the minimum value of the rms difference, 14.5 cm/s, is found at $136^o$. The values of the maximum correlation coefficient and the minimum rms difference show a minor difference. However, the angles detecting the maximum correlation coefficient and the minimum rms difference in the ideal pattern data are shifted about 10° to 30° from the angle of the M1 buoy. Also, the angles detecting the maximum correlation coefficient and the minimum rms difference in the measured pattern data are shifted about $0^o$ to 15° from the angle of the M1 buoy.

The scatter plots of the ideal and data were graphed against the M1 buoy radial data (Figure 19). The ideal measured data at $121^o$ gives a slope of 0.91 and intercepts of -6.71 (884 observations). The measured data at $121^o$ gives a slope of 0.95 and an intercept of 6.47 (1076 observations). A comparison of the slopes of ideal and measured data shows that the measured data is more accurate than the ideal data.

## 5. Summary from HF Radar - M1 Mooring Buoy Comparison

Another recent investigation compared the HF radar radial current components with those at 3.2 m depth from a bottom-mounted ADCP yielding rms speed differences of 7 to 19 cm/s (Emery et al., 2003). In this study, the M1 buoy measuring depths were from 12 to 20 meters. Due to the difference of the measured depths between the previous investigation and this study, general statistical data shows relatively larger differences than other ADCP comparisons that were measured from a depth of about 1 to 10 meters.

According to the HF radar – M1 buoy comparisons, results using the measured patterns at all four radar sites showed improved statistical values compared with results

using the ideal patterns at the angle looking toward the M1 mooring, except for the NPGS rms difference as shown in Table 2. Summary comparisons of the PPIN data show a slight improvement from the ideal to the measured data in the direction of the M1 buoy. The NPGS correlation coefficient shows a large improvement from the ideal to the measured data in the direction of the M1 buoy.

Moss Landing has the lowest correlation coefficient and the lowest rms difference of all four sites. This may be explained by the dominant current pattern in the region around Monterey Bay. In general, the current moves back and forth, north to south in the directions approaching or receding from PPIN or SCRZ. This current flow will give a large radial velocity at those sites compared to the Moss landing site, which is relatively perpendicular to the current flow.

All radar sites exhibited angular offsets relative to the direction of the M1 mooring as inferred by the angle of maximum correlation or the angle of the minimum rms difference. Angle shifts of 10˚ to 30˚ were obtained using the ideal patterns. Angle shifts obtained using the measured antenna patterns were, in general, smaller but shifts of 5˚ to 15˚ still exist, even though the local antenna pattern distortion was taken into account through the use of measured antenna patterns.

| R/D site | | Corr. Coef | rms Diff (cm/s) | Residual rms (cm/s) | # of obs | Angle of R/D site | Angle Shift |
|---|---|---|---|---|---|---|---|
| **SCRZ** | | **0.5** | **18.9** | **16.9** | **1073** | **-78˚** | |
| | | 0.42 | 15.2 | 12.9 | 1122 | -58˚ | 10˚ |
| | **Ideal** | 0.62 | 18.4 | 15.7 | 1126 | -68˚ | 10˚ |
| | | **0.62** | **18.1** | **16.5** | **942** | **-80˚** | |
| | | 0.51 | 15.5 | 14.2 | 1124 | -70˚ | 10˚ |
| | **Measured** | 0.65 | 20.6 | 17.6 | 968 | -90˚ | 10˚ |
| | **Improvement** | 0.12 | 0.8 | 0.4 | | | |
| **MLNG** | | **0.14** | **15.5** | **13. 4** | **1041** | **200˚** | |
| | | 0.49 | 12.8 | 12.3 | 957 | 215˚ | 15˚ |
| | **Ideal** | 0.43 | 12.7 | 12.2 | 1001 | 210˚ | 10˚ |
| | | **0.34** | **12.4** | **11.3** | **973** | **200˚** | |
| | **Measured** | 0.44 | 13.0 | 12.2 | 860 | 205˚ | 5˚ |
| | **Improvement** | 0.2 | 2.9 | 2.1 | | | |
| **NPGS** | | **0.25** | **17.4** | **13.1** | **637** | **131˚** | |
| | | 0.57 | 16.0 | 15.0 | 808 | 161˚ | 30˚ |
| | **Ideal** | 0.45 | 14.6 | 13.5 | 836 | 146˚ | 15˚ |
| | | **0.57** | **17.6** | **16.6** | **822** | **130˚** | |
| | | 0.53 | 14.9 | 14.5 | 616 | 140˚ | 10˚ |
| | **Measured** | 0.59 | 15.8 | 14.7 | 837 | 135˚ | 5˚ |
| | **Improvement** | 0.32 | -0.2 | -3.5 | | | |
| **PPIN** | | **0.58** | **18.3** | **17.2** | **884** | **121˚** | |
| | | 0.58 | 14.0 | 13.2 | 1023 | 151˚ | 30˚ |
| | **Ideal** | 0.63 | 15.8 | 14.4 | 1018 | 141˚ | 20˚ |
| | | **0.62** | **16.6** | **15.5** | **1076** | **121˚** | |
| | **Measured** | 0.51 | 14.5 | 13.5 | 1007 | 136˚ | 15˚ |
| | **Improvement** | 0.04 | 1.7 | 1.7 | | | |

**Table 2. Summary of Comparison Statistics for HF Radar vs. M1 Mooring Radial Current Speed Pairs**

## B. BASELINE ANALYSIS

M1 buoy data comparisons show that the radial current data obtained using measured patterns have better statistical performance than those obtained using ideal patterns. However the direction-finding technique still had errors in the range of $5^o$ to $15^o$ using the measured patterns. In this section, a second technique is used to investigate radar performance by comparing observations from radar pairs along the baseline connecting the two radar locations. Through these baseline comparisons, the direction-finding performance can be measured to determine if errors are still implied for radar-to-radar comparisons, which, unlike the mooring observations, measure exactly the same vertical and horizontal scales.

Four radar baselines exist in the Monterey Bay HF radar network: SCRZ – MLNG, SCRZ – NPGS, SCRZ – PPIN, and MLNG – PPIN baseline. The direction-finding performance of the ideal antenna patterns and the measured patterns using the MUSIC algorithm can be evaluated by comparing of the radial speed provided by two different sites along any baseline. Theoretically, the radial speed at the same grid point on the baseline would have the same magnitude but the opposite sign. As an example, one site would indicate that the given current was receding (negative sign), while the opposite site of the baseline should indicate that the current was approaching (positive sign).

Figure 20 illustrates a baseline overlaid between the SCRZ radar site and the MLNG radar site along with the relative positions and radial grid points from each radar site. The grid points of the SCRZ, NPGS, and PPIN sites were configured with 3 km increments in range and 5° increments in azimuth (angle), whereas the grid points of the MLNG site were configured with 1.5 km increments in range and 5° increments in azimuth. The center grid point pairings on the baselines between radar sites are shown on the figures below that accompany the descriptions of the four different baseline comparisons. These pairings were expected to provide the best agreement between radial currents measured at the individual radar sites.

Once the best grid point pairing were established, analyses were conducted by holding one grid point of the best grid point pairing constant and comparing radial values from that site to radial values from all angles at the same range from the opposite site. For instance, along the SCRZ-PPIN baseline, data from one 18 Km radial bin of the best grid point pairing emanating from SCRZ were compared with data from several 18 Km radial bins emanating from PPIN. Once the individual radial current data sets were selected, the same statistical methods were used to document the baseline comparisons, as were used with the M1 buoy data comparisons described above.

### 1. Santa Cruz-Moss Landing Baseline

Figure 20 illustrates a baseline overlaid between the SCRZ radar site and the MLNG radar site. The baseline angle to SCRZ (MLNG) site from MLNG (SCRZ) is 147º (-33$^{o}$). For the comparison of data from the best grid point bin of SCRZ and the MLNG measured radial bins, the expected highest correlated and the lowest rms

difference pairing would be the best grid point pairing of 145º/15 km from MLNG. The upper panel of Figure 21 illustrates the result, namely that the grid point of 160º has the highest correlation and the lowest rms difference, although the slow change of correlation and rms difference from 150º to 180º makes it difficult to choose the best angle for the comparisons in this case. Nonetheless, a 15º discrepancy existed from the MLNG site.

Looking from the opposite direction, the comparison of the best grid point bin of MLNG with several SCRZ measured radial bins is expected to have the highest correlated and lowest rms difference at the best grid point pairing of -35º/15 km from SCRZ. The lower panel of Figure 21 graphically illustrates that the expected best grid point pairing does not have the highest correlation or the lowest rms difference. SCRZ radial bin of the best pairing has the highest correlation and the lowest rms difference at –25º as indicated by the relatively sharp curves on the figure. Thus a clear 10º pointing discrepancy existed as seen from the SCRZ site.

The scatter plots of the ideal and measured radial baseline data are presented in Figure 22. The ideal data at -33º from the SCRZ radar site and 145º from the MLNG radar site gives a slope of 0.75 and intercept of –1.3 (718 observations). The measured data at -35º from the SCRZ radar site and 145º from the MLNG radar site gives a slope of 0.63 and an intercept of –3.8 (720 observations). A comparison of the ideal and measured scatter plots shows the surprising result that the ideal data is slightly more accurate than the measured data, which is not expected.

**2. Santa Cruz-NPGS Baseline**

Figure 23 illustrates a baseline overlaid between the SCRZ radar site and the NPGS radar site, and further shows the baseline angle to SCRZ (NPGS) site from NPGS (SCRZ) is 114º (-66º). For the comparison of the best grid point bin of SCRZ and the NPGS measured radial bins, the expected highest correlated and the lowest rms difference pairing would be the best grid point pairing of 115º/21 km from NPGS. The upper panel of Figure 24 illustrates the result that, instead, the 110º grid point has the highest correlation and the lowest rms difference. In this case, the observed best pairing at 110º is indicated by a relatively sharp drop of rms difference, as is seen in the figure. Thus, a 5º pointing discrepancy existed from the NPGS site.

For the comparison of the expected best grid point bin of NPGS and the SCRZ measured radial bins, the highest correlated and the lowest rms difference pairing would be expected to be found at the best grid point pairing of -65º/21 km from SCRZ. The lower panel of Figure 24 graphically illustrates the result that the best grid point pairing does not have the highest correlation or the lowest rms difference. Instead, the SCRZ radial bin has the highest correlation and the lowest rms difference at –70º as indicated by the relatively sharp curves in the figure. Thus, a 5º pointing discrepancy existed from the SCRZ site.

The scatter plots of the ideal and measured radial baseline data are presented in Figure (25). The ideal data at -68º from the SCRZ radar site and 116º from the NPGS radar site gives a slope of 0.28 and an intercept of –5.5 (409 observations). The measured data at -65º from the SCRZ radar site and 115º from the NPGS radar site gives a slope of 0.98 and an intercept of 3.1 (778 observations). A comparison of the scatter plots of the ideal and the measured data shows that the measured data is more accurate than the ideal data as expected.

**3. Santa Cruz-Point Pinos Baseline**

Figure 26 illustrates a baseline overlaid between the SCRZ radar site and the PPIN radar site and the baseline angle to SCRZ (PPIN) site from PPIN (SCRZ) is 109º (-71º). For the comparison of the best grid point bin of SCRZ and the PPIN measured radial bins, the expected highest correlated and the lowest rms difference pairing would be the best grid point pairing of 106º/18 km from PPIN. The upper panel of Figure 27 illustrates the result that the grid point at 111º has the highest correlation and the lowest rms difference as exhibited by the relatively sharp extrema in the figure. Thus, a 5º pointing discrepancy existed from the perspective of the PPIN site.

For the comparison of the best grid point bin of PPIN and the SCRZ measured radial bins, the highest correlated and the lowest rms difference pairing would be expected to be found at the best grid point pairing of -70º/18 km from SCRZ. The lower panel of Figure 27 illustrates the result that the grid point at -70º does, indeed, exhibit the highest correlation and lowest rms difference as expected with relatively sharp extrema at that angle providing confidence in the result. Therefore, there is no angular shift as viewed from the PPIN site.

The scatter plots of the ideal and measured baseline data are shown in Figure 28. The ideal data at -73$^{o}$ from the SCRZ radar site and 106$^{o}$ from the PPIN radar site gives a slope of 0.69 and an intercept of 9.7 (696 observations). The measured data at -70$^{o}$ from the SCRZ radar site and 106$^{o}$ from the PPIN radar site gives a slope of 0.8 and an intercept of 3.61 (791 observations). A comparison of the scatter plots of the ideal and the measured data shows that the measured data is more accurate than the ideal data, as expected.

**4. Moss Landing-Point Pinos Baseline**

Figure 29 illustrates the final baseline pairing between the MLNG radar site and the PPIN radar site. The baseline angle to MLNG (PPIN) site from PPIN (MLNG) is 55º (235$^{o}$). For the comparison of the best grid point bin of MLNG and the PPIN measured radial bins, the expected highest correlated and the lowest rms difference pairing would be the best grid point pairing of 56º/12 km from PPIN. The upper panel of Figure 30 illustrates the result that the grid point at 56º does, indeed, have the highest correlation and the lowest rms difference. However, the slow change of correlation and the rms difference from 46º to 66º makes it difficult to unambiguously choose the best fitted angle. The results support the conclusion that there is no angular shift viewed from the PPIN site.

For the comparison of the best grid point bin of PPIN and the MLNG measured radial bins, the highest correlated and the lowest rms difference pairing would be expected to be found at the best grid point pairing of 235º/10.5 km from the MLNG site. The lower panel of Figure 30 graphically illustrates these results that the best grid point pairing does not have the highest correlation or the lowest rms difference. The MLNG radial bin of the best pairing has the highest correlation and the lowest rms difference at 230º as indicated in the figure. Thus a 5º pointing discrepancy exists as viewed from the MLNG site.

The scatter plots of the ideal and measured baseline data are shown in Figure 31. The ideal data at 235$^{o}$ from the MLNG radar site and 56$^{o}$ from the PPIN radar site gives a slope of 0.56 and an intercept of 1.1 (503 observations). The measured data at 235$^{o}$ from the MLNG radar site and 56$^{o}$ from the PPIN radar site gives a slope of 0.66

and an intercept of 1.1 (790 observations). A comparison of the scatter plots of the ideal and the measured data shows that the measured data is more accurate than the ideal data as expected.

### 5. Summary from Baseline Comparison

According to the baseline comparisons, radial current data computed using the measured antenna patterns show improved statistical values compared with results based on the ideal antenna patterns. There is one exception for the SCRZ-MLNG baseline for which the results are similar, as shown in Table 3. Relatively large improvement is seen for the SCRZ-NPGS baseline when measured antenna patterns are used.

| Baseline | | Corr. Coef | rms Diff (cm/s) | Residual rms (cm/s) | Slope | Intercept | # of obs |
|---|---|---|---|---|---|---|---|
| **SCRZ - MLNG** | **Ideal** | 0.63 | 11.2 | 10.8 | 0.75 | -1.3 | 718 |
| | **Measured** | 0.6 | 12.9 | 11.6 | 0.63 | -3.8 | 720 |
| | **Improvement** | **-0.03** | **-1.7** | **-0.8** | | | |
| **SCRZ - NPGS** | **Ideal** | 0.44 | 28.5 | 11.2 | 0.28 | -5.5 | 409 |
| | **Measured** | 0.79 | 11.8 | 11.4 | 0.98 | 3.1 | 778 |
| | **Improvement** | **0.35** | **16.7** | **-0.2** | | | |
| **SCRZ - PPIN** | **Ideal** | 0.66 | 17.3 | 14.8 | 0.69 | 9.7 | 696 |
| | **Measured** | 0.83 | 10.6 | 9.9 | 0.8 | 3.61 | 791 |
| | **Improvement** | **0.17** | **6.7** | **4.9** | | | |
| **MLNG - PPIN** | **Ideal** | 0.57 | 13.3 | 10.8 | 0.56 | 3.8 | 503 |
| | **Measured** | 0.71 | 9.8 | 8.5 | 0.66 | 1.1 | 790 |
| | **Improvement** | **0.14** | **3.5** | **2.3** | | | |

**Table 3. Summary of Statistical Improvement from Ideal to Measured Pattern Data for HF Radar vs. HF Radar Baseline Radial Current Speed Pairs**

Also, the results of this comparison shows that for the angle looking toward the opposite site, the statistical values of the measured patterns yielded rms differences of 9.3 to 12.9 cm/s and correlation coefficients in the range 0.60 – 0.85. But 0˚ to 15˚ angular shifts for radial currents still exist with the use of measured antenna patterns as shown in Table 4.

| Baseline | | Corr. Coef | rms Diff (cm/s) | Residual rms (cm/s) | # of obs | Angle of R/D site | Angle Shift |
|---|---|---|---|---|---|---|---|
| SCRZ - MLNG | SCRZ side | **0.6** | **12.9** | **10.9** | **720** | **-35˚** | |
| | | 0.71 | 10.1 | 8.2 | 679 | -25˚ | 10˚ |
| | MLNG side | **0.6** | **12.9** | **11.8** | **720** | **145˚** | |
| | | 0.72 | 11.1 | 10.0 | 812 | 160˚ | 15˚ |
| SCRZ - NPGS | SCRZ side | **0.79** | **11.8** | **9.2** | **778** | **-65˚** | |
| | | 0.86 | 10.1 | 9.3 | 781 | -70˚ | 5˚ |
| | NPGS side | **0.79** | **11.8** | **12.7** | **778** | **115˚** | |
| | | 0.79 | 10.0 | 9.3 | 782 | 110˚ | 5˚ |
| SCRZ - PPIN | SCRZ side | **0.83** | **10.6** | **9.9** | **791** | **-70˚** | 0˚ |
| | PPIN side | **0.83** | **10.6** | **10.3** | **791** | **106˚** | |
| | | 0.85 | 10.1 | 9.6 | 984 | 111˚ | 5˚ |
| MLNG - PPIN | MLNG side | **0.71** | **9.8** | **9.2** | **790** | **235˚** | |
| | | 0.74 | 9.3 | 8.8 | 832 | 230˚ | 5˚ |
| | PPIN side | **0.71** | **9.8** | **9.9** | **790** | **56˚** | 0˚ |

**Table 4. Summary of Comparison Statistics for HF Radar vs. HF Radar Baseline Radial Current Speed Pairs**

There is no angular shift at the SCRZ radar site of the SCRZ – PPIN pair and at the PPIN radar site of the MLNG – PPIN pair with a correlation coefficient of 0.83 and 0.71, respectively. But for the comparison of the other sites, the angular shifts are between $5^o$ to 15˚.

In the comparison of the SCRZ – MLNG, SCRZ – NPGS, and SCRZ – PPIN baseline pairs, the angular shift of the SCRZ radar site is 10˚ to the MLNG radar site, 5˚ to the NPGS radar site, and a $0^o$ angular shift to the PPIN radar site. In the comparison of SCRZ – MLNG and MLNG – PPIN baseline pairs, the angular shift of the MLNG radar site is 15˚ to the SCRZ radar site and 5˚ to the PPIN radar site. There is no angular shift of the PPIN radar site to the SCRZ and MLNG radar sites. This angular shift of $0^o$ to $15^o$ in the baseline comparisons of the measured patterns is similar to the measured angular shift of the M1 buoy at 5-$15^o$. However, the angular shift of one radar site to another site is not constant. For example, there is no angular shift measured from SCRZ to PPIN, but there is a $5^o$ angular shift from SCRZ to NPGS, and a $10^o$ shift from SCRZ to MLNG.

## C. COMPARISON WITH DRIFTERS

Through use of the radial surface currents from the drifters it may be possible to see the statistical variations of the observed-to-radar comparisons as a function of angle from individual radar sites. Also, the performance change moving from the ideal to measured antenna patterns can be seen through these comparisons.

Radial surface current data from ideal and measured patterns from each radar site were compared with data from sixteen drifters deployed from 11 August to 5 September 2003. To create the paired data set, radial currents were selected from the HF radar grid point closest to the drifters' location at each drifter observation time. Individual pairs with more than two km distance between the radar and drifter data or more than 3˚ angular difference between two data points were removed to reduce spatial error. To compare radials from HF radar with current measurements from the drifters, the radial components of the drifter-derived velocities were computed in the direction of the various HF radar sites. After that, the same methods used to calculate the statistical comparisons with data from the M1 buoy radial velocities were applied to the paired HF radar-drifter radial current data. Both ideal and measured pattern data were compared over all locations. One important distinction in the computations involving the drifter-derived radial currents is that the radar-to-drifter comparison data were binned by angle as shown below since the drifter data covered a large range of angles unlike the case for the fixed location of the M1 buoy or the finite number of available baseline comparisons.

### 1. Drifter vs. SCRZ HF RADAR

The individual drifter positions, HF radar radial grid points, and the angles seen from the SCRZ site are illustrated in Figure 32. In total, 931 observations were used for the comparison. In addition, angles between -28˚ and -83˚ from east contained enough radial current pairs to investigate the statistical variation with angle and to assess the impact of using measured versus ideal antenna patterns.

Figure 33 shows the rms difference and correlation coefficients between radar-derived and drifter-derived radial currents as a function of angle. Results are shown for data produced using both ideal and measured antenna patterns. As shown below, there is some improvement obtained in the total radar-to-drifter comparison by using measured antenna patterns. However, the effect is not constant over the angles observed. There is

no significant or negative effect of measured patterns at angles from -38˚ to -28˚. The particular angle pointing toward the MLNG radar site shows a small negative improvement. This result is also supported by the SCRZ – MLNG baseline comparison, which showed negative improvement for this case.

In the angle range between –63$^{o}$ to –88$^{o}$, which include the angles to the M1 buoy, the PPIN radar site, and the NPGS radar site, there is significant improvement in the rms difference when measured antenna patterns are used. The correlation coefficients results in this angle range are variable. These results are consistent with the M1 buoy comparisons and the SCRZ – NPGS and the SCRZ – PPIN baseline comparisons.

The scatter plots of the HF radar ideal and measured radial data versus drifter radial data from the SCRZ radar site are graphed in Figure 34. The ideal data gives a slope of 0.48 and an intercept of 0.16 (931 observations). The measured data gives a slope of 0.64 and an intercept of 0.81. A comparison of the slopes of the ideal and the measured data shows that the measured data is more accurate than the ideal data with an improvement of 4.2 cm/s rms difference and a 0.09 correlation coefficient.

**2. Drifter vs. MLNG HF RADAR**

The individual drifter positions, HF radar radial grid points, and the angles seen from the MLNG site are illustrated in Figure 35. In total, 987 observations were used for the comparison. In addition, angles between 130˚ and 245˚ from east contained enough radial current pairs to investigate the statistical variation with angle.

Figure 36 shows the rms difference and correlation coefficients between radar-derived and drifter-derived radial currents as a function of angle. Positive improvement for the data produced using measured antenna patterns is shown only at some angles from 180˚ to 195˚. The angle toward the SCRZ radar site, 147$^{o}$, shows a negative improvement in terms of both the rms difference and the correlation coefficient. This result is also supported by the SCRZ – MLNG baseline comparison, which showed a small negative improvement when measured patterns were used. The angle toward the PPIN radar site, 235$^{o}$, shows a positive improvement in the rms difference with no change in the correlation coefficient.

The scatter plots of the HF radar ideal and measured radial data versus drifter radial data from the MLNG radar site are graphed in Figure 37. The ideal data gives a slope of 0.71 and an intercept of 0.39 (987 observations). The measured data gives a slope of 0.7 and an intercept of 0.5. A comparison of the scatter plots show that the measured data is less accurate than the ideal data with small negative improvements of –0.04 cm/s rms difference and a -0.02 correlation coefficient.

### 3. Drifter vs. NPGS HF RADAR

The individual drifter positions, HF radar radial grid points, and the angles seen from the NPGS site are illustrated in Figure 38. In total, 547 observations were used for the comparison. In addition, angles between 91˚ and 141˚ from east contained enough radial current pairs to investigate the statistical variation with angle.

Figure 39 illustrates the change of the rms difference and the correlation coefficient as a function of angle. Positive improvement for the data produced using measured antenna patterns is shown for all angles. This is the expected result of the direction-finding process using measured antenna patterns and the MUSIC algorithm.

The scatter plots of the HF radar ideal and measured radial data versus drifter radial data from the NPGS radar site are graphed in Figure 40. The ideal data gives a slope of 0.56 and an intercept of –9.03 (547 observations). The measured data gives a slope of 0.67 and an intercept of –1.97. A comparison of the scatter plots show that the measured data is more accurate than the ideal data with the significant improvements of 7.0 cm/s rms difference and a 0.29 correlation coefficient.

### 4. Drifter vs. PPIN HF RADAR

The individual drifter position, HF radar radial grid points and the angles seen from the PPIN site are illustrated in Figure 41. In total, 610 observations were used for the comparison. In addition, angles between 61˚ and 116˚ from east contained enough radial current pairs to investigate the statistical variation with angle.

Figure 42 illustrates the change of the rms difference and the correlation coefficient as a function of angle. Positive improvement for the data produced using measured antenna patterns is shown for nearly all the angles with small differences between the results for ideal data and measured data. This result suggests that the

measured pattern of the PPIN radar site is not distorted as much as, for example, the NPGS radar site. Thus the change of statistical values is relatively lower than the NPGS site.

The scatter plots of the HF radar ideal and measured radial data versus the drifter radial data from the PPIN radar site are graphed in Figure 43. The ideal data gives a slope of 0.72 and an intercept of 1.35 (610 observations). The measured data gives a slope of 0.8 and an intercept of 0.15. A comparison of the scatter plots show that the measured data is more accurate than the ideal data with the relatively small improvements of 1.4 cm/s rms difference and a 0.03 correlation coefficient.

### 5. Summary from Drifter Comparison

The drifter measurement depths were, approximately, eight meters while the HF radar measurement depth is from the surface to, approximately, one meter. In keeping with the differences of the measurement depths, the statistical data show relatively better comparisons than with the M1 buoy and lower values when compared to the baseline data.

According to the HF radar – drifter comparisons, data computed using the measured antenna patterns exhibit improved statistical values compared with data computed using the ideal antenna patterns in all cases, except at the MLNG radar site, as shown in Table 5. Summary comparisons of the PPIN data show a very small improvement from the ideal data to the measured data. The NPGS rms differences and the correlation coefficients show a large improvement from the ideal data to the measured data suggesting that highly distorted antenna patterns at the NPGS radar site have been significantly compensated for through the use of measured antenna patterns.

| R/D site | | Corr. coef | rms Diff (cm/s) | Residual rms (cm/s) | Slope | Intercept | # of obs |
|---|---|---|---|---|---|---|---|
| **SCRZ** | **Ideal** | **0.65** | **16.9** | **18. 7** | **0.48** | **0.16** | |
| | **Measured** | **0.74** | **12.7** | **13.1** | **0.64** | **0.81** | 931 |
| | **Improvement** | 0.09 | 4.2 | 5.6 | | | |
| **MLNG** | **Ideal** | **0.74** | **9.66** | **9.3** | **0.71** | **0.39** | |
| | **Measured** | **0.72** | **10.0** | **9.6** | **0.7** | **0.5** | 987 |
| | **Improvement** | -0.02 | -0.04 | -0.3 | | | |
| **NPGS** | **Ideal** | **0.48** | **17.4** | **20.0** | **0.56** | **-9.03** | |
| | **Measured** | **0.79** | **10.4** | **11.0** | **0.67** | **-1.97** | 547 |
| | **Improvement** | 0.29 | 7.0 | 9.0 | | | |
| **PPIN** | **Ideal** | **0.74** | **11.8** | **12.0** | **0.72** | **1.35** | |
| | **Measured** | **0.77** | **10.4** | **9.7** | **0.8** | **0.15** | 610 |
| | **Improvement** | 0.03 | 1.4 | 2.3 | | | |

**Table 5. Summary of Comparison Statistics for HF Radar vs. Drifter Radial Current Speed Pairs**

From the NPGS radar site at angles of 91°-141°, the correlation coefficients and the rms differences maintain high values, which are not scattered. Except for the 126° angle, all other angles show a marked improvement from the ideal to measured patterns. From the PPIN radar site, the correlation coefficients and the rms differences maintain high values, which are also not scattered. Also, there is statistical improvement in the ideal to measured patterns. However, the PPIN improvement is smaller than the NPGS improvement.

The SCRZ and MLNG drifter comparisons show some marked improvement through some angle ranges while other angle ranges did not improve or showed negative improvement. There is an angular shift in the M1 buoy comparison and baseline comparison in the angle ranges that show negative improvement compared with the drifter observations. At the MLNG radar site the total angular range is from 130° to 245°, but improvements in the rms differences and correlation coefficients can only be seen for angles 165° to 195°. As a result, the composite statistical comparisons using the measured pattern are worse than those for the ideal pattern for the MLNG radar site.

# IV. DISCUSSION

## A. POINTING ERRORS IN THE MUSIC ALGORITHM

Through various comparisons in this study, it was shown that the use of measured antenna patterns provides better direction finding than using the ideal antenna patterns. Thus, it is recommended to use the measured antenna patterns for current mapping when using CODAR SeaSonde HF radar. However, pointing errors still exist when using the measured patterns and, in some cases, little improvement or slightly worse performance than the results using ideal antenna patters were observed.

The CODAR SeaSonde systems use the MUSIC algorithm for direction finding, which requires accurate receive antenna patterns. Errors in the antenna patterns translate into pointing errors of the ocean current mapping. There are two issues that may cause pointing errors in the field operations of the MUSIC algorithm that are discussed here: 1) Smoothing of measured antenna pattern and 2) Signal ratios of two loop antennae.

### 1. Smoothing of Measured Antenna Pattern

Actual antenna patterns measured by the transponder may not be good to use directly in the MUSIC algorithm for a heavily distorted pattern. Figure 44 shows the raw, measured antenna patterns (a) at MLNG radar site, $5^{o}$ smoothed line (b), $10^{o}$ smoothed line (c), and $20^{o}$ smoothed line (d). Given the limited number of degrees of freedom represented by the three SeaSonde receive antenna elements, the MUSIC algorithm cannot be expected to account for all of the small-scale variability in the observed antenna patterns. Hence, some angular smoothing is requested but the optimal amount of smoothing is not known.

Figure 45 shows the raw, measured antenna patterns at the SCRZ site (a), MLNG site (b), NPGS site (c), and PPIN site (d). The noisiest antenna pattern is shown at the MLNG radar site broadcasting 24.6 MHz signals that is about twice the frequency of the others.

### 2. Signal Ratio between Two Loop Antennae

At the most basic level, the direction finding system uses the arctangent of signal ratio between the two crossed-loop antennas normalized by the monopole antenna. to

determine the direction of the target. Figure 46 shows the ideal antenna pattern and its signal ratio. It is quite clear how to determine the bearing with the signal ratio of the ideal pattern because there is only one point of bearing for a certain signal ratio. If there is the same signal ratio of the receive antenna at two or more bearings due to the distorted antenna pattern, it is not simple to distinguish which is which, even though the distorted antenna pattern was taken into account in the algorithm. In the case of the more sophisticated MUSIC algorithm, which applies a statistical, eigenfunction approach to the direction finding, it is possible to tolerate some additional ambiguity in the signal ratios, but the multi-valued nature of the observed signal ratios still provides a good indication of when to expect increased numbers of pointing errors. Figures 47 to 50 illustrate the measured antenna patterns and signal ratios of the four radar sites in Monterey Bay. These figures show that the same signal ratio of the receive antenna could be found at several angles except for the NPGS measured antenna pattern.

## B. SUMMARY

High-Frequency (HF) radars have been developed mainly to measure surface currents since the first identification of the Doppler spectrum of sea echo by Crombie (1955). There are two types of HF radar systems in use, which differ mainly in the direction finding: a beam forming system used in OSCR and WERA, and a direction finding system used in the CODAR SeaSonde.

The CODAR SeaSonde using the MUSIC algorithm for direction finding can use either ideal or measured antenna patterns. The measured patterns of the receive antenna can be measured by small battery-operated transponders and the system accuracy of CODAR SeaSonde is dependent on the distortion of the measured pattern.

In this study, the performance of a network of four CODAR (Coastal Ocean Dynamics Application Radar) SeaSonde HF radars deployed around Monterey Bay, CA, was described for the period between July to September 2003. Comparisons were made in Monterey Bay with moored velocity observations, with four radar baseline pairs, and with velocity observations from sixteen drifter deployments. Statistical values, such as the correlation coefficient, rms difference, residual rms difference, slope, and intercept, were used for this study.

All systems measured ocean surface current and all vector currents are translated into radial current components in the direction of the various radar sites. Measurement depths were ~1 m deep for the HF radar-derived currents, 12 to 20 m for the ADCP bin nearest to the surface at the M1 mooring site, and ~8 m for the drifter-derived velocity estimates. In relation to the difference of the measured depths, general statistical data comparisons showed relatively high correlations using the baseline data and lower correlations with the M1 buoy data.

First, the HF radar – M1 buoy comparisons of radial current components yielded improvements of -0.2 to 2.9 cm/s rms differences and 0.04 to 0.32 correlation coefficients between radar data using ideal and measured antenna patterns. In the measured pattern case, the maximum value of the correlation coefficient, 0.62, was found at the SCRZ and the PPIN radar site and the minimum value of the correlation coefficient, 0.34, was found at the MLNG radar site. The PPIN data showed a very small improvement from the ideal to the measured data, but the NPGS correlation coefficient showed a large improvement from the ideal to the measured data. Also, these comparisons indicated angular shifts of 10˚ to 30˚ for radial currents produced using ideal antenna patterns. Angular shifts of 5˚ to 15˚ for radial currents still existed even though the local antenna pattern distortion was taken into account by using measured antenna patterns.

Second, the baseline comparisons of radial current components yield improvements of -1.7 to 16.7 cm/s rms differences and -0.03 to 0.35 correlation coefficients between radar data using ideal and measured antenna patterns. In the measured pattern, the maximum value of the correlation coefficient, 0.83, was found at the SCRZ - PPIN baseline and the minimum value of the correlation coefficient, 0.60, was found at the SCRZ - MLNG baseline. The SCRZ – NPGS baseline data showed a large improvement in statistical values from the ideal to the measured data, but a small negative improvement was seen at the SCRZ – MLNG baseline. Also, these comparisons indicated angular shifts of 0˚ to 15˚ for radial currents produced using measured antenna patterns, similar to the measured angular shift based on comparisons with the M1 buoy of 5-15$^{o}$. Particularly, the angular shift of one radar site to another sites was not constant. For instance, there was no angular shift measured from SCRZ to PPIN, but there was a 5$^{o}$

angular shift from SCRZ to NPGS, and a $10^o$ shift from SCRZ to MLNG. Furthermore, the HF radar system accuracies were evaluated through these baseline analyses using the same HF radar system.

Lastly, comparisons of radial current components with drifters yielded improvements of -0.04 to 7.00 cm/s rms differences and -0.02 to 0.29 correlation coefficients between radar data using ideal and measured antenna patterns. The PPIN data showed a very small improvement, the NPGS data a large improvement, and the MLNG data a small worsening from the ideal to the measured pattern. In the measured pattern, the maximum value of the correlation coefficient, 0.79, was found at the NPGS radar site and the minimum value of the correlation coefficient, 0.72, was found at the MLNG radar site.

Due to the scattered distribution of the sixteen drifters across Monterey Bay, it was possible to see the statistical values and their variation at several angles from one radar site. The drifter comparisons at the SCRZ and the MLNG radar site showed some marked improvement through some angle ranges while other angle ranges did not or showed negative improvement. In particular the angle of $-33^o$ ($147^o$) toward the MLNG (SCRZ) radar site from the SCRZ (MLNG) radar site showed negative improvement of statistical values, which was already shown in the SCRZ – MLNG baseline comparison. At the MLNG radar site, the smaller distribution of drifters within the positive improvement angular range was less than the negative improvement range, resulting in overall statistical correlations of the measured pattern, which were slightly worse than the ideal pattern values. The correlation coefficients and the rms differences of the NPGS and the PPIN radar site maintained positive improvements and high values within most of the angular range. However, the PPIN improvement was small while the NPGS improvement was significant. Through the comparisons of the drifters with the HF radar data, it is clear that the pointing errors vary with angle. The drifter comparisons, in particular, provided an important, new look at the performance of the MUSIC algorithm with respect to the three-element receive antenna configuration of the SeaSonde. It is highly recommended that additional drifter experiments, particularly with shallower, 1-m instruments, be conducted to better elucidate the relationship of pointing errors as a function of angle and the observed angular antenna patterns.

Finally, it is highly recommended that simulation experiments be conducted in which known current patterns and known antenna distortions are used with the MUSIC algorithm in order to develop spatial error models based on the shape of the observed antenna patterns. Furthermore, it is possible that some coastal locations are not acceptable SeaSonde HF radar sites due to the level and nature of the antenna pattern distortions at the site. Follow-on studies to this one with drifters and with simulation experiments should aim to describe these "unacceptable" antenna pattern distortions as a guide to further expansion of coastal ocean monitoring networks using HF radar instruments.

THIS PAGE INTENTIONALLY LEFT BLANK

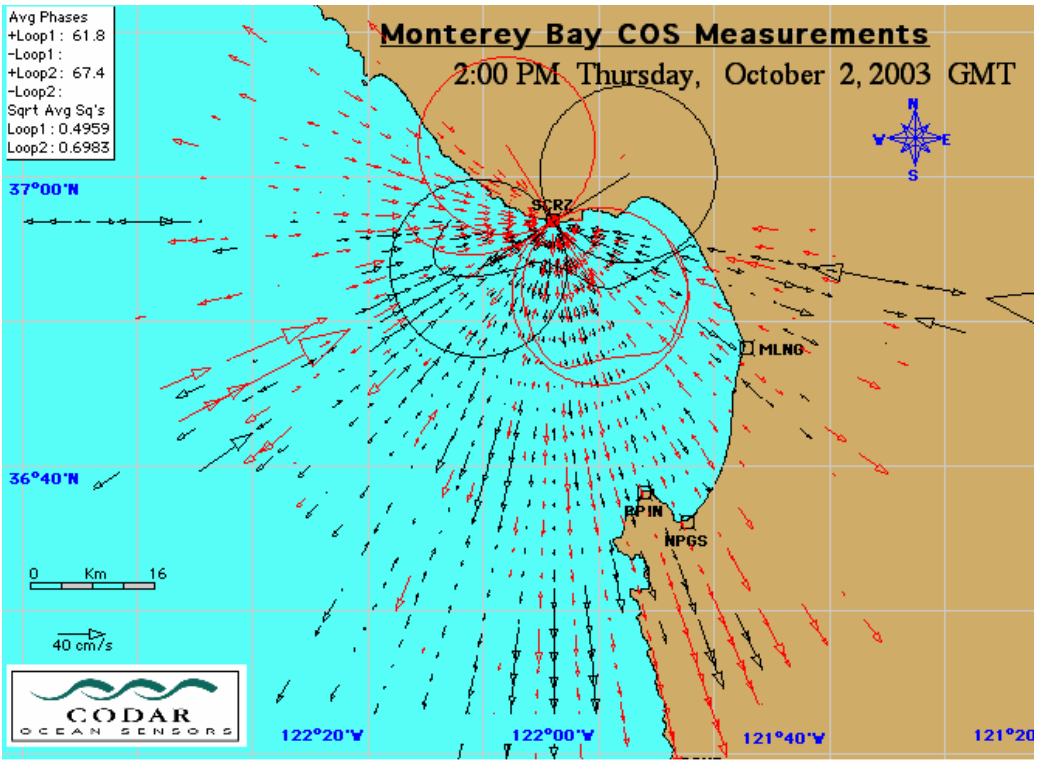


Figure 1. An Example of the Radial Current Vectors for the SCRZ Radar Site based on the Ideal (Black) and Measured (Red) Antenna Patterns.

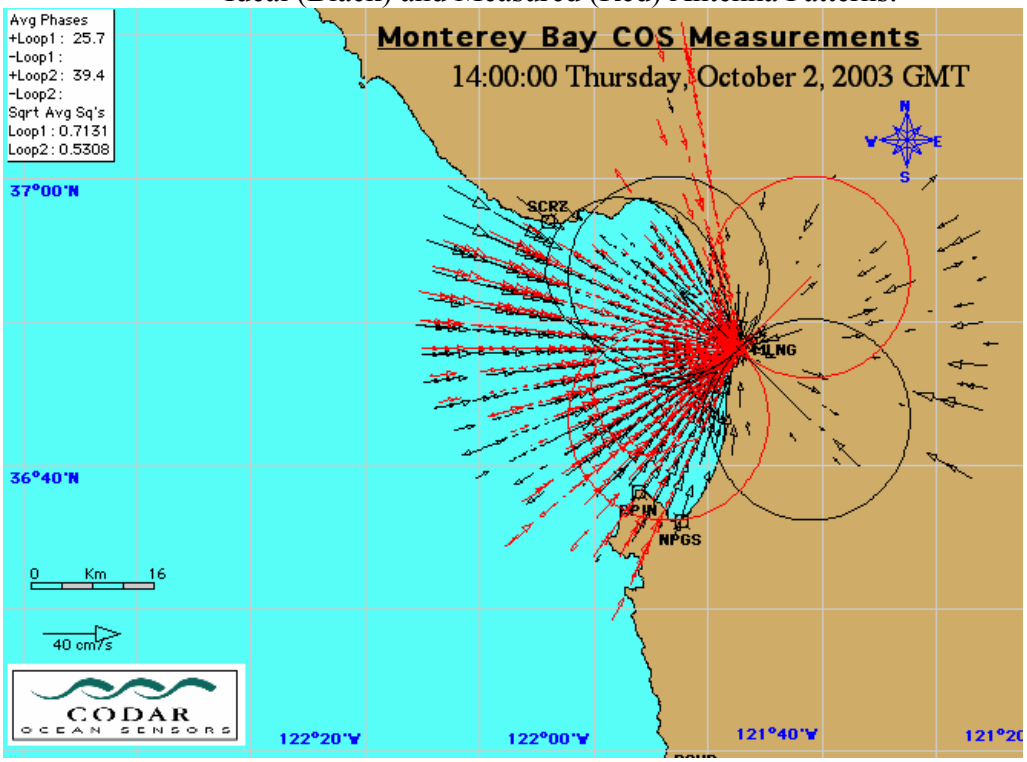


Figure 2. An Example of the Radial Current Vectors for the MLNG Radar Site based on the Ideal (Black) and Measured (Red) Antenna Patterns.

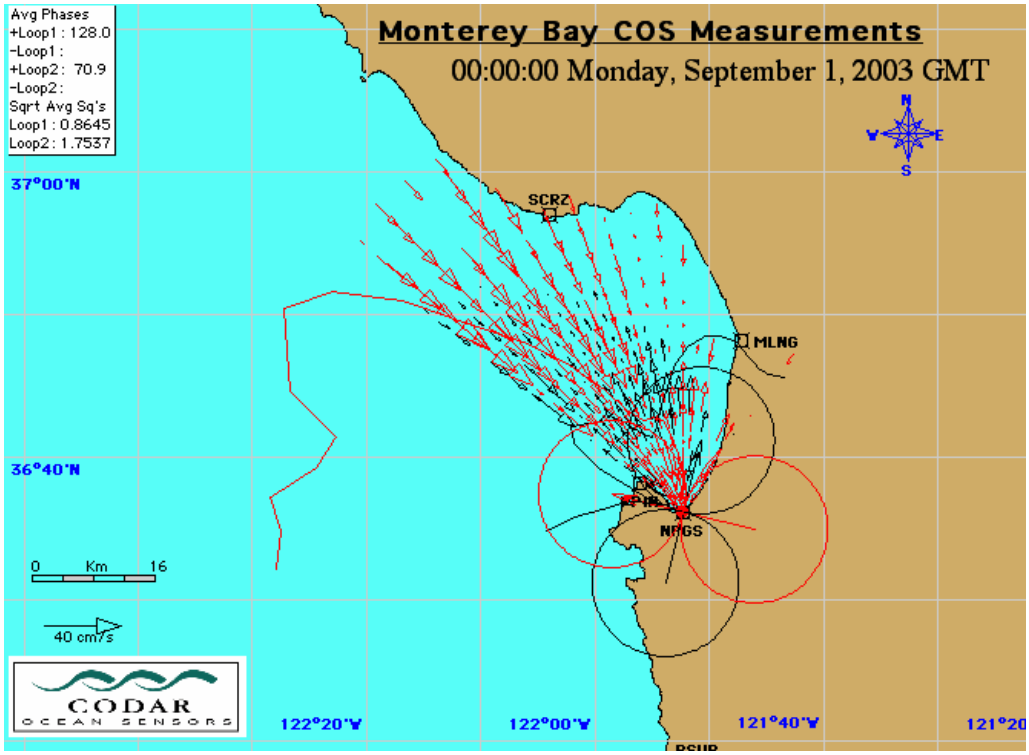


Figure 3. An Example of the Radial Current Vectors for the NPGS Radar Site based on the Ideal (Black) and Measured (Red) Antenna Patterns.

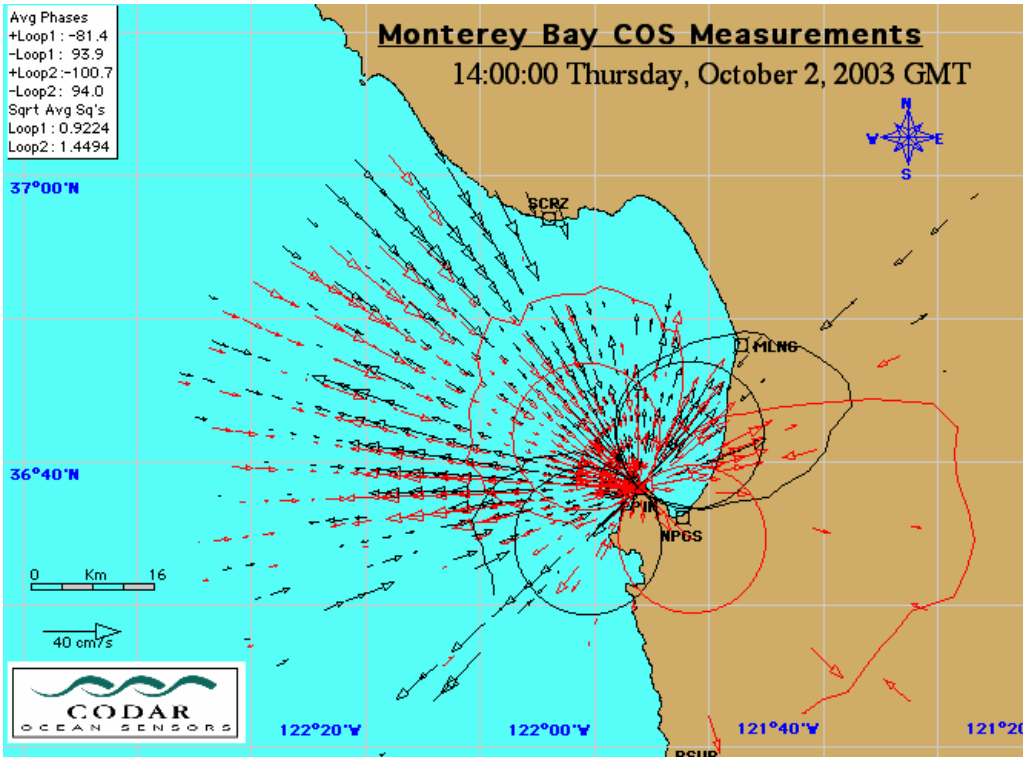


Figure 4. An Example of the Radial Current Vectors for the PPIN Radar Site based on the Ideal (Black) and Measured (Red) Antenna Patterns.

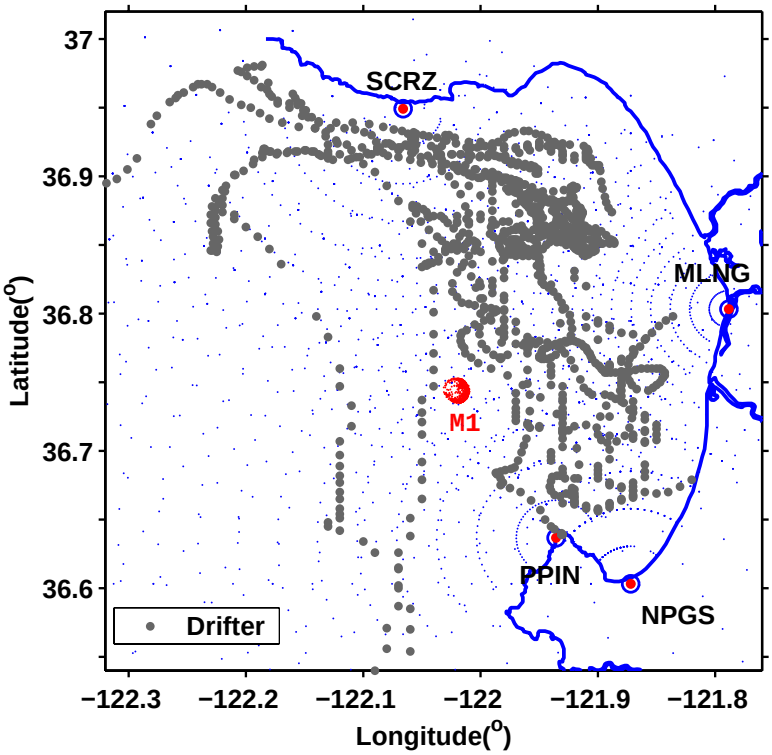


Figure 5. Locations of the Four HF Radar Sites, M1 Buoy and Drifters.

Figure 6. Drifter with Its Drogue Shortly After Deployment.

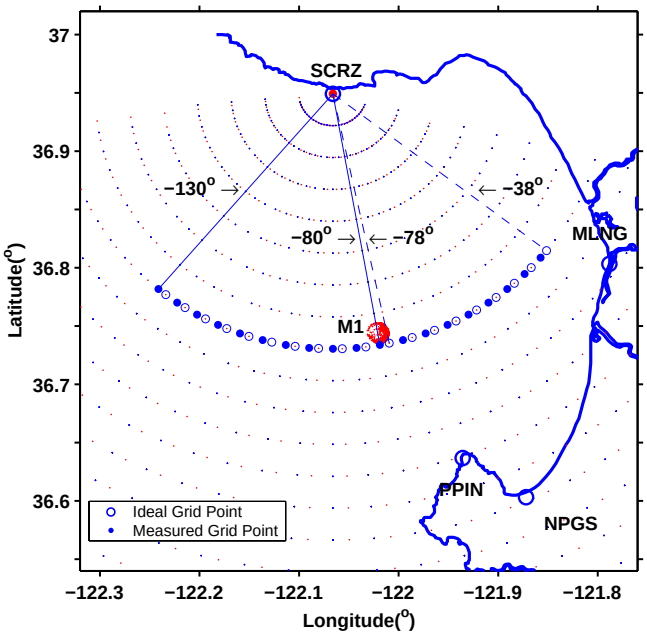


Figure 7. M1 Buoy and SCRZ Radial Grid Points. $-78^{o}$ indicates the Closest Grid Point of Ideal Data to the M1 Buoy and $-80^{o}$ the Closest Grid Point of Measured Data to the Buoy.

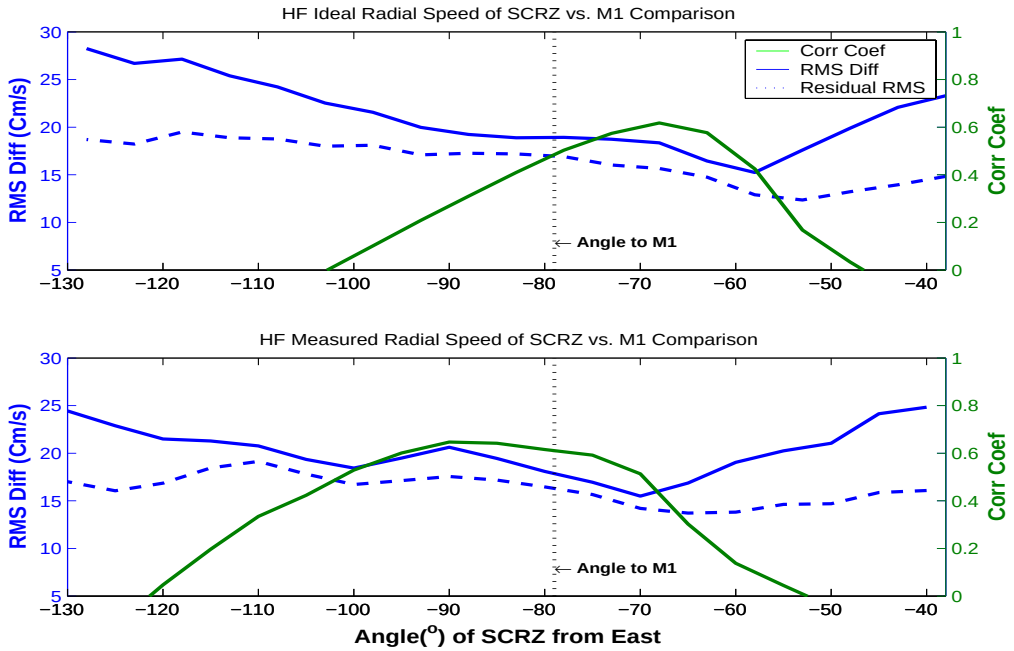


Figure 8. Correlation Coefficient and rms Difference Plots of M1 Buoy Radial Data vs. SCRZ Ideal (upper panel) and Measured Data (lower panel).

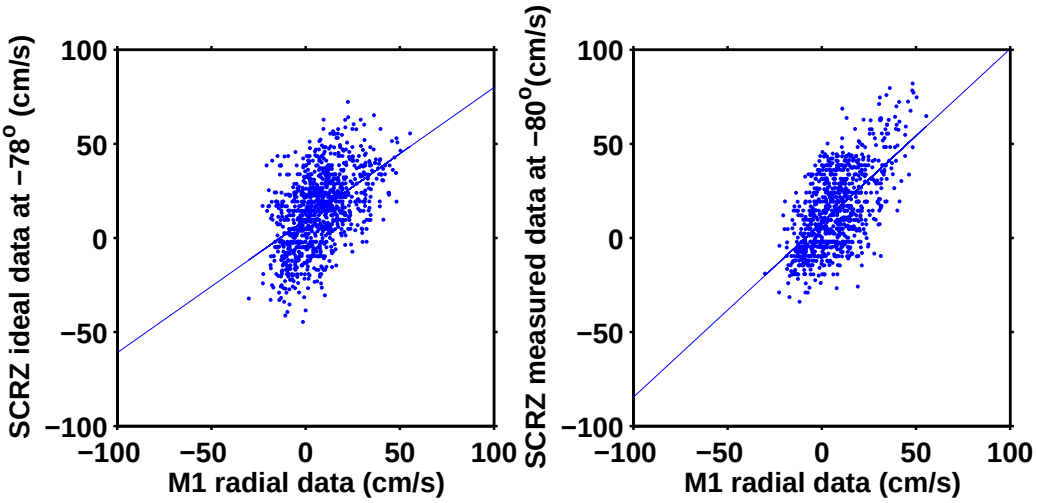


Figure 9. Scatter Plot of M1 Buoy Radial Data vs. SCRZ HF Radial Data. Ideal Data (left panel) yield Slope of 0.7 and y Intercept of 9.52. Measured Data (right panel) yield Slope of 0.93 and y Intercept of 7.96, respectively.

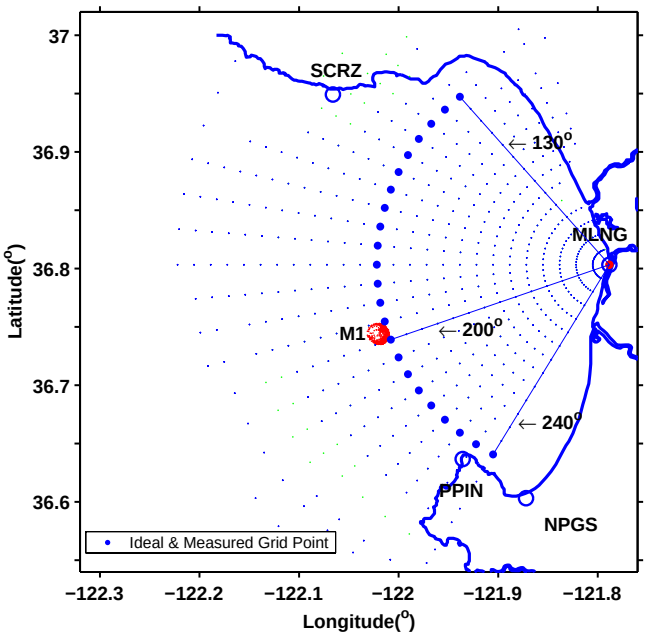


Figure 10. M1 Buoy and MLNG Radial Grid Points.

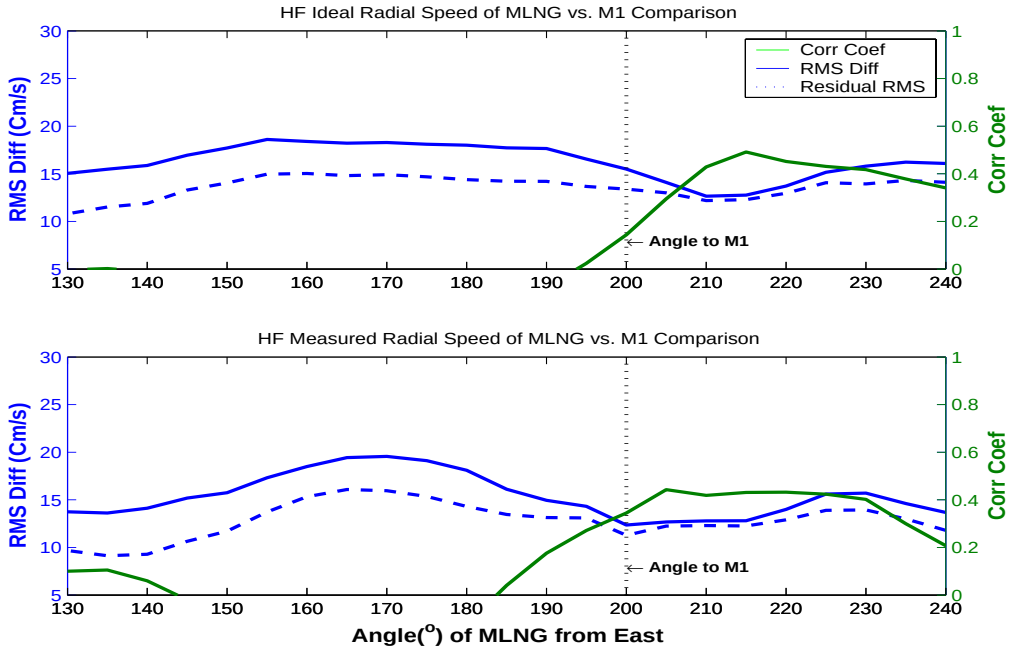


Figure 11. Correlation Coefficient and rms Difference Plots of M1 Buoy Radial Data vs. MLNG Ideal (upper panel) and Measured data (lower panel).

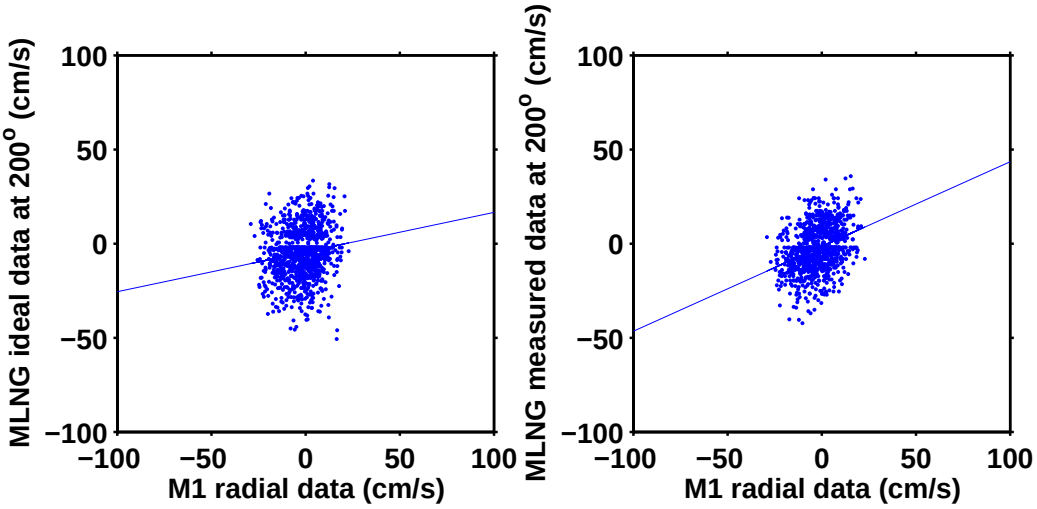


Figure 12. Scatter Plot of M1 Buoy Radial Data vs. MLNG HF Radial Data. Ideal Data (left panel) yield Slope of 0.21 and y Intercept of –4.41. Measured Data (right panel) yield Slope of 0.45 and y Intercept of –1.43, respectively.

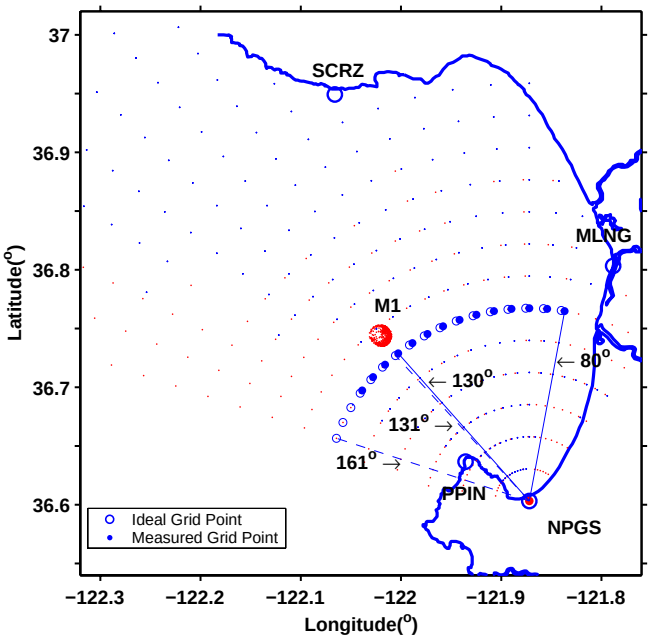


Figure 13. M1 Buoy and NPGS Radial Grid Points.

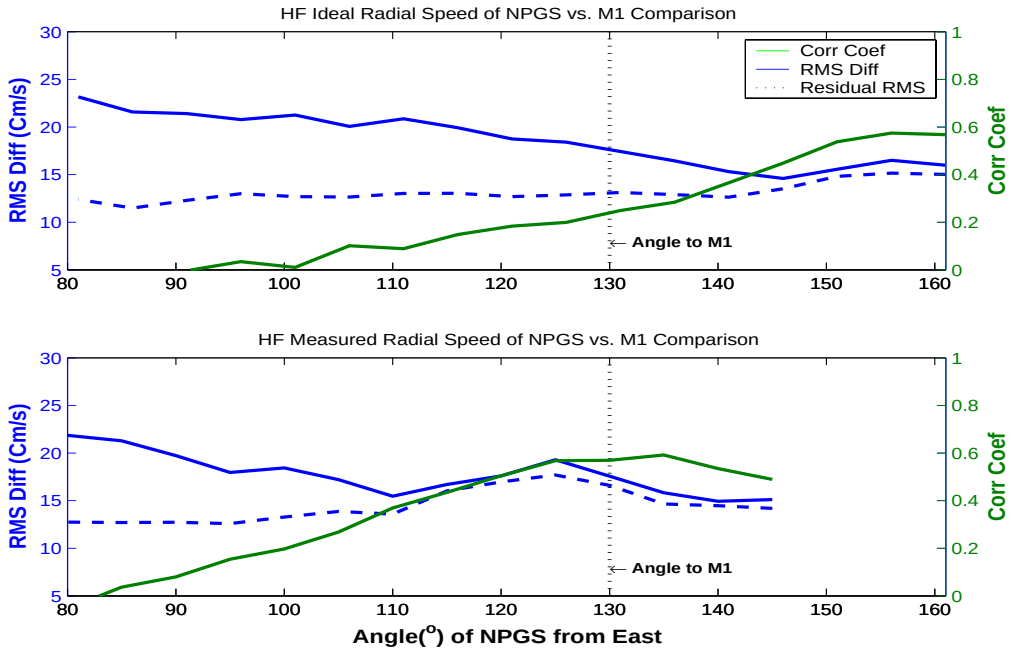


Figure 14. Correlation Coefficient and rms Difference Plots of M1 Buoy Radial Data vs. NPGS Ideal (upper panel) and Measured Data (lower panel).

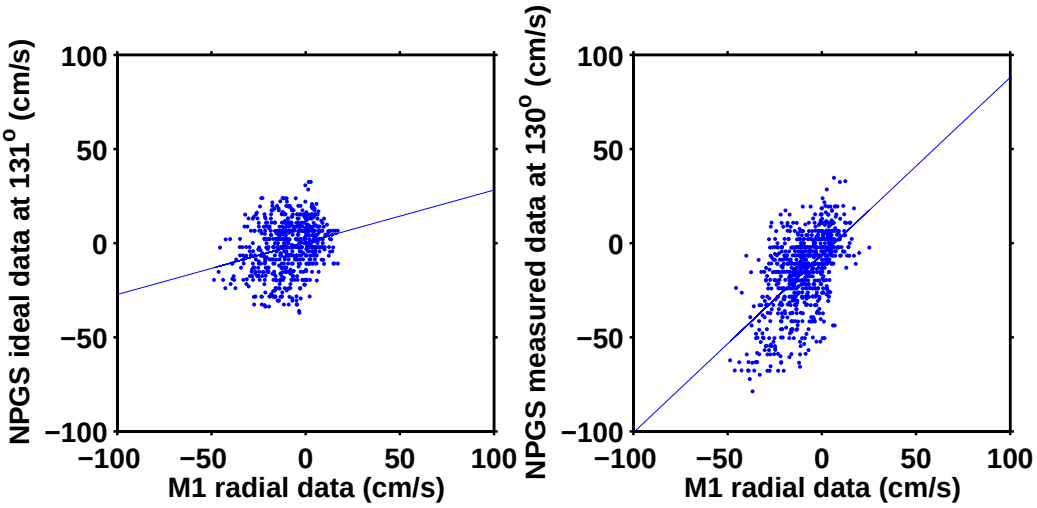


Figure 15. Scatter Plot of M1 Buoy Radial Data vs. NPGS HF Radial Data. Ideal Data (left panel) yield Slope of 0.28 and y Intercept of 0.48. Measured Data (right panel) yield Slope of 0.94 and y Intercept of –6.24, respectively.

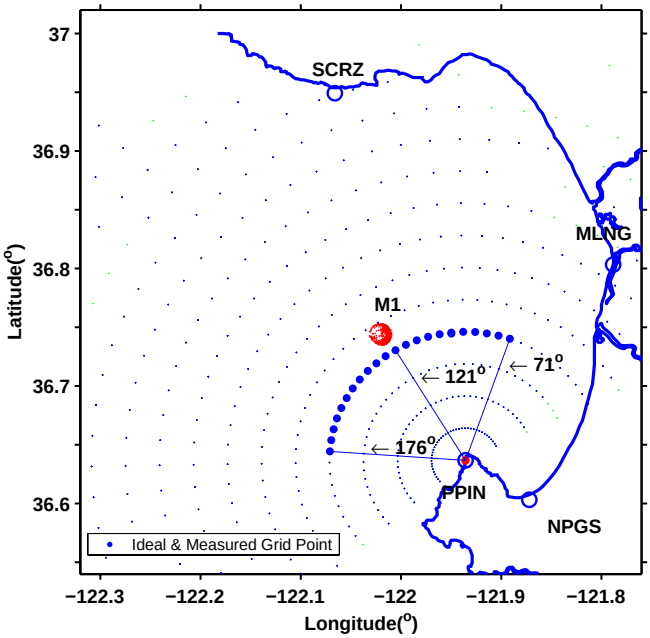


Figure 16. M1 Buoy and PPIN Radial Grid Points.

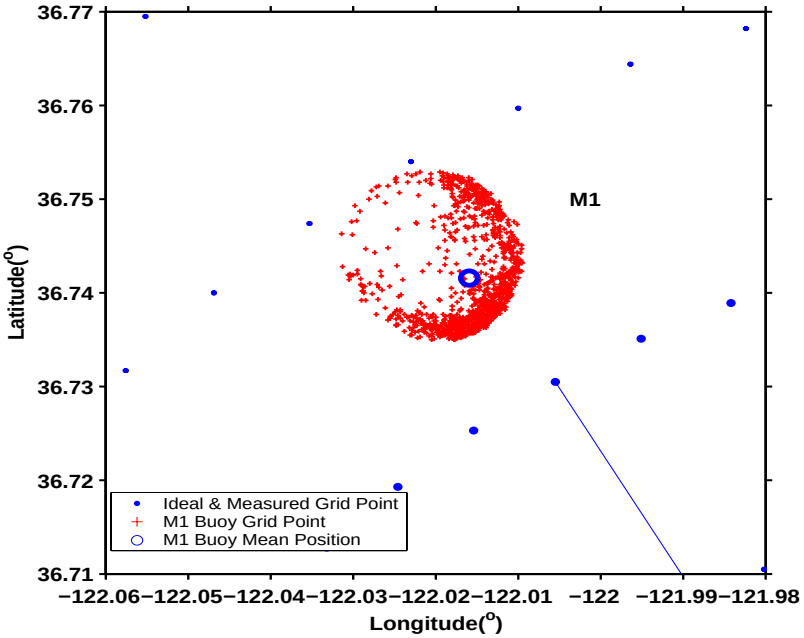


Figure 17. Wide Circle of M1 Buoy Grid Points and Its Neighboring PPIN Radial Grid Points. Blue Circle in the Red Indicates the Mean Position of the M1 Buoy.

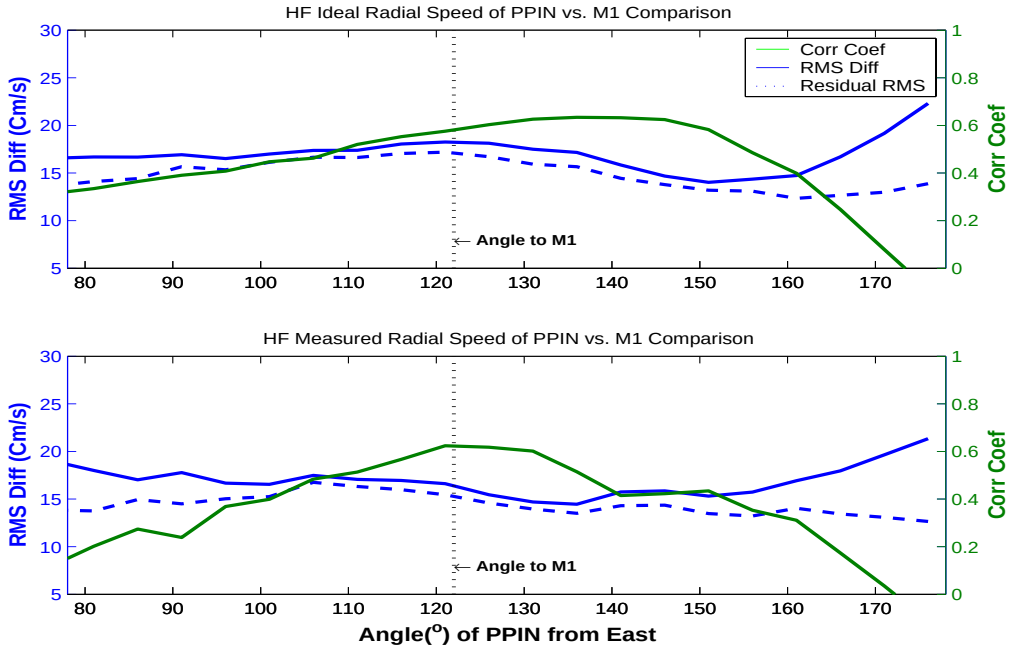


Figure 18. Correlation Coefficient and rms Difference Plots of M1 Buoy Radial Data vs. PPIN Ideal (upper panel) and Measured Data (lower panel).

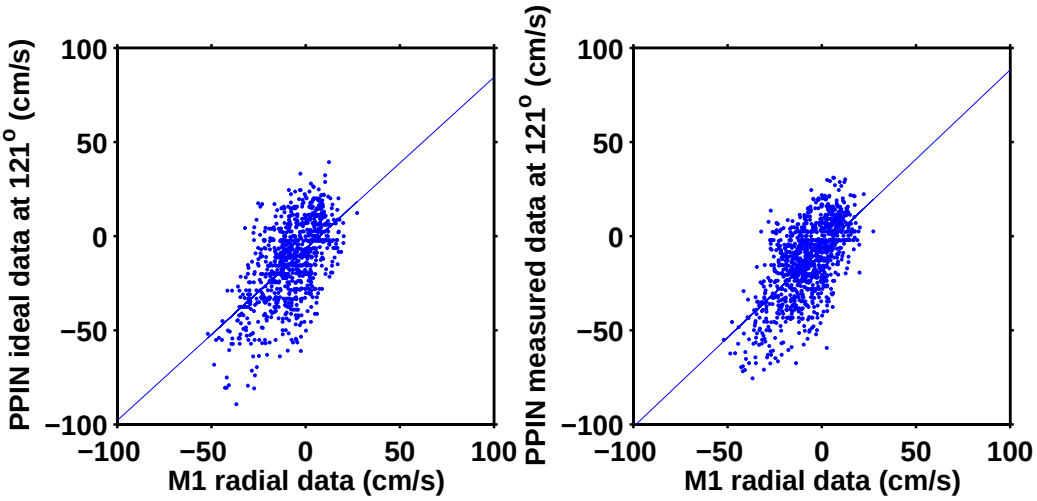


Figure 19. Scatter Plot of M1 Buoy Radial Data vs. PPIN HF Radial Data. Ideal Data (left panel) yield Slope of 0.91 and y Intercept of –6.71. Measured Data (right panel) yield Slope of 0.95 and y Intercept of 6.47, respectively.

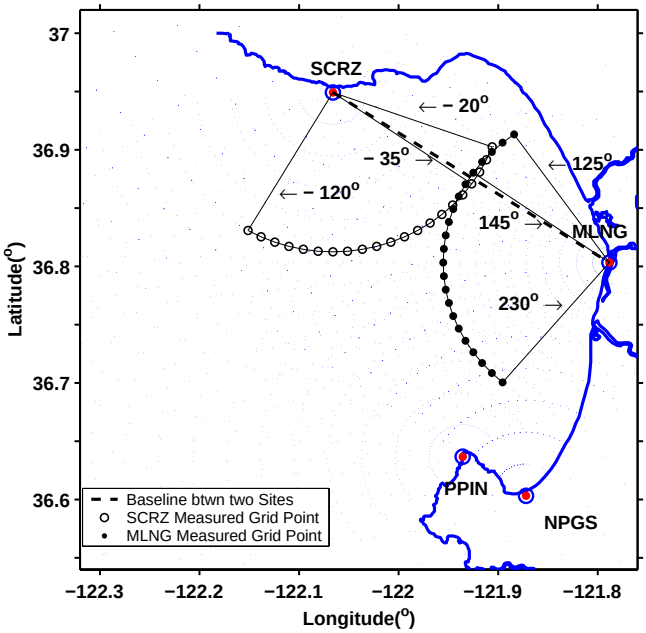


Figure 20. SCRZ – MLNG Baseline and Grid Points of Measured Radial Data.

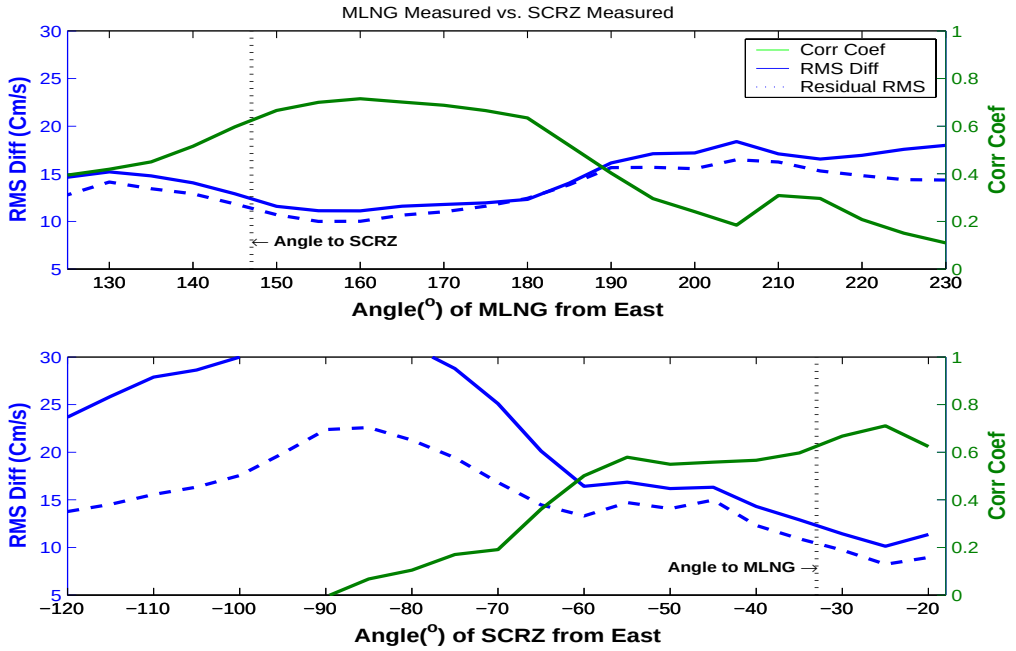


Figure 21. Correlation Coefficient and rms Difference Plots of MLNG vs. SCRZ HF Measured Radial Data. MLNG HF Measured Radial Data at Several Angles vs. SCRZ HF Measured Radial Data at –35˚ (upper panel) and SCRZ HF Measured Radial Data at Several Angles vs. MLNG at 145˚ (lower panel).

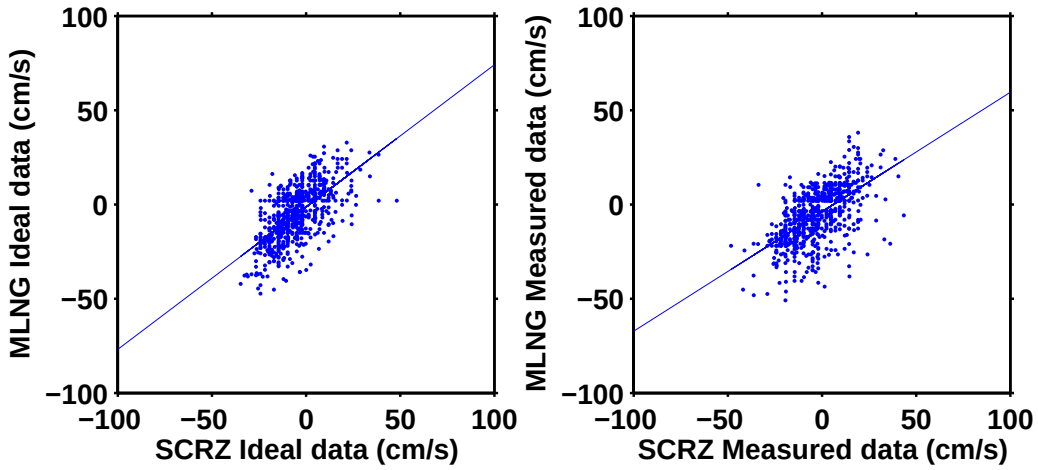


Figure 22. Scatter Plot of MLNG vs. SCRZ HF Radial Data. Ideal Data (left panel) yield Slope of 0.75 and y Intercept of –1.3. Measured Data (right panel) yield Slope of 0.63 and y Intercept of –3.8, respectively.

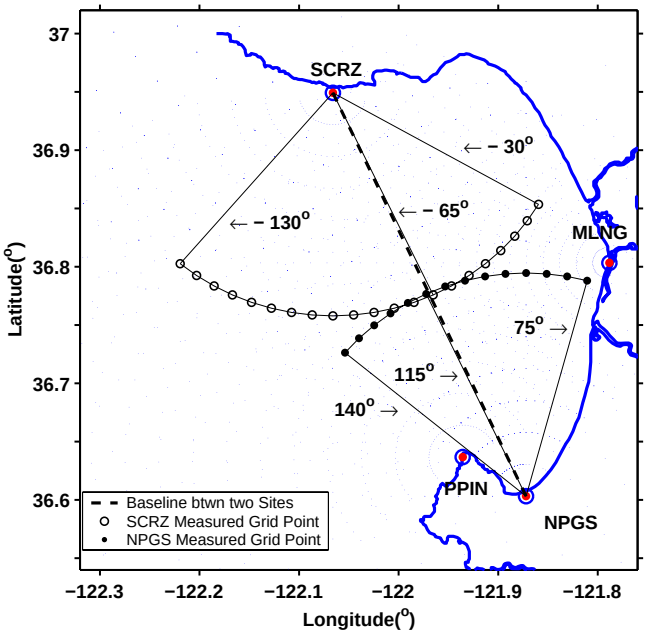


Figure 23. SCRZ – NPGS Baseline and Grid Points of Measured Radial Data.

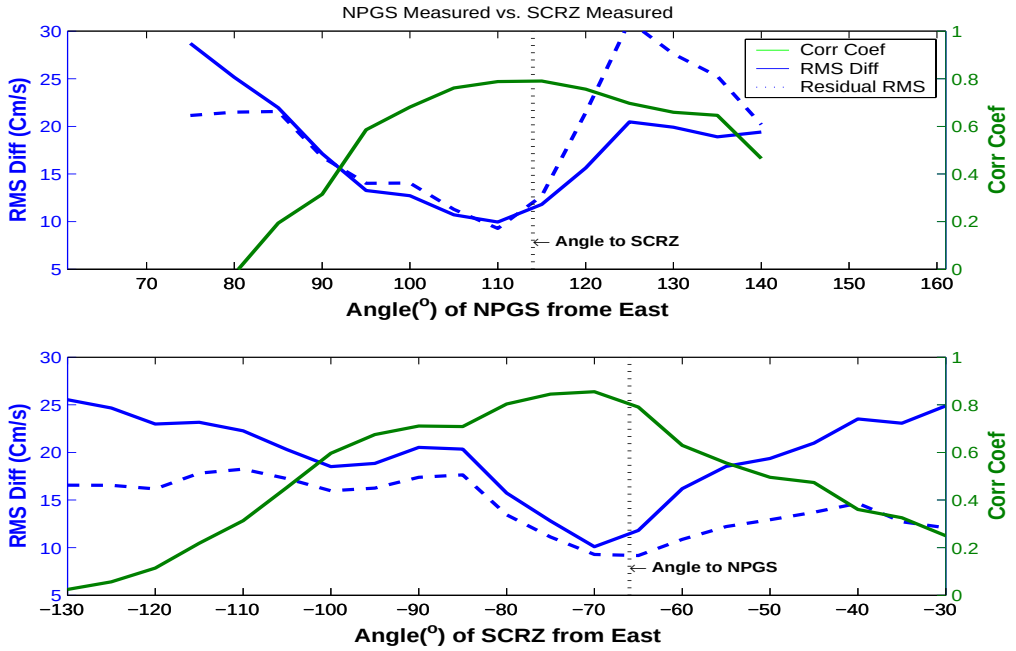


Figure 24. Correlation Coefficient and rms Difference Plots of NPGS vs. SCRZ HF Measured Radial Data. NPGS HF Measured Radial Data at Several Angles vs. SCRZ HF Measured Radial Data at -65˚ (upper panel) and SCRZ HF Measured Radial Data at Several Angles vs. NPGS at 115˚ (lower panel).

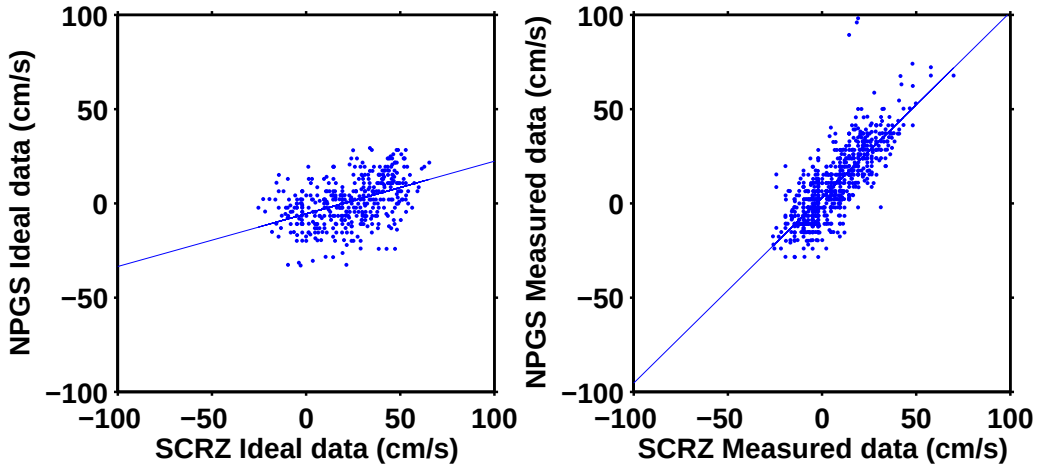


Figure 25. Scatter Plot of NPGS vs. SCRZ HF Radial Data. Ideal Data (left panel) yield Slope of 0.28 and y Intercept of –5.5. Measured Data (right panel) yield Slope of 0.98 and y Intercept of 3.1, respectively.

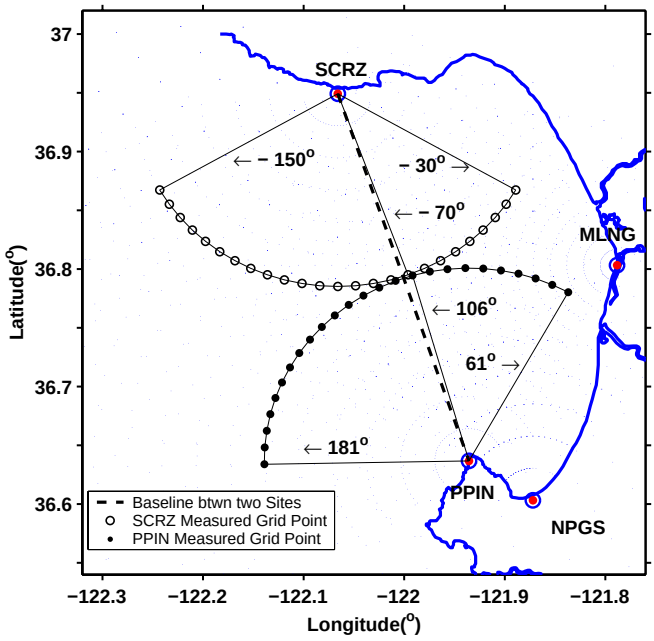


Figure 26. SCRZ – PPIN Baseline and Grid Points of Measured Radial Data.

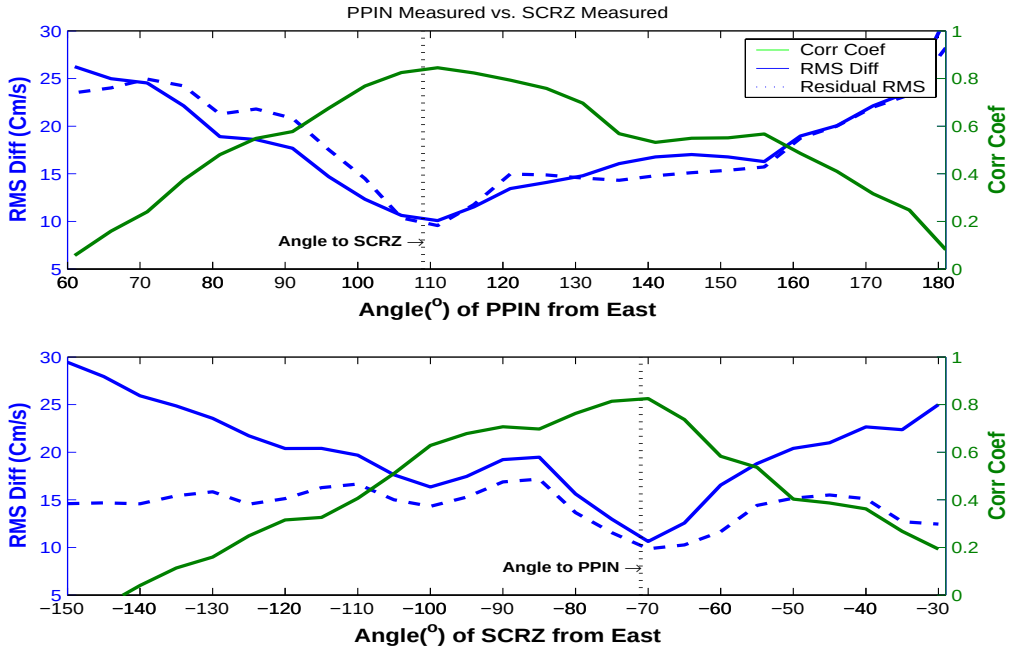


Figure 27. Correlation Coefficient and rms Difference Plots of PPIN vs. SCRZ HF Measured Radial Data. PPIN HF Measured Radial Data at Several Angles vs. SCRZ HF Measured Radial Data at -70˚ (upper panel) and SCRZ HF Measured Radial Data at Several Angles vs. PPIN at 111˚ (lower panel).

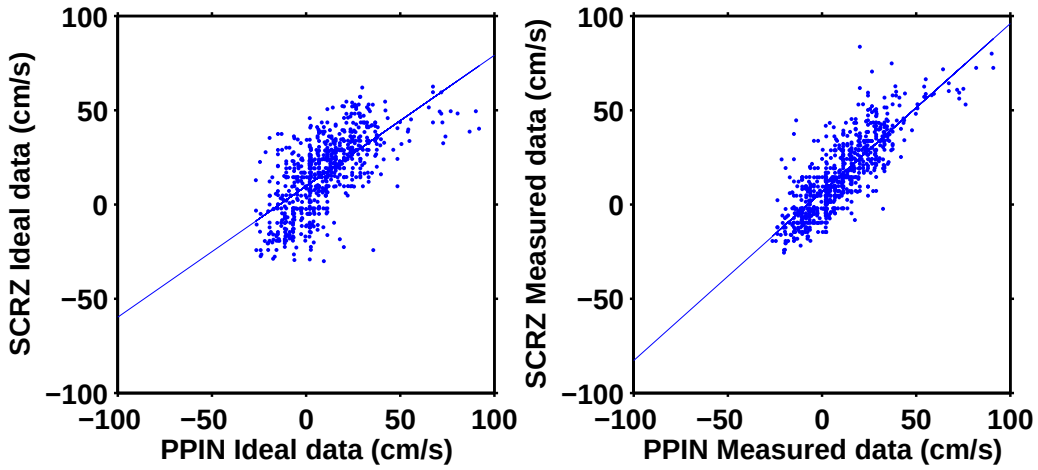


Figure 28. Scatter Plot of PPIN vs. SCRZ HF Radial Data. Ideal Data (left panel) yield Slope of 0.69 and y Intercept of 9.7. Measured Data (right panel) yield Slope of 0.98 and y Intercept of 3.61, respectively.

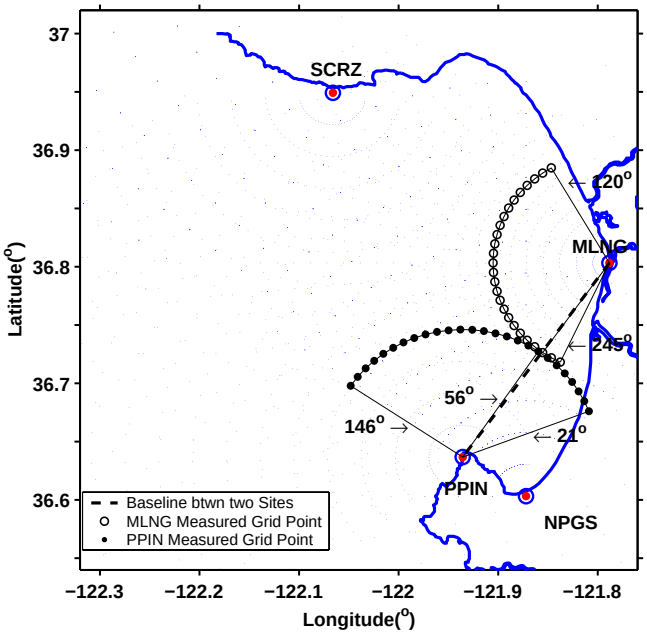


Figure 29. MLNG – PPIN Baseline and Grid Points of Measured Radial Data.

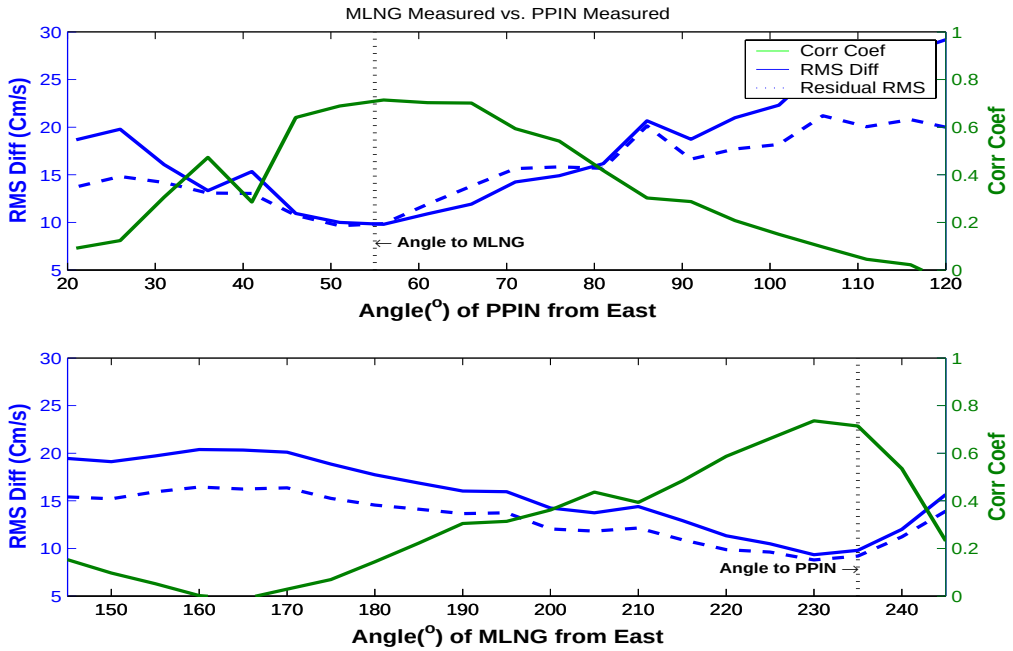


Figure 30. Correlation Coefficient and rms Difference Plots of PPIN vs. MLNG HF Measured Radial Data. PPIN HF Measured Radial Data at Several Angles vs. MLNG HF Measured Radial Data at 235˚ (upper panel) and MLNG HF Measured Radial Data at Several Angles vs. PPIN at 56˚ (lower panel).

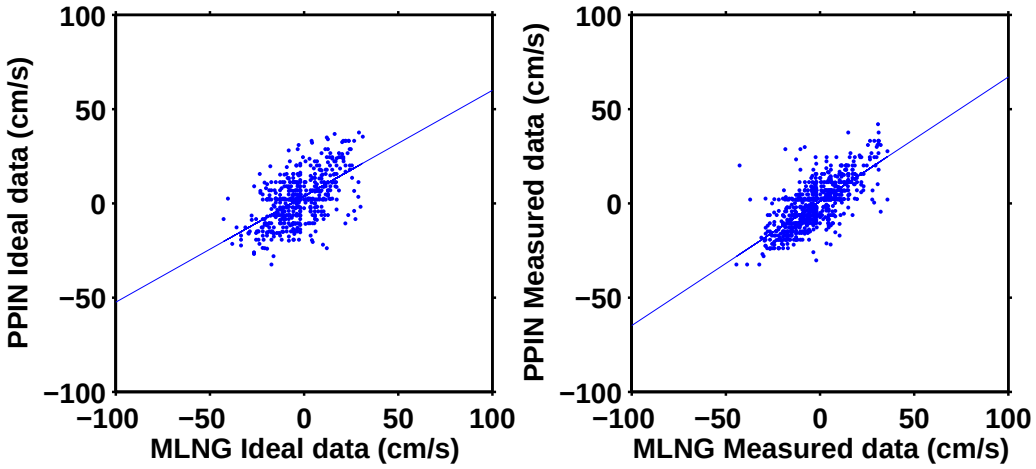


Figure 31. Scatter Plot of PPIN vs. MLNG HF Radial Data. Ideal Data (left panel) yield Slope of 0.56 and y Intercept of 3.8. Measured Data (right panel) yield Slope of 0.66 and y Intercept of 1.1, respectively.

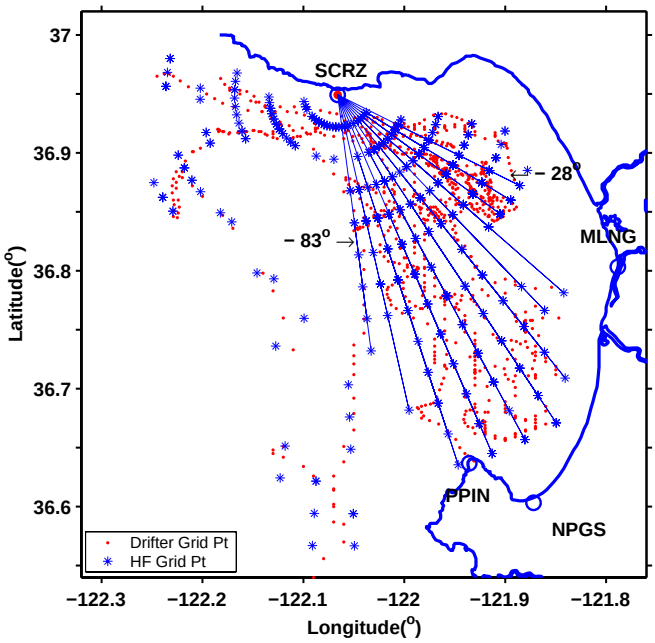


Figure 32. Grid Points of SCRZ HF Measured Radial Data (blue star) and Drifter Position (red dot). Blue Lines Indicate Grid Points of HF Data in the Same Angle from the Radar Site.

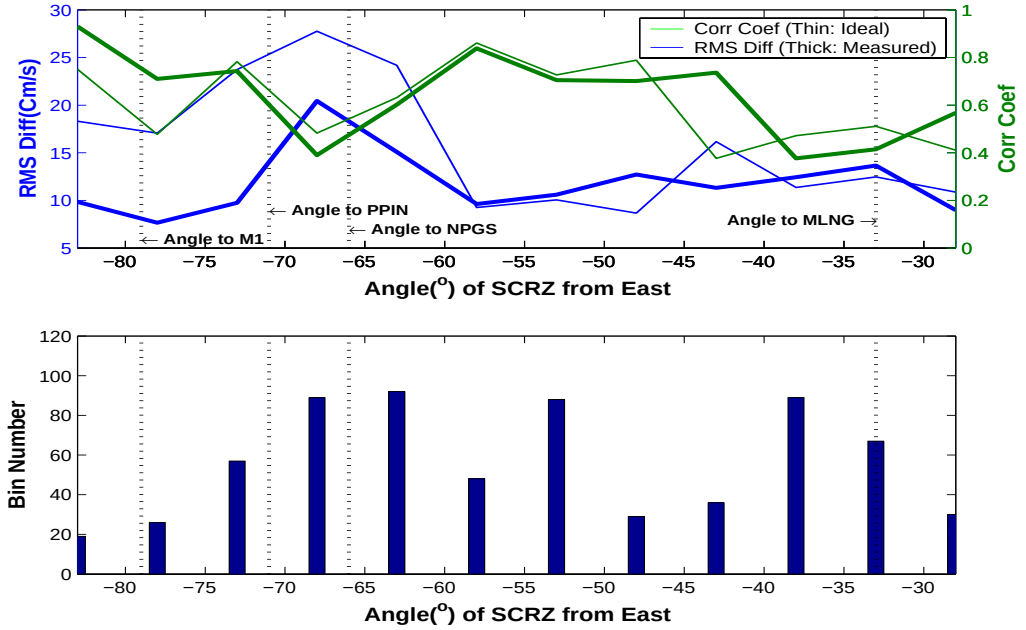


Figure 33. Correlation Coefficient and rms Difference Plot of Drifter Radial Data vs. SCRZ HF Radial Data (upper panel, ideal: thin line, measured: thick line). Number of Observations at Each Angle is shown at the Lower Panel.

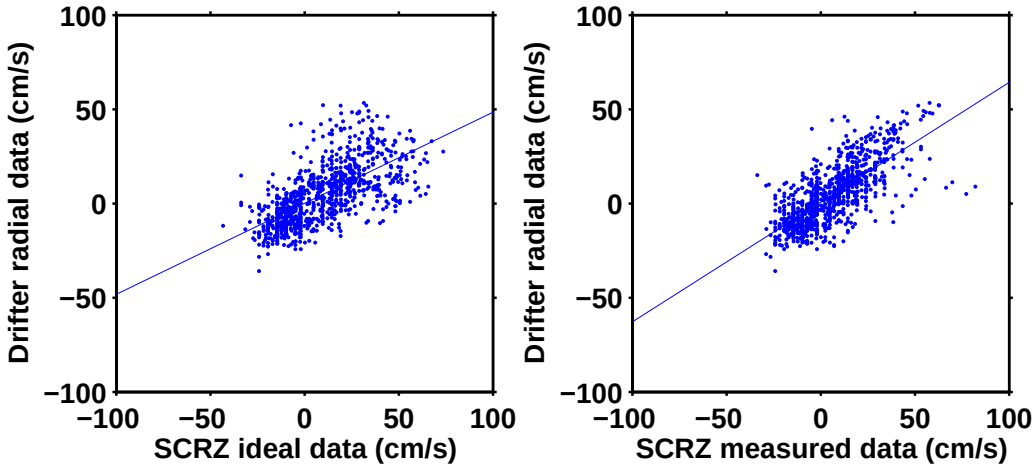


Figure 34. Scatter Plot of Drifter Radial Data vs. SCRZ HF Radial Data. Ideal Data (left panel) yield Slope of 0.48 and y Intercept of 0.16. Measured Data (right panel) yield Slope of 0.64 and y Intercept of 0.81, respectively.

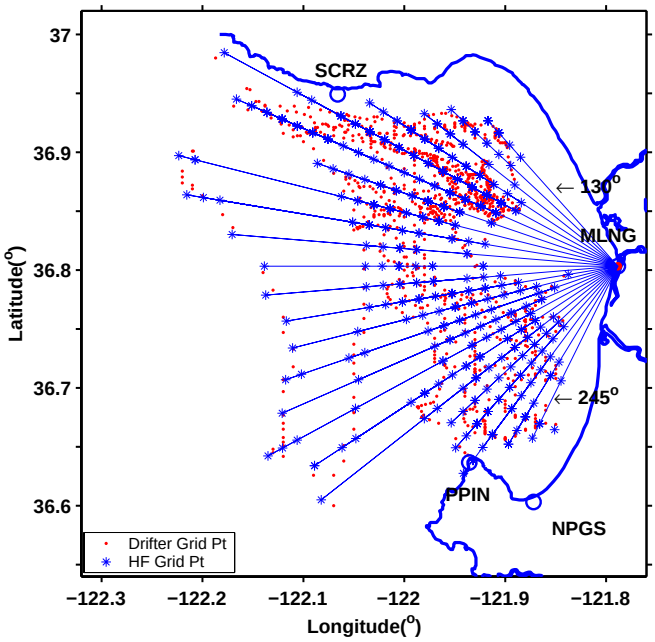


Figure 35. Grid Points of MLNG HF Measured Radial Data (blue star) and Drifter Position (red dot). Blue Lines Indicate Grid Points of HF Data in the Same Angle from the Radar Site.

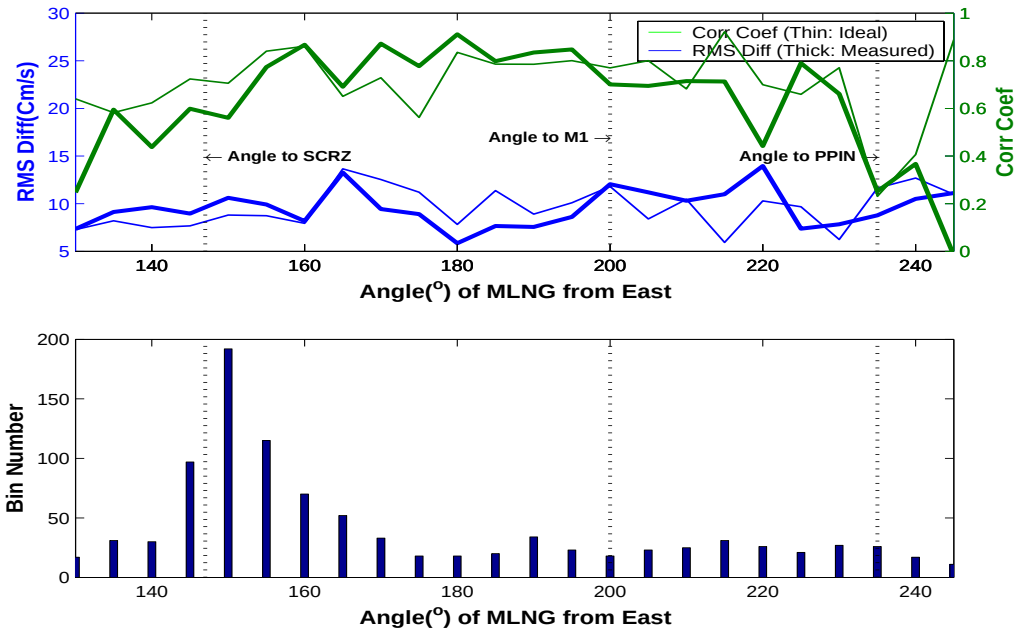


Figure 36. Correlation Coefficient and rms Difference Plot of Drifter Radial Data vs. MLNG HF Radial Data (upper panel, ideal: thin line, measured: thick line). Number of Observations at Each Angle is shown at the Lower Panel.

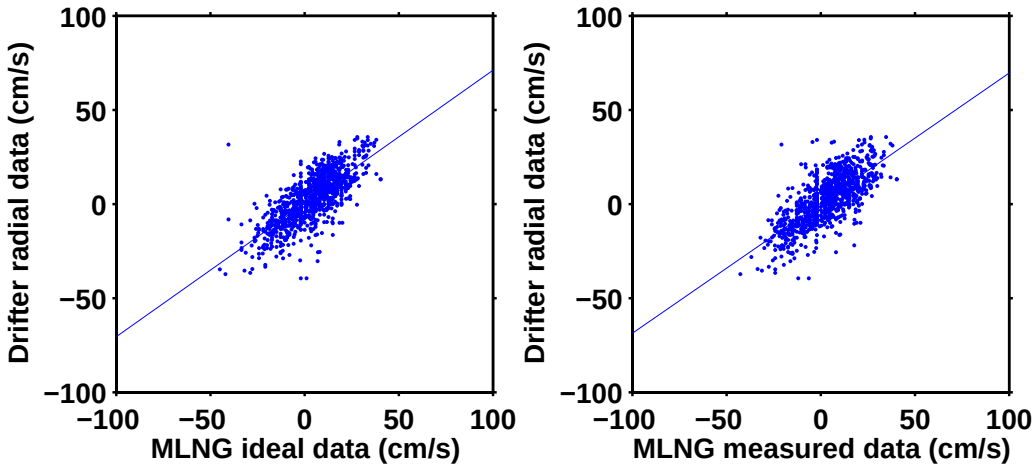


Figure 37. Scatter Plot of Drifter Radial Data vs. MLNG HF Radial Data. Ideal Data (left panel) yield Slope of 0.71 and y Intercept of 0.39. Measured Data (right panel) yield Slope of 0.7 and y Intercept of 0.5, respectively.

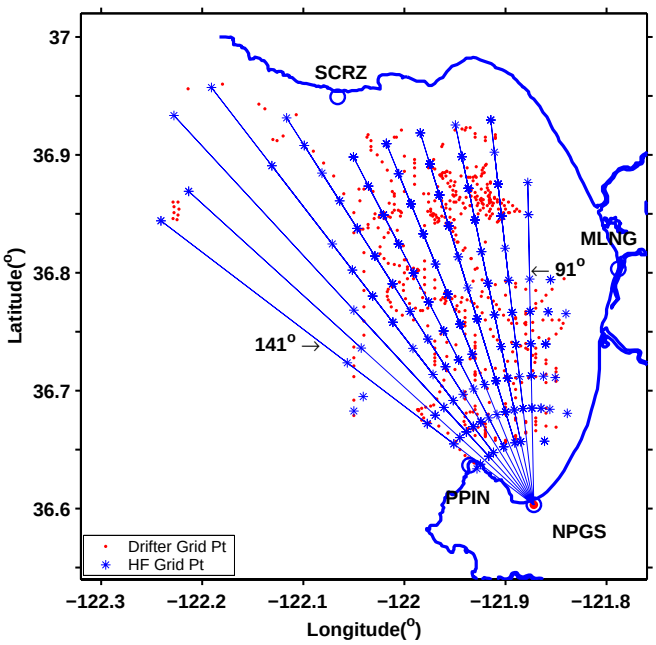


Figure 38. Grid Points of NPGS HF Measured Radial Data (blue star) and Drifter Position (red dot). Blue Lines Indicate Grid Points of HF Data in the Same Angle from the Radar Site.

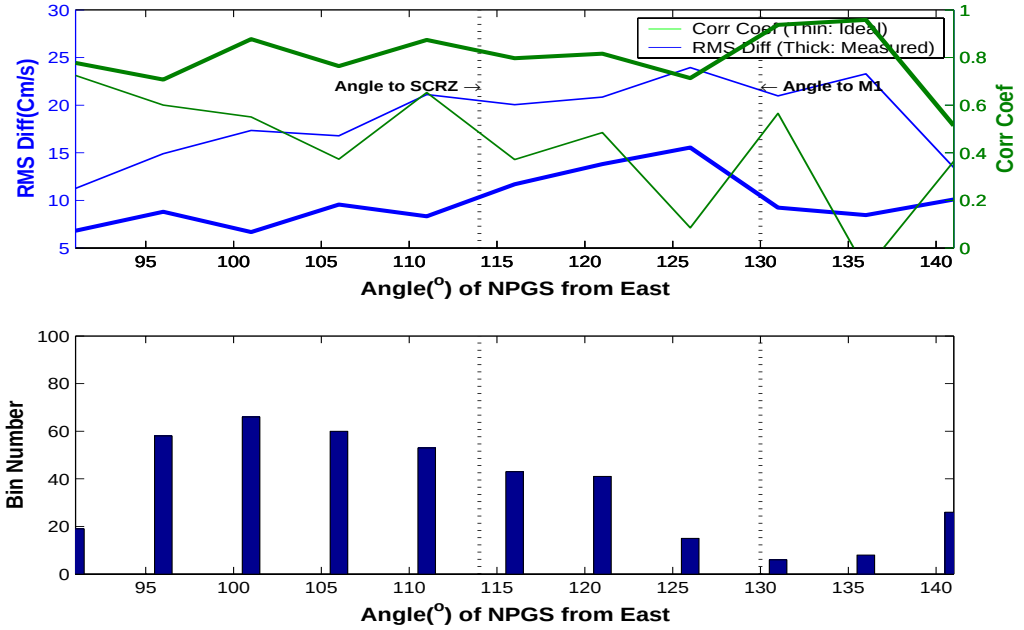


Figure 39. Correlation Coefficient and rms Difference Plot of Drifter Radial Data vs. NPGS HF Radial Data (upper panel, ideal: thin line, measured: thick line). Number of Observations at Each Angle is shown at the Lower Panel.

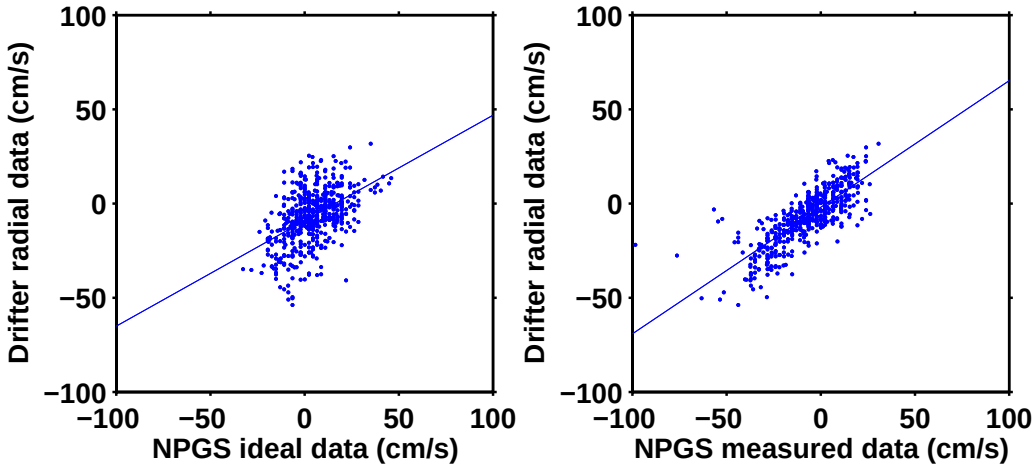


Figure 40. Scatter Plot of Drifter Radial Data vs. NPGS HF Radial Data. Ideal Data (left panel) yield Slope of 0.56 and y Intercept of –1.97. Measured Data (right panel) yield Slope of 0.67 and y Intercept of 0.81, respectively.

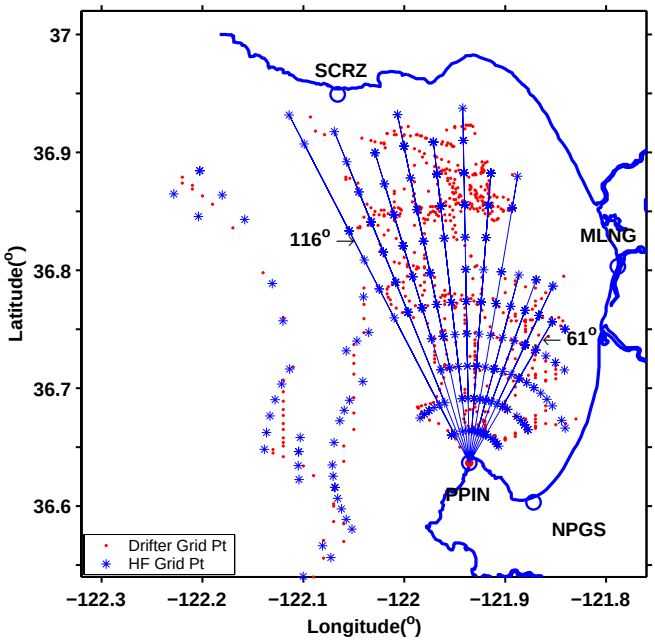


Figure 41. Grid Points of PPIN HF Measured Radial Data (blue star) and Drifter Position (red dot). Blue Lines Indicate Grid Points of HF Data in the Same Angle from the Radar Site.

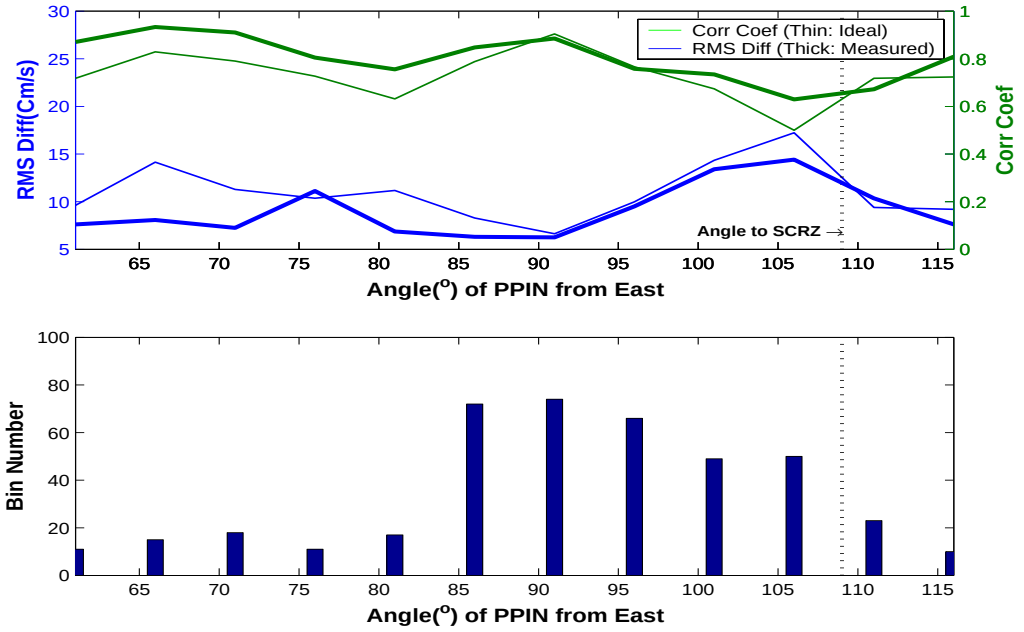


Figure 42. Correlation Coefficient and rms Difference Plot of Drifter Radial Data vs. PPIN HF Radial Data (upper panel, ideal: thin line, measured: thick line). Number of Observations at Each Angle is shown at the Lower Panel.

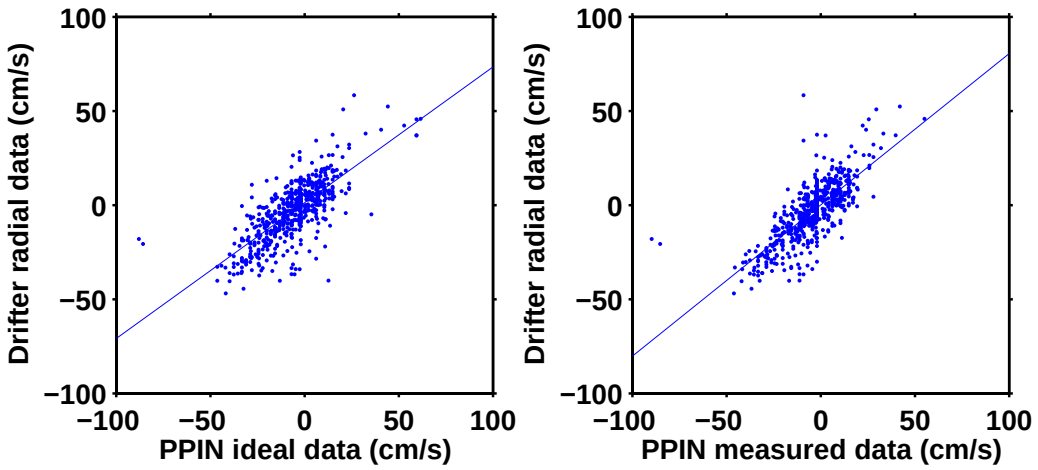


Figure 43. Scatter Plot of Drifter Radial Data vs. PPIN HF Radial Data. Ideal Data (left panel) yield Slope of 0.72 and y Intercept of 1.35. Measured Data (right panel) yield Slope of 0.8 and y Intercept of 0.15, respectively.

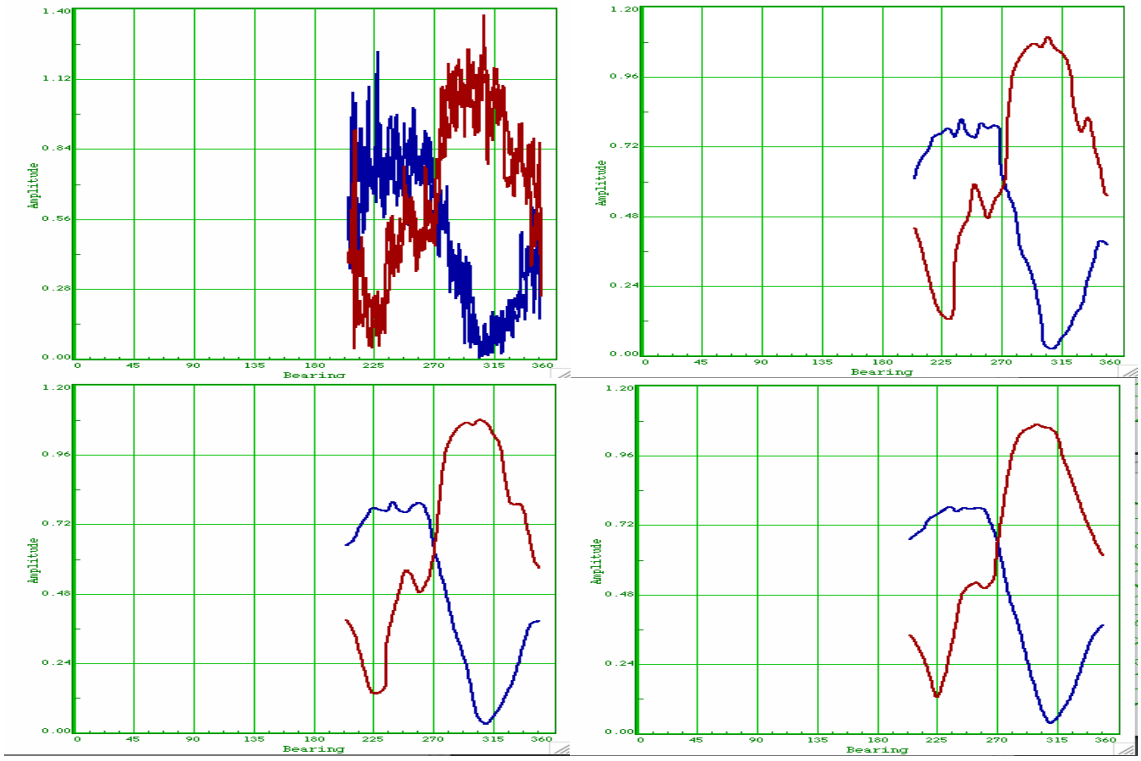


Figure 44. Measured Antenna Patterns of MLNG Radar Site. Left-upper Panel (a) is Raw Measured Antenna Pattern, Right-upper Panel (b) is 5° Smoothed, Left-lower Panel (c) is 10° Smoothed, and Right-lower Panel (d) is 20° Smoothed.

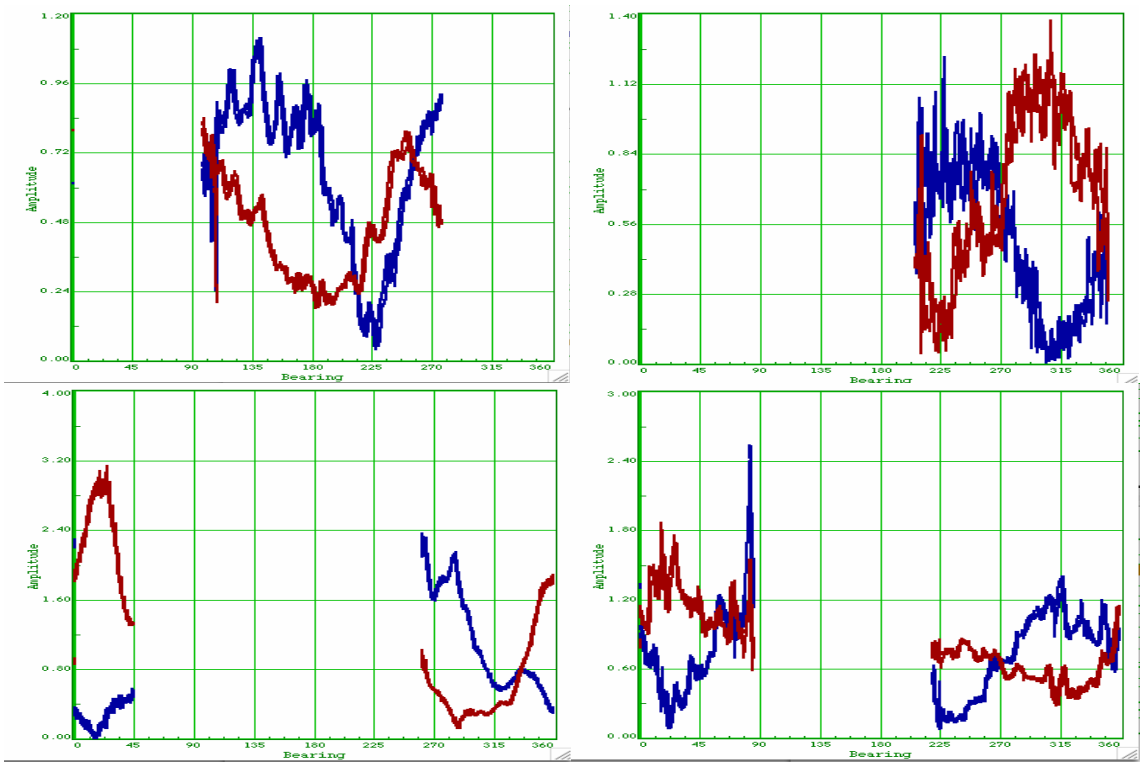


Figure 45. Raw Measured Antenna Patterns of Each Radar Site. Left-upper Panel (a) is the Measured Antenna Pattern at SCRZ Radar Site, Right-upper Panel (b) is MLNG, Left-lower Panel (c) is NPGS, and Right-lower Panel (d) is PPIN.

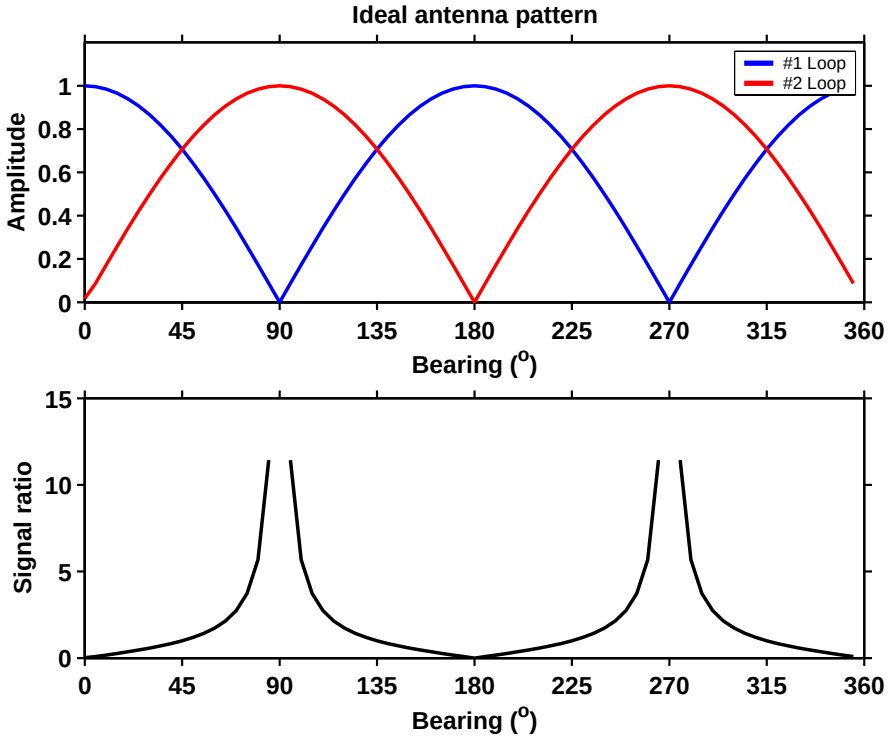


Figure 46. Ideal Antenna Pattern and Its Signal Ratio

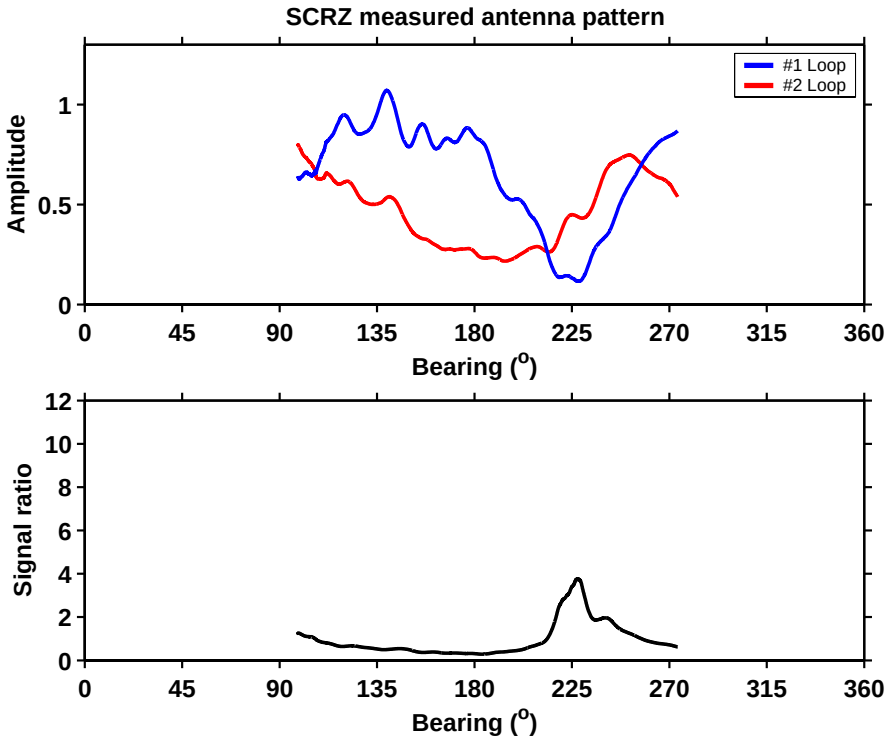


Figure 47. Measured Antenna Pattern and Its Signal Ratio at SCRZ Radar Site

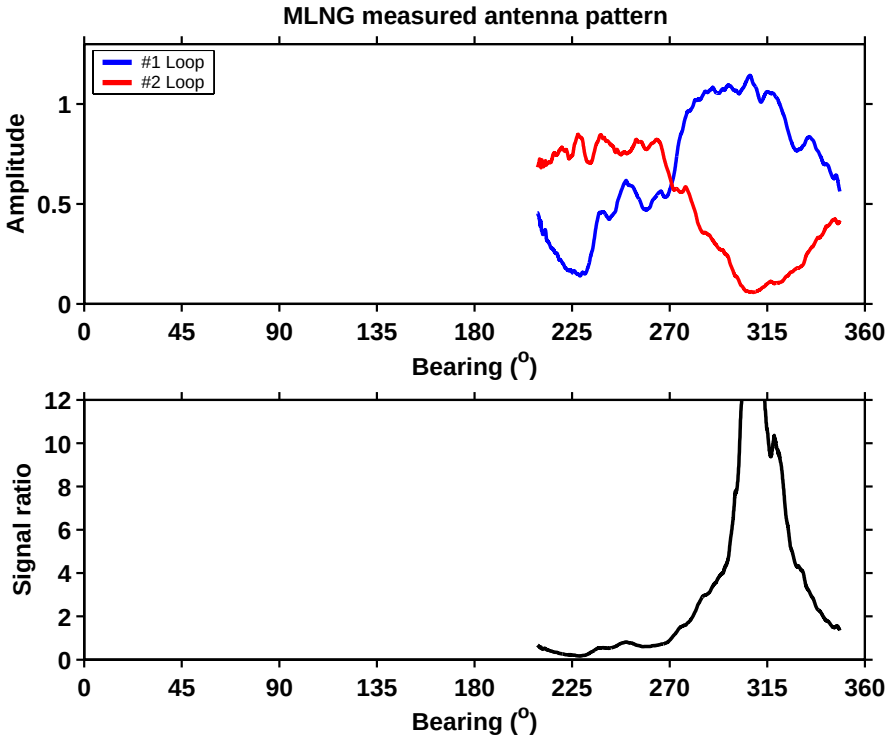


Figure 48. Measured Antenna Pattern and Its Signal Ratio at MLNG Radar Site

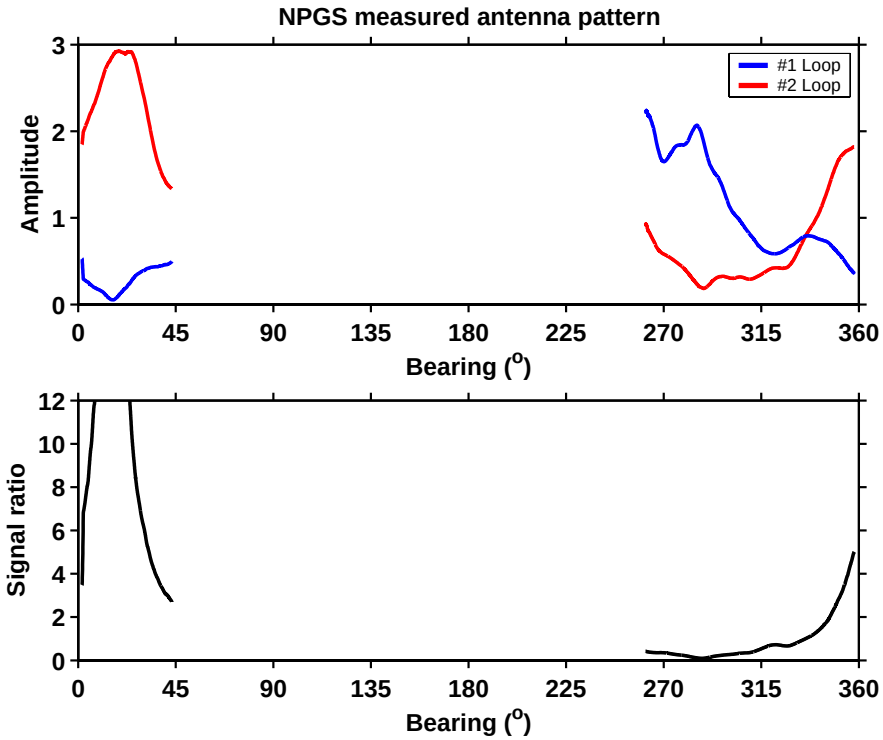


Figure 49. Measured Antenna Pattern and Its Signal Ratio at NPGS Radar Site

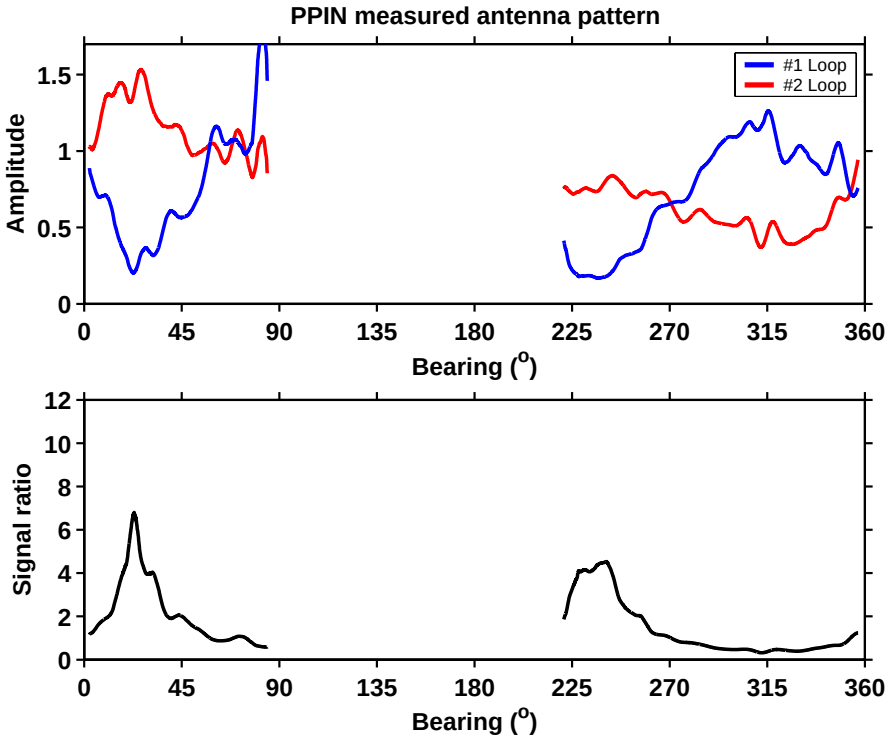


Figure 50. Measured Antenna Pattern and Its Signal Ratio at PPIN Radar Site

THIS PAGE INTENTIONALLY LEFT BLANK

# APPENDIX: TABLES

| Angles of SCRZ | Corr. Coef | rms Diff (cm/s) | Residual rms (cm/s) | Slope | Intercept | # of obs |
|---|---|---|---|---|---|---|
| **-38˚** | -0.13 | 23.3 | 14.8 | -0.13 | 0.34 | 648 |
| **-43˚** | -0.09 | 22.1 | 14.0 | -0.08 | 1.06 | 855 |
| **-48˚** | 0.03 | 19.9 | 13.2 | 0.03 | 1.25 | 1034 |
| **-53˚** | 0.17 | 17.6 | 12.4 | 0.15 | 2.17 | 1113 |
| **-58˚** | 0.42 | 15.2 | 12.9 | 0.43 | 5.05 | 1122 |
| **-63˚** | 0.58 | 16.4 | 14.8 | 0.74 | 8.05 | 1125 |
| **-68˚** | 0.62 | 18.4 | 15.7 | 0.88 | 10.24 | 1126 |
| **-73˚** | 0.57 | 18.7 | 16.0 | 0.8 | 10.67 | 1116 |
| **-78˚** | 0.5 | 18.9 | 16.9 | 0.7 | 9.52 | 1073 |
| **-83˚** | 0.41 | 18. 9 | 17.2 | 0.56 | 7.73 | 1023 |
| **-88˚** | 0.31 | 19.2 | 17.3 | 0.41 | 6.29 | 874 |
| **-93˚** | 0.21 | 20.0 | 17.1 | 0.26 | 5.92 | 798 |
| **-98˚** | 0.1 | 21.6 | 18.1 | 0.14 | 5.16 | 672 |
| **-103˚** | 0.0 | 22.5 | 18.0 | -0.01 | 5.09 | 645 |
| **-108˚** | -0.09 | 24.2 | 18.8 | -0.13 | 4.09 | 547 |
| **-113˚** | -0.16 | 25.4 | 18. 9 | -0.23 | 4.6 | 539 |
| **-118˚** | -0.25 | 27.2 | 19.5 | -0.36 | 3.73 | 475 |
| **-123˚** | -0.27 | 26.7 | 18.2 | -0.37 | 3.77 | 483 |
| **-128˚** | -0.34 | 28.3 | 18.7 | -0.49 | 1.94 | 438 |

**Table A-1. Comparison Statistics for SCRZ HF Radar (Ideal Pattern) vs. M1 Mooring Radial Current Speed Pairs.**

| Angles of SCRZ | Corr. Coef | rms Diff (cm/s) | Residual rms (cm/s) | Slope | Intercept | # of obs |
|---|---|---|---|---|---|---|
| **-40˚** | -0.12 | 24.8 | 16.1 | -0.13 | 1.5 | 550 |
| **-45˚** | -0.13 | 24.2 | 15.9 | -0.15 | 2.18 | 416 |
| **-50˚** | -0.04 | 21.0 | 14.7 | -0.05 | 2.65 | 606 |
| **-55˚** | 0.04 | 20.3 | 14.6 | 0.05 | 2.8 | 681 |
| **-60˚** | 0.14 | 19.0 | 13.8 | 0.13 | 1.82 | 999 |
| **-65˚** | 0.3 | 16.9 | 13.7 | 0.31 | 3.74 | 1111 |
| **-70˚** | 0.51 | 15.5 | 14.2 | 0.6 | 5.28 | 1124 |
| **-75˚** | 0.59 | 17.0 | 15. 7 | 0.82 | 7.23 | 1091 |
| **-80˚** | 0.62 | 18.1 | 16.5 | 0.93 | 7.96 | 942 |
| **-85˚** | 0.64 | 19.5 | 17.2 | 1.03 | 8.91 | 850 |
| **-90˚** | 0.65 | 20.6 | 17. 6 | 1.05 | 10.4 | 968 |
| **-95˚** | 0.6 | 19.5 | 17.1 | 0.92 | 9.82 | 1098 |
| **-100˚** | 0.53 | 18.4 | 16.7 | 0.74 | 8.67 | 1109 |
| **-105˚** | 0.42 | 19.4 | 17.8 | 0.59 | 7.79 | 1101 |
| **-110˚** | 0.33 | 20.8 | 19.1 | 0.48 | 6.98 | 1003 |
| **-115˚** | 0.2 | 21.3 | 18. 5 | 0.26 | 6.94 | 1012 |
| **-120˚** | 0.05 | 21.5 | 16.9 | 0.06 | 5.5 | 1061 |
| **-125˚** | -0.12 | 22.9 | 16.1 | -0.14 | 4.72 | 1080 |
| **-130˚** | -0.17 | 24.4 | 17.0 | -0.21 | 3.32 | 971 |

**Table A-2. Comparison Statistics for SCRZ HF Radar (Measured Pattern) vs. M1 Mooring Radial Current Speed Pairs.**

| Angles of MLNG | Corr. Coef | rms Diff (cm/s) | Residual rms (cm/s) | Slope | Intercept | # of obs |
|---|---|---|---|---|---|---|
| **240˚** | 0.34 | 16.1 | 14.1 | 0.56 | 5.82 | 646 |
| **235˚** | 0.38 | 16.2 | 14.3 | 0.63 | 6.08 | 743 |
| **230˚** | 0.42 | 15.8 | 13.9 | 0.7 | 6.39 | 815 |
| **225˚** | 0.43 | 15.2 | 14.1 | 0.74 | 4.64 | 853 |
| **220˚** | 0.45 | 13.7 | 13.0 | 0.72 | 3.08 | 923 |
| **215˚** | 0.49 | 12.8 | 12.3 | 0.76 | 2.18 | 957 |
| **210˚** | 0.43 | 12.7 | 12.2 | 0.63 | -0.5 | 1001 |
| **205˚** | 0.29 | 14.1 | 13.0 | 0.43 | -2.7 | 1035 |
| **200˚** | 0.14 | 15.5 | 13. 4 | 0.21 | -4.41 | 1041 |
| **195˚** | 0.02 | 16.5 | 13.7 | 0.04 | -4.78 | 1044 |
| **190˚** | -0.07 | 17.7 | 14.2 | -0.11 | -4.36 | 1052 |
| **185˚** | -0.09 | 17.7 | 14.2 | -0.14 | -3.52 | 1045 |
| **180˚** | -0.11 | 18.0 | 14.4 | -0.18 | -2.82 | 1039 |
| **175˚** | -0.09 | 18.1 | 14.7 | -0.14 | -2.13 | 1028 |
| **170˚** | -0.09 | 18.3 | 14.9 | -0.14 | -1.21 | 1030 |
| **165˚** | -0.07 | 18.2 | 14.8 | -0.12 | -0.18 | 1025 |
| **160˚** | -0.06 | 18.4 | 15.0 | -0.09 | 0.87 | 1006 |
| **155˚** | -0.07 | 18.6 | 15.0 | -0.12 | 1.56 | 974 |
| **150˚** | -0.04 | 17.7 | 14.0 | -0.07 | 2.21 | 956 |
| **145˚** | -0.02 | 17.0 | 13.3 | -0.03 | 2.53 | 924 |
| **140˚** | -0.01 | 15.9 | 11.9 | -0.01 | 2.76 | 847 |
| **135˚** | 0.0 | 15.5 | 11.5 | 0.0 | 2.7 | 815 |
| **130˚** | 0.0 | 15.0 | 10.8 | 0.0 | 2.93 | 700 |

**Table A-3. Comparison Statistics for MLNG HF Radar (Ideal Pattern) vs. M1 Mooring Radial Current Speed Pairs.**

| Angles of MLNG | Corr. Coef | rms Diff (cm/s) | Residual rms (cm/s) | Slope | Intercept | # of obs |
|---|---|---|---|---|---|---|
| **240˚** | 0.21 | 13.7 | 11.8 | 0.28 | 0.34 | 690 |
| **235˚** | 0.3 | 14.6 | 13.0 | 0.45 | 3.26 | 871 |
| **230˚** | 0.4 | 15.7 | 13.9 | 0.67 | 5.9 | 870 |
| **225˚** | 0.42 | 15.6 | 13.9 | 0.71 | 6.02 | 912 |
| **220˚** | 0.43 | 14.0 | 12.9 | 0.67 | 3.84 | 991 |
| **215˚** | 0.43 | 13.0 | 12.3 | 0.64 | 0.89 | 991 |
| **210˚** | 0.42 | 13.0 | 12.3 | 0.62 | -0.8 | 965 |
| **205˚** | 0.44 | 13.0 | 12.2 | 0.65 | -0.74 | 860 |
| **200˚** | 0.34 | 12.4 | 11.3 | 0.45 | -1.43 | 973 |
| **195˚** | 0.27 | 14.3 | 13.1 | 0.4 | -2.88 | 975 |
| **190˚** | 0.18 | 14.9 | 13.1 | 0.25 | -3.37 | 1046 |
| **185˚** | 0.04 | 16.1 | 13.5 | 0.06 | -3.77 | 1061 |
| **180˚** | -0.12 | 18.1 | 14.3 | -0.19 | -3.68 | 1063 |
| **175˚** | -0.14 | 19.1 | 15.4 | -0.23 | -3.18 | 1058 |
| **170˚** | -0.13 | 19.6 | 16.0 | -0.22 | -2.18 | 1041 |
| **165˚** | -0.1 | 19.4 | 16.0 | -0.17 | -0.77 | 1036 |
| **160˚** | -0.05 | 18.5 | 15.3 | -0.08 | 0.47 | 1030 |
| **155˚** | -0.04 | 17.3 | 13.7 | -0.06 | 1.65 | 1024 |
| **150˚** | -0.02 | 15.8 | 11.7 | -0.02 | 2.44 | 971 |
| **145˚** | -0.02 | 15.2 | 10.6 | -0.02 | 3.1 | 851 |

| | | | | | | |
|---|---|---|---|---|---|---|
| **140˚** | 0.06 | 14.1 | 9. 3 | 0.06 | 4.14 | 715 |
| **135˚** | 0.1 | 13.6 | 9.1 | 0.11 | 3.62 | 679 |
| **130˚** | 0.1 | 13.7 | 9.7 | 0.1 | 2.57 | 617 |

**Table A-4. Comparison Statistics for MLNG HF Radar (Measured Pattern) vs. M1 Mooring Radial Current Speed Pairs.**

| Angles of NPGS | Corr. Coef | rms Diff (cm/s) | Residual rms (cm/s) | Slope | Intercept | # of obs |
|---|---|---|---|---|---|---|
| **161˚** | 0.57 | 16.0 | 15.0 | 0.84 | -6.59 | 808 |
| **156˚** | 0.57 | 16.5 | 15.2 | 0.87 | -7.54 | 845 |
| **151˚** | 0.54 | 15.6 | 14.8 | 0.78 | -5.99 | 847 |
| **146˚** | 0.45 | 14.6 | 13.5 | 0.56 | -3.1 | 836 |
| **141˚** | 0.37 | 15.3 | 12.6 | 0.41 | -0.64 | 815 |
| **136˚** | 0.28 | 16.4 | 12.9 | 0.31 | -0.3 | 753 |
| **131˚** | 0.25 | 17.4 | 13.1 | 0.28 | 0.48 | 637 |
| **126˚** | 0.2 | 18.4 | 12.9 | 0.22 | 1.48 | 540 |
| **121˚** | 0.18 | 18.7 | 12.7 | 0.2 | 2.32 | 492 |
| **116˚** | 0.15 | 19.9 | 13.0 | 0.16 | 1.58 | 411 |
| **111˚** | 0.09 | 20. 9 | 13.0 | 0.1 | 1.47 | 355 |
| **106˚** | 0.1 | 20.1 | 12.6 | 0.11 | 1.13 | 333 |
| **101˚** | 0.01 | 21.3 | 12.7 | 0.01 | 1.24 | 320 |
| **96˚** | 0.03 | 20.8 | 13.0 | 0.04 | 1.42 | 286 |
| **91˚** | 0.0 | 21.4 | 12. 3 | 0.0 | 1.89 | 282 |
| **86˚** | -0.09 | 21.6 | 11.5 | -0.08 | 1.23 | 231 |
| **81˚** | -0.13 | 23.2 | 12.4 | -0.12 | 1.26 | 208 |

**Table A-5. Comparison Statistics for NPGS HF Radar (Ideal Pattern) vs. M1 Mooring Radial Current Speed Pairs.**

| Intercept | Corr. Coef | rms Diff (cm/s) | Residual rms (cm/s) | Slope | Intercept | # of obs |
|---|---|---|---|---|---|---|
| **145˚** | 0.49 | 15.1 | 14.2 | 0.62 | -2.91 | 312 |
| **140˚** | 0.53 | 14.9 | 14.5 | 0.74 | -4.21 | 616 |
| **135˚** | 0.59 | 15.8 | 14.7 | 0.88 | -6.91 | 837 |
| **130˚** | 0.57 | 17.6 | 16.6 | 0.94 | -6.24 | 822 |
| **125˚** | 0.57 | 19.3 | 17.7 | 1.0 | -7.65 | 804 |
| **120˚** | 0.5 | 17. 6 | 17.0 | 0.81 | -5.8 | 830 |
| **115˚** | 0.43 | 16.7 | 16.0 | 0.62 | -3.98 | 751 |
| **110˚** | 0.37 | 15.5 | 13.6 | 0.44 | -2.37 | 786 |
| **105˚** | 0.27 | 17.2 | 13.9 | 0.32 | -0.31 | 682 |
| **100˚** | 0.2 | 18.4 | 13.3 | 0.22 | 0.5 | 619 |
| **95˚** | 0.15 | 18.0 | 12.6 | 0.16 | 0.03 | 699 |
| **90˚** | 0.08 | 19.7 | 12.7 | 0.09 | 1.13 | 534 |
| **85˚** | 0.04 | 21.3 | 12.7 | 0.04 | 2.21 | 413 |
| **80˚** | -0.05 | 21. 9 | 12.8 | 0.06 | 0.19 | 222 |

**Table A-6. Comparison Statistics for NPGS HF Radar (Measured Pattern) vs. M1 Mooring Radial Current Speed Pairs.**

| Angles of PPIN | Corr. Coef | rms Diff (cm/s) | Residual rms (cm/s) | Slope | Intercept | # of obs |
|---|---|---|---|---|---|---|
| **176°** | -0.09 | 22.3 | 13.9 | -0.09 | 1.51 | 1023 |
| **171°** | 0.08 | 19.2 | 13.0 | 0.08 | 0.35 | 1044 |
| **166°** | 0.25 | 16.7 | 12.7 | 0.25 | -0.98 | 1055 |
| **161°** | 0.4 | 14.7 | 12.3 | 0.41 | -2.34 | 1047 |
| **156°** | 0.49 | 14.4 | 13.1 | 0.55 | -3.89 | 1037 |
| **151°** | 0.58 | 14.0 | 13.2 | 0.72 | -5.13 | 1023 |
| **146°** | 0.62 | 14.7 | 13.8 | 0.84 | -5.87 | 996 |
| **141°** | 0.63 | 15.8 | 14.4 | 0.9 | -7.14 | 1018 |
| **136°** | 0.63 | 17.2 | 15.7 | 0.97 | -7.23 | 997 |
| **131°** | 0.63 | 17.5 | 15.9 | 0.97 | -7.45 | 971 |
| **126°** | 0.6 | 18.1 | 16.7 | 0.95 | -7.4 | 924 |
| **121°** | 0.58 | 18.3 | 17.2 | 0.91 | -6.71 | 884 |
| **116°** | 0.55 | 18.0 | 17.0 | 0.84 | -6.69 | 827 |
| **111°** | 0.52 | 17.4 | 16.6 | 0.75 | -5.7 | 804 |
| **106°** | 0.46 | 17.4 | 16.7 | 0.65 | -4.49 | 726 |
| **101°** | 0.45 | 17.0 | 16.1 | 0.6 | -3.95 | 729 |
| **96°** | 0.41 | 16.5 | 15.3 | 0.53 | -2.6 | 667 |
| **91°** | 0.39 | 16.9 | 15.7 | 0.52 | -2.15 | 669 |
| **86°** | 0.36 | 16.7 | 14.4 | 0.44 | -1.15 | 629 |
| **81°** | 0.33 | 16.7 | 14.1 | 0.39 | -1.53 | 628 |
| **76°** | 0.31 | 16.6 | 13.6 | 0.36 | -0.9 | 622 |
| **71°** | 0.28 | 17.5 | 13.8 | 0.32 | -0.31 | 597 |

**Table A-7. Comparison Statistics for PPIN HF Radar (Ideal Pattern) vs. M1 Mooring Radial Current Speed Pairs.**

| Angles of PPIN | Corr. Coef | rms Diff (cm/s) | Residual rms (cm/s) | Slope | Intercept | # of obs |
|---|---|---|---|---|---|---|
| **176°** | -0.11 | 21.3 | 12.7 | -0.11 | 1.07 | 1084 |
| **171°** | 0.03 | 19.6 | 13.1 | 0.04 | 0.14 | 1058 |
| **166°** | 0.17 | 18.0 | 13.4 | 0.18 | -1.17 | 1000 |
| **161°** | 0.31 | 16.9 | 14.0 | 0.34 | -2.7 | 807 |
| **156°** | 0.35 | 15.7 | 13.2 | 0.37 | -3.75 | 849 |
| **151°** | 0.43 | 15.3 | 13.5 | 0.48 | -3.09 | 513 |
| **146°** | 0.42 | 15.9 | 14.4 | 0.5 | -3.86 | 701 |
| **141°** | 0.42 | 15.8 | 14.3 | 0.5 | -4.64 | 855 |
| **136°** | 0.51 | 14.5 | 13.5 | 0.63 | -4.63 | 1007 |
| **131°** | 0.6 | 15.0 | 13.9 | 0.81 | -5.39 | 1038 |
| **126°** | 0.62 | 15.5 | 14.6 | 0.88 | -5.75 | 1081 |
| **121°** | 0.62 | 16.6 | 15.5 | 0.95 | 6.47 | 1076 |
| **116°** | 0.57 | 17.0 | 16.0 | 0.84 | -6.45 | 1072 |
| **111°** | 0.51 | 17.1 | 16.3 | 0.75 | -5.57 | 1059 |
| **106°** | 0.48 | 17.5 | 16.8 | 0.7 | -5.41 | 859 |
| **101°** | 0.4 | 16.5 | 15.3 | 0.51 | -3.56 | 1044 |
| **96°** | 0.37 | 16.7 | 15.0 | 0.46 | -2.34 | 830 |
| **91°** | 0.24 | 17.8 | 14.5 | 0.28 | -1.81 | 816 |
| **86°** | 0.27 | 17.0 | 14.9 | 0.36 | -3.1 | 471 |
| **81°** | 0.2 | 18.0 | 13.8 | 0.22 | -1.16 | 827 |
| **76°** | 0.12 | 19.1 | 13.8 | 0.12 | -2.22 | 647 |
| **71°** | 0.03 | 20.1 | 14.2 | 0.04 | -2.24 | 604 |

**Table A-8. Comparison Statistics for PPIN HF Radar (Measured Pattern) vs. M1 Mooring Radial Current Speed Pairs.**

| Angles of SCRZ | Corr. Coef | rms Diff (cm/s) | Residual rms (cm/s) | Slope | Intercept | # of obs |
|---|---|---|---|---|---|---|
| **-120˚** | -0.11 | 23.7 | 13.8 | -0.11 | 5.82 | 904 |
| **-115˚** | -0.13 | 25.86 | 14.5 | -0.13 | 8.42 | 886 |
| **-110˚** | -0.15 | 27.89 | 15.6 | -0.17 | 10.09 | 871 |
| **-105˚** | -0.07 | 28.63 | 16.3 | -0.08 | 12.41 | 926 |
| **-100˚** | -0.04 | 30.0 | 17.6 | -0.05 | 14.01 | 933 |
| **-95˚** | -0.03 | 33.3 | 19.9 | -0.05 | 16.74 | 911 |
| **-90˚** | -0.01 | 35. 3 | 22.4 | -0.01 | 18.74 | 821 |
| **-85˚** | 0.07 | 33.3 | 22.6 | 0.13 | 18.54 | 676 |
| **-80˚** | 0.1 | 31.1 | 21.3 | 0.18 | 16.83 | 759 |
| **-75˚** | 0.17 | 28.8 | 19.4 | 0.25 | 14.64 | 909 |
| **-70˚** | 0.19 | 25.1 | 16.8 | 0.24 | 11.4 | 956 |
| **-65˚** | 0.36 | 20.1 | 14.5 | 0.4 | 8.24 | 952 |
| **-60˚** | 0.5 | 16.4 | 13.3 | 0.56 | 5.3 | 863 |
| **-55˚** | 0.58 | 16.9 | 14.7 | 0.73 | 6.28 | 515 |
| **-50˚** | 0.55 | 16.2 | 14.1 | 0.66 | 5.25 | 394 |
| **-45˚** | 0.56 | 16.3 | 15.0 | 0.74 | 4.18 | 332 |
| **-40˚** | 0.57 | 14.3 | 12.3 | 0.59 | 2.39 | 499 |
| **-35˚** | 0.6 | 12.9 | 10.9 | 0.56 | 0.25 | 720 |
| **-30˚** | 0.67 | 11.4 | 9.7 | 0.6 | -0.89 | 687 |
| **-25˚** | 0.71 | 10.1 | 8.2 | 0.59 | -2.23 | 679 |
| **-20˚** | 0.62 | 11.4 | 8.9 | 0.51 | -3.22 | 631 |

**Table A-9. Comparison Statistics for SCRZ – MLNG HF Radar Baseline Radial Current Speed Pairs (Measured Pattern). One Radial Bin of the Best Grid Point Pairing from MLNG vs. Several Radial Bins from SCRZ.**

| Angles of MLNG | Corr. Coef | rms Diff (cm/s) | Residual rms (cm/s) | Slope | Intercept | # of obs |
|---|---|---|---|---|---|---|
| **230˚** | 0.11 | 18.0 | 14.3 | 0. 1 | 1.37 | 720 |
| **225˚** | 0.15 | 17.6 | 14.4 | 0.13 | 1.35 | 739 |
| **220˚** | 0.21 | 16.9 | 14.8 | 0.18 | 2.98 | 795 |
| **215˚** | 0.3 | 16.5 | 15.3 | 0.26 | 4.08 | 796 |
| **210˚** | 0.31 | 17.1 | 16.2 | 0.27 | 5.43 | 776 |
| **205˚** | 0.18 | 18.4 | 16. 5 | 0.16 | 5.78 | 705 |
| **200˚** | 0.24 | 17.2 | 15.5 | 0.21 | 4.24 | 765 |
| **195˚** | 0.3 | 17.1 | 15.7 | 0.28 | 4.73 | 758 |
| **190˚** | 0.4 | 16.1 | 15.6 | 0.38 | 5.02 | 821 |
| **185˚** | 0.52 | 14.0 | 13.9 | 0.49 | 3.57 | 822 |
| **180˚** | 0.63 | 12.3 | 12.4 | 0.62 | 2.96 | 822 |
| **175˚** | 0.67 | 11.9 | 11.6 | 0.69 | 2.28 | 810 |
| **170˚** | 0.69 | 11.8 | 11.0 | 0.76 | 1.69 | 805 |
| **165˚** | 0.7 | 11.6 | 10.7 | 0.79 | 1.21 | 807 |
| **160˚** | 0.72 | 11.1 | 10.0 | 0.8 | 0.23 | 812 |
| **155˚** | 0.7 | 11.1 | 10.0 | 0.75 | -1.05 | 809 |
| **150˚** | 0.67 | 11.6 | 10.7 | 0.69 | -2.68 | 792 |
| **145˚** | 0.6 | 12.9 | 11.8 | 0.64 | -3.82 | 720 |
| **140˚** | 0.52 | 14.1 | 12.9 | 0.54 | -5.11 | 671 |
| **135˚** | 0.45 | 14.8 | 13.4 | 0.46 | -6.0 | 632 |
| **130˚** | 0.42 | 15.2 | 14.1 | 0.41 | -6.58 | 603 |
| **125˚** | 0.39 | 14.6 | 12.8 | 0.39 | -4.43 | 550 |

**Table A-10. Comparison Statistics for SCRZ – MLNG HF Radar Baseline Radial Current Speed Pairs (Measured Pattern). One Radial Bin of the Best Grid Point Pairing from SCRZ vs. Several Radial Bins from MLNG.**

| Angles of SCRZ | Corr. Coef | rms Diff (cm/s) | Residual rms (cm/s) | Slope | Intercept | # of obs |
|---|---|---|---|---|---|---|
| **-170˚** | -0.41 | 37.8 | 15. 4 | -0.37 | -4.51 | 404 |
| **-165˚** | -0.3 | 38.3 | 14.9 | -0.24 | -7.18 | 423 |
| **-160˚** | -0.25 | 41.0 | 14.7 | -0.2 | -7.93 | 296 |
| **-155˚** | -0.19 | 32.1 | 15.5 | -0.16 | -2.7 | 471 |
| **-150˚** | -0.16 | 29.3 | 14.3 | -0.12 | -2.44 | 621 |
| **-145˚** | -0.07 | 27.8 | 14.1 | -0.06 | -2.52 | 654 |
| **-140˚** | -0.05 | 27.2 | 15.1 | -0.04 | -0.34 | 692 |
| **-135˚** | -0.04 | 27.1 | 16.5 | -0.03 | 1.3 | 649 |
| **-130˚** | 0.02 | 25.5 | 16.6 | 0.02 | 3.01 | 677 |
| **-125˚** | 0.06 | 24.7 | 16.5 | 0.05 | 4.3 | 745 |
| **-120˚** | 0.11 | 23.0 | 16.2 | 0.10 | 6.79 | 742 |
| **-115˚** | 0.22 | 23.2 | 17.8 | 0.21 | 8.51 | 724 |
| **-110˚** | 0.31 | 22.3 | 18.2 | 0.33 | 8.74 | 717 |
| **-105˚** | 0.45 | 20.3 | 17.3 | 0.47 | 9.17 | 767 |
| **-100˚** | 0.6 | 18.5 | 16.0 | 0.64 | 9.84 | 779 |
| **-95˚** | 0.67 | 18.8 | 16.2 | 0.8 | 10.58 | 762 |
| **-90˚** | 0.71 | 20.5 | 17.4 | 0.92 | 11.56 | 694 |
| **-85˚** | 0.71 | 20.3 | 17.6 | 0.96 | 10.5 | 598 |
| **-80˚** | 0.8 | 15.7 | 13.4 | 0.97 | 8.41 | 651 |
| **-75˚** | 0.85 | 12.8 | 11.1 | 0.94 | 6.79 | 758 |
| **-70˚** | 0.86 | 10.1 | 9.3 | 0.82 | 3.82 | 781 |
| **-65˚** | 0.79 | 11.8 | 9.2 | 0.64 | 0.42 | 778 |
| **-60˚** | 0.63 | 16.2 | 10.9 | 0.47 | -1.62 | 705 |
| **-55˚** | 0.56 | 18.5 | 12.2 | 0.41 | -1.68 | 491 |
| **-50˚** | 0.5 | 19.4 | 12.9 | 0.38 | -2.6 | 391 |
| **-45˚** | 0.47 | 21.0 | 13.7 | 0.38 | -3.42 | 280 |
| **-40˚** | 0.36 | 23.5 | 14.7 | 0.28 | -3.1 | 383 |
| **-35˚** | 0.33 | 23.1 | 12.7 | 0.23 | -5.05 | 527 |
| **-30˚** | 0.25 | 24.9 | 12.1 | 0.16 | -6.09 | 473 |

**Table A-11. Comparison Statistics for SCRZ – NPGS HF Radar Baseline Radial Current Speed Pairs (Measured Pattern). One Radial Bin of the Best Grid Point Pairing from NPGS vs. Several Radial Bins from SCRZ.**

| Angles of NPGS | Corr. Coef | rms Diff (cm/s) | Residual rms (cm/s) | Slope | Intercept | # of obs |
|---|---|---|---|---|---|---|
| **75˚** | -0.21 | 28.7 | 21. 2 | -0.17 | 0.6 | 153 |
| **80˚** | -0.02 | 25.1 | 21.5 | -0.02 | -0.46 | 251 |
| **85˚** | 0.19 | 22.0 | 21.6 | 0.15 | -3.04 | 408 |
| **90˚** | 0.31 | 17.1 | 16.8 | 0.23 | -0.56 | 561 |
| **95˚** | 0.59 | 13.3 | 14.0 | 0.49 | -1.41 | 697 |
| **100˚** | 0.68 | 12.7 | 14.0 | 0.63 | -2.65 | 617 |
| **105˚** | 0.76 | 10.7 | 11.3 | 0.75 | -1.78 | 703 |
| **110˚** | 0.79 | 10.0 | 9.3 | 0.82 | 1.4 | 782 |
| **115˚** | 0.79 | 11.8 | 12.7 | 0.98 | 3.07 | 778 |
| **120˚** | 0.76 | 15.6 | 21.5 | 1.05 | 7.42 | 823 |
| **125˚** | 0.7 | 20.5 | 31.1 | 1.05 | 12.46 | 796 |
| **130˚** | 0.66 | 19.9 | 27.6 | 0.93 | 12.4 | 819 |
| **135˚** | 0.65 | 18.9 | 25.3 | 0.81 | 13.15 | 825 |
| **140˚** | 0.47 | 19.4 | 20.2 | 0.59 | 11.36 | 605 |

**Table A-12. Comparison Statistics for SCRZ – NPGS HF Radar Baseline Radial Current Speed Pairs (Measured Pattern). One Radial Bin of the Best Grid Point Pairing from SCRZ vs. Several Radial Bins from NPGS.**

| Angles of SCRZ | Corr. Coef | rms Diff (cm/s) | Residual rms (cm/s) | Slope | Intercept | # of obs |
|---|---|---|---|---|---|---|
| **-150˚** | -0.18 | 29.4 | 14.6 | -0.14 | -2.21 | 675 |
| **-145˚** | -0.05 | 28.0 | 14.7 | -0.04 | -2.88 | 706 |
| **-140˚** | 0.04 | 25.9 | 14.6 | 0.03 | -2.2 | 729 |
| **-135˚** | 0.11 | 24.9 | 15.4 | 0.1 | -1.65 | 695 |
| **-130˚** | 0.16 | 23.6 | 15.8 | 0.14 | 0.12 | 686 |
| **-125˚** | 0.25 | 21.7 | 14.5 | 0.21 | 0.09 | 770 |
| **-120˚** | 0.32 | 20.4 | 15.1 | 0.28 | 2.11 | 757 |
| **-115˚** | 0.33 | 20.4 | 16.3 | 0.32 | 4.67 | 723 |
| **-110˚** | 0.41 | 19.7 | 16.7 | 0.42 | 6.39 | 708 |
| **-105˚** | 0.51 | 17.6 | 15.0 | 0. 5 | 6.83 | 773 |
| **-100˚** | 0.63 | 16.4 | 14.3 | 0.64 | 8.02 | 782 |
| **-95˚** | 0.68 | 17.5 | 15.3 | 0.78 | 9.61 | 771 |
| **-90˚** | 0.71 | 19.2 | 16.9 | 0.91 | 9.98 | 664 |
| **-85˚** | 0.7 | 19.5 | 17.2 | 0.94 | 9.64 | 585 |
| **-80˚** | 0.76 | 15.6 | 13.7 | 0. 9 | 8.33 | 651 |
| **-75˚** | 0.81 | 13.0 | 11.5 | 0.89 | 6.65 | 760 |
| **-70˚** | 0.83 | 10.6 | 9.9 | 0.8 | 3.61 | 791 |
| **-65˚** | 0.74 | 12. 6 | 10.3 | 0.62 | 1.13 | 790 |
| **-60˚** | 0.58 | 16.6 | 11.6 | 0.46 | -0.86 | 717 |
| **-55˚** | 0.54 | 18.8 | 14.4 | 0.47 | -0.45 | 461 |
| **-50˚** | 0.4 | 20.4 | 15.2 | 0.37 | -1.53 | 382 |
| **-45˚** | 0.39 | 21.0 | 15.5 | 0.36 | -1.93 | 302 |
| **-40˚** | 0.36 | 22.7 | 15.1 | 0.31 | -3.18 | 418 |
| **-35˚** | 0.27 | 22.4 | 12.7 | 0.2 | -3.82 | 606 |
| **-30˚** | 0.19 | 25.0 | 12.5 | 0.13 | 5.61 | 530 |

**Table A-13. Comparison Statistics for SCRZ – PPIN HF Radar Baseline Radial Current Speed Pairs (Measured Pattern). One Radial Bin of the Best Grid Point Pairing from PPIN vs. Several Radial Bins from SCRZ.**

| Angles of PPIN | Corr. Coef | rms Diff (cm/s) | Residual rms (cm/s) | Slope | Intercept | # of obs |
|---|---|---|---|---|---|---|
| **181˚** | 0.08 | 31.3 | 28.2 | 0.08 | -9.05 | 856 |
| **176˚** | 0.25 | 23.6 | 23.3 | 0.20 | -4.93 | 1056 |
| **171˚** | 0.32 | 22.1 | 22.0 | 0.27 | -3.52 | 1029 |
| **166˚** | 0.41 | 20.0 | 20.0 | 0.37 | -1.39 | 952 |
| **161˚** | 0.49 | 19.04 | 18.7 | 0.45 | 0.11 | 726 |
| **156˚** | 0.57 | 16.3 | 15.7 | 0.53 | 1.37 | 842 |
| **151˚** | 0.55 | 16.8 | 15.4 | 0.52 | 3.8 | 556 |
| **146˚** | 0.55 | 17.0 | 15.1 | 0.56 | 2.99 | 732 |
| **141˚** | 0.53 | 16.8 | 14.8 | 0.52 | 5.17 | 816 |
| **136˚** | 0.57 | 16.1 | 14.3 | 0.57 | 5.47 | 999 |
| **131˚** | 0. 7 | 14.8 | 14. 6 | 0.77 | 6.52 | 1044 |
| **126˚** | 0.76 | 14.1 | 14.9 | 0.89 | 5.63 | 1059 |
| **121˚** | 0.79 | 13.4 | 15.0 | 0.95 | 5.09 | 1058 |
| **116˚** | 0.82 | 11.5 | 11.8 | 0.94 | 3.25 | 1040 |
| **111˚** | 0.85 | 10.1 | 9.6 | 0.9 | 1.46 | 984 |
| **106˚** | 0.83 | 10.6 | 10.3 | 0.85 | 0.04 | 791 |
| **101˚** | 0.77 | 12.3 | 14.5 | 0.66 | -1.51 | 978 |
| **96˚** | 0.68 | 14.7 | 17.5 | 0.54 | -2.07 | 781 |
| **91˚** | 0.58 | 17.7 | 20.8 | 0.42 | -2.96 | 779 |
| **86˚** | 0.55 | 18.6 | 21.8 | 0.41 | -2.47 | 444 |
| **81˚** | 0.48 | 18.9 | 21.3 | 0.34 | -2.42 | 795 |
| **76˚** | 0.37 | 22.1 | 24.2 | 0.27 | -3.32 | 599 |
| **71˚** | 0.24 | 24.5 | 24.9 | 0.18 | -3.3 | 565 |
| **66˚** | 0.16 | 25.0 | 24.0 | 0.12 | -2.36 | 580 |
| **61˚** | 0.07 | 26.2 | 23.5 | 0.04 | -1.76 | 637 |

**Table A-14. Comparison Statistics for SCRZ – PPIN HF Radar Baseline Radial Current Speed Pairs (Measured Pattern). One Radial Bin of the Best Grid Point Pairing from SCRZ vs. Several Radial Bins from PPIN.**

| Angles of MLNG | Corr. Coef | rms Diff (cm/s) | Residual rms (cm/s) | Slope | Intercept | # of obs |
|---|---|---|---|---|---|---|
| **245˚** | 0.23 | 15.7 | 13.9 | 0.32 | -2.31 | 550 |
| **240˚** | 0.54 | 12.0 | 11.2 | 0.66 | -2.67 | 551 |
| **235˚** | 0.71 | 9.8 | 9.2 | 0.77 | -2.13 | 790 |
| **230˚** | 0.74 | 9.3 | 8.8 | 0.78 | -1.83 | 832 |
| **225˚** | 0.66 | 10.5 | 9.6 | 0.7 | -1.98 | 831 |
| **220˚** | 0.59 | 11.3 | 9.9 | 0.59 | -2.65 | 875 |
| **215˚** | 0.48 | 12.9 | 10.9 | 0.5 | -3.76 | 888 |
| **210˚** | 0.39 | 14.4 | 12.1 | 0.43 | -3.95 | 866 |
| **205˚** | 0.44 | 13.7 | 11.8 | 0.48 | -3.64 | 807 |
| **200˚** | 0.36 | 14.3 | 12.0 | 0.39 | -3.04 | 846 |
| **195˚** | 0.31 | 16.0 | 13.7 | 0.38 | -3.52 | 834 |
| **190˚** | 0.3 | 16.0 | 13.7 | 0.36 | -3.85 | 907 |
| **185˚** | 0.22 | 16.9 | 14.1 | 0.27 | -3.19 | 906 |
| **180˚** | 0.14 | 17.7 | 14.5 | 0.18 | -2.67 | 903 |
| **175˚** | 0.07 | 18.9 | 15.3 | 0.09 | -2.09 | 897 |
| **170˚** | 0.03 | 20.1 | 16.4 | 0.04 | -1.52 | 880 |
| **165˚** | -0.01 | 20.3 | 16.2 | -0.02 | -0.76 | 880 |
| **160˚** | 0.0 | 20.4 | 16.4 | 0.0 | 0.6 | 885 |
| **155˚** | 0.05 | 19.7 | 15.9 | 0.07 | 2.43 | 890 |
| **150˚** | 0.1 | 19.1 | 15.2 | 0.12 | 4.12 | 886 |

| | | | | | | |
|---|---|---|---|---|---|---|
| **145°** | 0.15 | 19.4 | 15.4 | 0.2 | 6.29 | 841 |
| **140°** | 0.2 | 19.5 | 15.0 | 0.26 | 8.15 | 799 |
| **135°** | 0.2 | 19.6 | 15.2 | 0.25 | 8.1 | 782 |
| **130°** | 0.2 | 19.9 | 15.6 | 0.26 | 8.0 | 753 |
| **125°** | 0.18 | 19.5 | 15.6 | 0.23 | 6.4 | 675 |
| **120°** | 0.18 | 18.8 | 15.3 | 0.24 | 5.06 | 474 |

**Table A-15. Comparison Statistics for MLNG – PPIN HF Radar Baseline Radial Current Speed Pairs (Measured Pattern). One Radial Bin of the Best Grid Point Pairing from PPIN vs. Several Radial Bins from MLNG.**

| Angles of PPIN | Corr. Coef | rms Diff (cm/s) | Residual rms (cm/s) | Slope | Intercept | # of obs |
|---|---|---|---|---|---|---|
| **146°** | -0.18 | 25.4 | 16.1 | -0.21 | 8.27 | 607 |
| **141°** | -0.15 | 25.0 | 16.2 | -0.18 | 8.82 | 748 |
| **136°** | -0.12 | 25.0 | 16.8 | -0.15 | 9.25 | 872 |
| **131°** | -0.15 | 27.4 | 17.4 | -0.21 | 11.3 | 891 |
| **126°** | -0.1 | 28.2 | 18.5 | -0.14 | 12.05 | 929 |
| **121°** | -0.06 | 29.5 | 19.8 | -0.1 | 13.47 | 925 |
| **116°** | 0.02 | 28.0 | 20. 8 | 0.03 | 12.9 | 924 |
| **111°** | 0.05 | 26.9 | 20.0 | 0.07 | 11.52 | 912 |
| **106°** | 0.1 | 26.5 | 21.2 | 0.14 | 11.36 | 739 |
| **101°** | 0.15 | 22.3 | 18.2 | 0.19 | 8.21 | 898 |
| **96°** | 0.21 | 21.0 | 17.7 | 0.26 | 6.91 | 718 |
| **91°** | 0.29 | 18.7 | 16.6 | 0.32 | 5.48 | 703 |
| **86°** | 0.3 | 20.7 | 20.1 | 0.33 | 8.16 | 408 |
| **81°** | 0.42 | 16.2 | 15.7 | 0.45 | 4.91 | 712 |
| **76°** | 0.54 | 14.9 | 15.8 | 0.55 | 5.3 | 567 |
| **71°** | 0.59 | 14.2 | 15.6 | 0.62 | 5.25 | 523 |
| **66°** | 0.7 | 11.9 | 13.8 | 0.68 | 4.76 | 588 |
| **61°** | 0.7 | 10.9 | 11.9 | 0.67 | 3.33 | 664 |
| **56°** | 0.71 | 9.8 | 9.9 | 0.66 | 1.14 | 790 |
| **51°** | 0.69 | 10.0 | 9.6 | 0.63 | -0.37 | 793 |
| **46°** | 0.64 | 10.9 | 10.7 | 0.56 | -1.65 | 686 |
| **41°** | 0.29 | 15.3 | 13.0 | 0.26 | 0.73 | 840 |
| **36°** | 0.47 | 13.3 | 13.1 | 0.39 | -3.5 | 507 |
| **31°** | 0.31 | 16.1 | 14.2 | 0.27 | -1.66 | 300 |
| **26°** | 0.12 | 19.8 | 14.8 | 0.13 | -3.52 | 314 |
| **21°** | 0.09 | 18.7 | 13.7 | 0.1 | 1.09 | 757 |

**Table A-16. Comparison Statistics for MLNG – PPIN HF Radar Baseline Radial Current Speed Pairs (Measured Pattern). One Radial Bin of the Best Grid Point Pairing from MLNG vs. Several Radial Bins from PPIN.**

| Angels of SCRZ | | Corr. coef | rms Diff (cm/s) | Residual rms (cm/s) | Slope | Intercept | # of obs |
|---|---|---|---|---|---|---|---|
| **Ideal Total** | | 0.65 | 16.9 | 18. 7 | 0.48 | 0.16 | 931 |
| **Measured Total** | | 0.74 | 12.7 | 13.1 | 0.64 | 0.81 | 931 |
| **Ideal** | **-83º** | 0.75 | 18.3 | 29.7 | 1.46 | -3.57 | 19 |
| | **-78º** | 0.48 | 17.1 | 19.8 | 0.37 | -3.49 | 26 |
| | **-73º** | 0.78 | 23. 7 | 31.6 | 0.4 | -5.46 | 57 |
| | **-68º** | 0.48 | 27. 8 | 33.0 | 0.32 | 1.24 | 89 |
| | **-63º** | 0.63 | 24.2 | 31.0 | 0.46 | -2.3 | 92 |
| | **-58º** | 0.86 | 9.2 | 12.2 | 0.86 | -3.78 | 48 |
| | **-53º** | 0.73 | 10.1 | 9.1 | 0.83 | 0.59 | 88 |
| | **-48º** | 0.79 | 8.7 | 8.4 | 0.76 | 1.88 | 29 |
| | **-43º** | 0.38 | 16.2 | 15.4 | 0.29 | -1.25 | 36 |
| | **-38º** | 0.47 | 11.4 | 11.5 | 0.37 | -1.36 | 89 |
| | **-33º** | 0.51 | 12.5 | 13.8 | 0.47 | 1.32 | 67 |
| | **-28º** | 0.41 | 10.9 | 10.5 | 0.3 | -6.72 | 30 |
| **Measured** | **-83º** | 0.93 | 9.8 | 10.2 | 0.92 | -0.44 | 19 |
| | **-78º** | 0.71 | 7.7 | 7.0 | 0.84 | -0.57 | 26 |
| | **-73º** | 0.74 | 9.7 | 10.1 | 0.73 | -1.62 | 57 |
| | **-68º** | 0.39 | 20.4 | 20.5 | 0.27 | 6.48 | 89 |
| | **-63º** | 0.6 | 15.1 | 14.5 | 0.56 | 6.19 | 92 |
| | **-58º** | 0.84 | 9.6 | 11.1 | 0.73 | 3.71 | 48 |
| | **-53º** | 0.71 | 10. 6 | 9.8 | 0.8 | 2.65 | 88 |
| | **-48º** | 0.7 | 12.7 | 14.0 | 0.51 | 2.4 | 29 |
| | **-43º** | 0.74 | 11.3 | 12.8 | 0.54 | -2.11 | 36 |
| | **-38º** | 0.38 | 12.4 | 11. 9 | 0.27 | -3.45 | 89 |
| | **-33º** | 0.41 | 13.7 | 13.3 | 0.29 | -2.58 | 67 |
| | **-28º** | 0.57 | 9.0 | 9.0 | 0.45 | -5.27 | 30 |

**Table A-17. Comparison Statistics for SCRZ HF Radar vs. Drifter Radial Current Speed Pairs.**

| Angles of MLNG | | Corr. coef | rms Diff (cm/s) | Residual rms (cm/s) | Slope | Intercept | # of obs |
|---|---|---|---|---|---|---|---|
| **Ideal Total** | | 0.74 | 9.7 | 9.3 | 0.71 | 0.39 | 987 |
| **Measured Total** | | 0.72 | 10.0 | 9.6 | 0.7 | 0.5 | 987 |
| **Ideal** | **130˚** | 0.64 | 7.3 | 8.6 | 0.35 | 3.66 | 17 |
| | **135˚** | 0.58 | 8. 2 | 9.3 | 0.25 | 7.71 | 31 |
| | **140˚** | 0.62 | 7. 5 | 9.2 | 0.46 | 6.18 | 30 |
| | **145˚** | 0.72 | 7.7 | 7.9 | 0.63 | 2.9 | 97 |
| | **150˚** | 0.71 | 8.8 | 8.2 | 0.7 | 1.37 | 192 |
| | **155˚** | 0.84 | 8.7 | 9.0 | 0.84 | -0.3 | 115 |
| | **160˚** | 0.86 | 7.9 | 9.3 | 0.8 | -3.18 | 70 |
| | **165˚** | 0.65 | 13.7 | 13.7 | 0.55 | -0.36 | 52 |
| | **170˚** | 0.73 | 12.5 | 15.6 | 0.65 | -7.91 | 33 |
| | **175˚** | 0.56 | 11.2 | 9.5 | 0.67 | -3.48 | 18 |
| | **180˚** | 0.84 | 7.8 | 8.4 | 0.73 | 0.46 | 18 |
| | **185˚** | 0.79 | 11.4 | 14.0 | 0.52 | -2.76 | 20 |
| | **190˚** | 0.79 | 8.9 | 9.3 | 0.68 | -2.06 | 34 |
| | **195˚** | 0.8 | 10.1 | 10.7 | 0.68 | -1.62 | 23 |
| | **200˚** | 0.77 | 11.8 | 16.6 | 1.11 | 5.89 | 18 |
| | **205˚** | 0.8 | 8.4 | 10.2 | 0.85 | 4.01 | 23 |
| | **210˚** | 0.68 | 10.5 | 11.6 | 0.76 | 3.82 | 25 |

| | | | | | | | |
|---|---|---|---|---|---|---|---|
| | **215˚** | 0.92 | 5.9 | 6.1 | 0.95 | -0.98 | 31 |
| | **220˚** | 0.7 | 10.3 | 10.4 | 0.9 | 2.51 | 26 |
| | **225˚** | 0.66 | 9.7 | 9.0 | 0.65 | 1.08 | 21 |
| | **230˚** | 0.77 | 6.2 | 6.4 | 0.67 | 4.29 | 27 |
| | **235˚** | 0.23 | 11.6 | 11.3 | 0.14 | -0.09 | 26 |
| | **240˚** | 0.41 | 12.7 | 14.0 | 0.29 | -4.17 | 17 |
| | **245˚** | 0.89 | 11.0 | 18.4 | 0.72 | -8.4 | 11 |
| **Measured** | **130˚** | 0.25 | 7.4 | 6.9 | 0.19 | 3.82 | 17 |
| | **135˚** | 0.59 | 9.1 | 10. 5 | 0.23 | 7.72 | 31 |
| | **140˚** | 0.44 | 9.6 | 11.2 | 0.33 | 7.24 | 30 |
| | **145˚** | 0.6 | 9.0 | 8.6 | 0.54 | 2.11 | 97 |
| | **150˚** | 0.56 | 10.6 | 9.4 | 0.59 | 1.44 | 192 |
| | **155˚** | 0.77 | 9.9 | 9.5 | 0.84 | -0.03 | 115 |
| | **160˚** | 0.87 | 8. 2 | 9.8 | 0.75 | -3.21 | 70 |
| | **165˚** | 0.69 | 13.3 | 13.8 | 0.56 | -0.16 | 52 |
| | **170˚** | 0.87 | 9.4 | 12. 4 | 0.67 | -5.84 | 33 |
| | **175˚** | 0.78 | 8.9 | 8.8 | 0.72 | -1.98 | 18 |
| | **180˚** | 0.91 | 5.8 | 6.6 | 0.8 | -0.51 | 18 |
| | **185˚** | 0.8 | 7.7 | 8.3 | 0.84 | -2.61 | 20 |
| | **190˚** | 0.84 | 7.6 | 7.8 | 0.75 | -1.39 | 34 |
| | **195˚** | 0.85 | 8.6 | 9.4 | 0.79 | -2.83 | 23 |
| | **200˚** | 0.7 | 12.0 | 10.7 | 0.79 | 0.84 | 18 |
| | **205˚** | 0.69 | 11.2 | 13.5 | 0.69 | 5.25 | 23 |
| | **210˚** | 0.72 | 10.3 | 13.3 | 0.9 | 5.17 | 25 |
| | **215˚** | 0.71 | 11.0 | 10.7 | 0.81 | 2.92 | 31 |
| | **220˚** | 0.44 | 13.9 | 11.7 | 0.53 | 2.28 | 26 |
| | **225˚** | 0.79 | 7.4 | 7.1 | 0.84 | 1.06 | 21 |
| | **230˚** | 0.66 | 7.8 | 8.0 | 0.55 | 4.95 | 27 |
| | **235˚** | 0.25 | 8.8 | 7.7 | 0.21 | 0.13 | 26 |
| | **240˚** | 0.37 | 10.5 | 10.6 | 0.3 | -3.4 | 17 |
| | **245˚** | -0.02 | 11.1 | 9.4 | -0.01 | -3.12 | 11 |

**Table A-18. Comparison Statistics for MLNG HF Radar vs. Drifter Radial Current Speed Pairs.**

| **Angles of NPGS** | | **Corr. coef** | **rms Diff (cm/s)** | **Residual rms (cm/s)** | **Slope** | **Intercept** | **# of obs** |
|---|---|---|---|---|---|---|---|
| **Ideal Total** | | 0.48 | 17.4 | 20.3 | 0.56 | -9.03 | 547 |
| **Measured Total** | | 0.79 | 10.4 | 11.0 | 0.67 | -1.97 | 547 |
| **Ideal** | **91˚** | 0.72 | 11.3 | 14.6 | 0.59 | -6.26 | 19 |
| | **96˚** | 0.6 | 14.9 | 18.7 | 0.43 | -6.43 | 58 |
| | **101˚** | 0.55 | 17.3 | 21.7 | 0.52 | -8.49 | 66 |
| | **106˚** | 0.37 | 16.8 | 17.7 | 0.33 | -7.62 | 60 |
| | **111˚** | 0.65 | 21.1 | 35.4 | 0.95 | -16.78 | 53 |
| | **116˚** | 0.37 | 20.0 | 22.5 | 0.58 | -12.27 | 43 |
| | **121˚** | 0.49 | 20.8 | 25.8 | 0.97 | -9.26 | 41 |
| | **126˚** | 0.09 | 23.9 | 17.5 | 0.12 | -4.89 | 15 |
| | **131˚** | 0.57 | 21.0 | 27.5 | 0.87 | -11.25 | 6 |
| | **136˚** | -0.09 | 23.3 | 19.0 | -0.11 | -13.88 | 8 |
| | **141˚** | 0.36 | 13.4 | 14.2 | 0.24 | -7.83 | 26 |
| **Measured** | **91˚** | 0.78 | 6.8 | 6.5 | 0.78 | -1.70 | 19 |
| | **96˚** | 0.71 | 8.8 | 10.0 | 0.57 | -3.27 | 58 |
| | **101˚** | 0.88 | 6.7 | 7.0 | 0.79 | -1.08 | 66 |

| | | | | | | | |
|---|---|---|---|---|---|---|---|
| | **106˚** | 0.76 | 9.6 | 10.7 | 0.59 | -1.88 | 60 |
| | **111˚** | 0.87 | 8.3 | 8.2 | 0.87 | -0.64 | 53 |
| | **116˚** | 0.8 | 11.7 | 14.0 | 0.82 | 2.45 | 43 |
| | **121˚** | 0.82 | 13.8 | 14.4 | 0.75 | 0.18 | 41 |
| | **126˚** | 0.71 | 15.5 | 16.1 | 0.6 | -0.39 | 15 |
| | **131˚** | 0.94 | 9.2 | 13.1 | 0.93 | -5.56 | 6 |
| | **136˚** | 0.96 | 8.5 | 12.4 | 0.53 | -6.57 | 8 |
| | **141˚** | 0.51 | 10.1 | 10.8 | 0.36 | -6.38 | 26 |

**Table A-19. Comparison Statistics for NPGS HF Radar vs. Drifter Radial Current Speed Pairs.**

| **Angles of PPIN** | | **Corr. coef** | **rms Diff (cm/s)** | **Residual rms (cm/s)** | **Slope** | **Intercept** | **# of obs** |
|---|---|---|---|---|---|---|---|
| **Ideal Total** | | 0.74 | 11.8 | 12.0 | 0.72 | 1.35 | 610 |
| **Measured Total** | | 0.77 | 10.4 | 9.7 | 0.8 | 0.15 | 610 |
| **Ideal** | **61˚** | 0.72 | 9.6 | 11.2 | 0.57 | -2.54 | 11 |
| | **66˚** | 0.83 | 14.1 | 16.7 | 0.88 | 5.12 | 15 |
| | **71˚** | 0.79 | 11.3 | 13.5 | 0.69 | 1.94 | 18 |
| | **76˚** | 0.73 | 10.4 | 12.7 | 0.55 | -0.57 | 11 |
| | **81˚** | 0.63 | 11.2 | 13.4 | 0.45 | -1.11 | 17 |
| | **86˚** | 0.79 | 8.3 | 9.1 | 0.64 | -0.68 | 72 |
| | **91˚** | 0.9 | 6.6 | 7.9 | 0.86 | 1.82 | 74 |
| | **96˚** | 0.77 | 10.0 | 10.9 | 0.76 | 2.33 | 66 |
| | **101˚** | 0.67 | 14.3 | 13.9 | 0.61 | -3.24 | 49 |
| | **106˚** | 0.5 | 17.2 | 17. 4 | 0.4 | -2.45 | 50 |
| | **111˚** | 0.72 | 9.4 | 9.4 | 0.88 | 2.47 | 23 |
| | **116˚** | 0.72 | 9.2 | 8.3 | 0.81 | -1.17 | 10 |
| **Measured** | **61˚** | 0.87 | 7.6 | 10.2 | 0.66 | -6.27 | 11 |
| | **66˚** | 0.93 | 9.1 | 7.9 | 0.94 | -0.41 | 15 |
| | **71˚** | 0.91 | 7.2 | 8. 9 | 0.79 | -2.97 | 18 |
| | **76˚** | 0.81 | 11.1 | 14.6 | 0.51 | -6.50 | 11 |
| | **81˚** | 0.76 | 6.9 | 7.3 | 0.63 | -1.99 | 17 |
| | **86˚** | 0.85 | 6.3 | 6.4 | 0.79 | -0.68 | 72 |
| | **91˚** | 0.89 | 6.3 | 6.0 | 0.95 | -0.27 | 74 |
| | **96˚** | 0.76 | 9.5 | 9.9 | 0.85 | 2.23 | 66 |
| | **101˚** | 0.73 | 13.4 | 13.7 | 0.64 | -4.07 | 49 |
| | **106˚** | 0.63 | 14.4 | 14. 9 | 0.52 | -1.95 | 50 |
| | **111˚** | 0.67 | 10.3 | 10.0 | 0.75 | 2.67 | 23 |
| | **116˚** | 0.81 | 7.6 | 7.3 | 0.96 | -0.2 | 10 |

**Table A-20. Comparison Statistics for PPIN HF Radar vs. Drifter Radial Current Speed Pairs.**

# LIST OF REFERENCES


Barrick, D.E., and B.J. Lipa, 1986: Correcting for Distorted Antenna Patterns in CODAR Ocean Surface Measurements. *IEEE Journal of Oceanic Engineering*, **OE-11** (2), 304-309.

Barrick, D.E., and B.J. Lipa, 1997: Evolution of bearing determination in HF current mapping radars. *Oceanography*, **10** (2), 72-75.

Chapman, R.D., L.K. Shay, H.C. Graber, J.B. Edson, A. Karachintsev, C.L. Trump, and D.B. Ross, 1997: On the accuracy of HF radar surface current measurements: Intercomparison with ship-based sensors. *J. Geophys. Res.*, **102** (C8), 18,737-18,748.

Crombie, D.D., 1955: Doppler Spectrum of Sea Echo at 13.56 Mc/s. *Nature*, **175**, 681-682.

Emery, B.M., L. Washburn, and J.A. Harlan, 2003: Evaluating radial current measurements from CODAR high frequency radars with moored current meters. http://www.icess.ucsb.edu/~emery/papers/ 8 June/2004

Fernandez, D.M., H.C. Graber, J.D. Paduan and D.E. Barrick, 1997: Mapping wind direction with HF radar. *Oceanography*, **10**, 93-95.

Frisch, A.S., and B.L. Weber, 1980: A new technique for measuring tidal currents by using a two-site HF Doppler Radar System. *J. Geophys. Res.*, **85** (C1), 485-493.

Gurgel, K.-W., G. Antonischski, H.-H. Essen, and T. Schlick, 1999: Wellen radar (WERA): a new ground wave radar for remote sensing. *Coastal Engineering*, **37**, 219-234.

Hammond, T.M., C. Pattiaratchi, D. Eccles, M. Osborne, L. Nash, and M. Collins, 1987: Ocean surface current radar vector measurements on the inner continental shelf. *Cont. Shelf Res.* **7**, 411-431.

Kohut, J.T., and S.M. Glenn, 2003: Improving HF radar surface current measurements with measured antenna beam patterns. *Journal of Atmospheric and Oceanic Technology*. **20**, 1303.

Melton, D.C., 1995: Remote sensing and validation of surface currents from HF radar. Master's Thesis, Naval Postgraduate School, Monterey, CA.

Paduan, J.D. and H.C. Graber, 1997: Introduction to High-Frequency radar: Realty and myth. *Oceanography*, **10**, 36-39.

Schmidt, R.O., 1986: Multiple Emitter Location and Signal Parameter Estimation. *IEEE Trans. Antennas Propag.*, **AP-34** (3), 276-280.

Stewart, R.H., and J.W. Joy, 1974: HF radio measurements of surface currents. *Deep-Sea Res.*, **21**, 1039-1049.

Wyatt, L. R., 1997: The ocean wave directional spectrum. *Oceanography*, **10**, 85-89.

# INITIAL DISTRIBUTION LIST

1. Dudley Knox Library
   Naval Postgraduate School
   Monterey, California

2. Dr. Jeffrey D. Paduan
   Department of Oceanography, OC/PD
   Naval Postgraduate School
   Monterey, California

3. Dr. Steven Ramp
   Department of Oceanography, OC/RA
   Naval Postgraduate School
   Monterey, California

4. Dr. Mary L. Batteen
   Department of Oceanography, OC/BV
   Naval Postgraduate School
   Monterey, California

5. Dr. Leslie Rosenfeld
   Department of Oceanography, OC/RO
   Naval Postgraduate School
   Monterey, California

6. Dr. Crtis A. Collins
   Department of Oceanography, OC/CO
   Naval Postgraduate School
   Monterey, California

7. Dr. Hyong Rok Kim
   Department of Oceanography, OC
   Naval Postgraduate School
   Monterey, California

8. Dr. Sunghae Park
   Department of Oceanography, OC
   Naval Postgraduate School
   Monterey, California

9. Dr. Donald Barrick, President
   Codar Ocean Sensors, Ltd.
   Los Altos, California

10. Dr. Scott Glenn
Institute of Marine & Coastal Sciences
Rutgers University
New Brunswick, New Jersey

11. Dr. Libe Washburn
Department of Geography
Institute for Computational Earth System Science
University of California, Santa Barbara
Santa Barbara, California